UNIVERSITÉ DE SHERBROOKE

Faculté de génie

Département de génie chimique et de génie biotechnologique

Développement de modèles CFD appliqués à des lits fluidisés pour la gazéification des déchets

Development of CFD models applied to fluidized beds for waste gasification

Thèse de doctorat

Spécialité: génie chimique

Leonardo Tricomi

Jury : Jean-Michel LAVOIE Pr. (Directeur, Génie chimique)

David CHIARAMONTI (Co-directeur, Ing., Ph. D Mech. Eng., Florence)

Micaël BOULET (Enerkem , CFD specialist)

Bernard MARCOS (Ing., Ph. D, Génie chimique)

José Luis Sánchez CEBRIÁN (Profesor Titular, Ingeniería química, Zaragoza)

Sherbrooke (Québec) Canada October 2017

To all those who supported me through this experience…

Summary

The thesis work is part of a project that aims to develop a reliable CFD model to investigate the fluid-dynamics of a fluidized bubbling bed during gasification of refuse derived fuel (RDF) from sorted municipal solid waste (MSW).

Gasification is a thermochemical process that converts carbon-containing materials into syngas. In this specific context scaling up is challenging because it implies dealing with a complex chemistry combined to heat and mass transfer phenomena in a multi-phase fluid environment. CFD modeling could represent a potential tool to predict the impact of the reactor configuration and operating conditions on gas yield, composition and potential contaminants.

Validation of CFD simulations for such systems has been so far possible using different sophisticated experimental tools, allowing to link the model with experimental data. However, such high tech equipment may not always be available, especially at industrial scale.

Hence, this work focuses on investigating the accuracy and numerical sensitivity of two different CFD models employed in the characterization of dense solid-particle flows in bubbling fluidized beds. The key parameter adopted to describe and quantify the dynamic behavior of this multiphase system is the power spectral density (PSD) distribution of pressure fluctuations. This PSD function was used to assess the accuracy of CFD models using one set of operating condition. The same type of analysis, extended to a wider range of operating conditions, may lead to a robust validation of the numerical models presented in this work. In spite of his measurement simplicity, pressure drop data present a strong connection with the bed fluid-dynamics and its interpretation could help to improve the fluidized bed technologies very fast, pushing CFD models closer to applications.

Résumé

Le but de ce projet est de développer un modèle CFD fiable pour étudier la dynamique des fluides d'un lit fluidisé en régime bullant pendant la gazéification de combustibles solides de récupération (CSR) triés à partir de déchets solides municipaux (DSM).

La gazéification est un processus thermochimique qui convertit les matériaux contenant du carbone en gaz de synthèse. La mise à l'échelle est difficile dans ce cas car elle implique une chimie complexe combinée aux phénomènes de transfert de chaleur et de masse dans un environnement fluide multiphasique. La modélisation CFD représente un outil potentiel pour prédire l'impact de la configuration du réacteur et des conditions de fonctionnement sur le rendement, la composition et les contaminants potentiels du gaz.

La validation des simulations CFD pour de tels systèmes a été jusqu'à présent possible grâce à l'utilisation de différents outils expérimentaux sophistiqués, permettant de lier le modèle aux données expérimentales. Toutefois, un tel équipement de pointe n'est pas toujours disponible, en particulier à l'échelle industrielle.

Par conséquent, ce travail se concentre sur l'étude de la précision et de la sensibilité numérique de deux modèles CFD différents, utilisés dans la caractérisation des flux de particules solides denses dans les lits fluidisés bouillonnants. Le paramètre clé adopté pour décrire et quantifier le comportement dynamique de ce système multiphase est la distribution de la densité spectrale de puissance (DSP) des fluctuations de pression. La fonction DSP a été utilisée pour évaluer la précision des modèles CFD en utilisant un ensemble de conditions de fonctionnement. Le même type d'analyse, étendu à une plus large gamme de conditions de fonctionnement, peut conduire à une validation robuste des modèles numériques présentés dans ce travail. En dépit de sa simplicité de mesure, les données de chute de pression présentent une importante corrélation avec les lits fluidisés, de plus, leur interprétation pourrait aider à améliorer ces technologies très rapidement, poussant les modèles CFD plus près des applications.

Mots clés : lit fluidisé bouillonnant, fluctuations de pression, modèles CFD–TFM/DPM, densité spectrale de puissance (PSD), la théorie cinétique du flux granulaire (KTGF)

Acknowledgments

A very special and personal thank goes to Mr. Lavoie, professor at the Université de Sherbrooke, who gave me the great opportunity of doing my PhD in Canada while being of a vital support all the way through.

I would also dedicate a heartfelt thanks to Mr. Chiaramonti, professor on contract at the University of Florence, for his decisive help to find and finalize the chance for a PhD in Canada together with emeritus professor Esteban Chornet.

I would also like to thank Mr. Micaël Boulet, CFD specialist in Enerkem, and Mr. Tommaso Melchiori, Post Doc. at prof. Lavoie's Chair, both for having worked close to me, supporting my project with brilliant idea and always be present to find solutions necessary for the advancement of my Ph.D. project.

I sincerely thank Enerkem as one of the main industrial partners of the prof. Lavoie's Chair, for having contributed to finance this project as well as for having provided me with technical support and a pleasant working environment where I carried out most of my PhD.

At this regards I am very much grateful to Aca Minić, technician in Enerkem, and Simon Kelley technician at the Chair, for their precious technical support in assembling the experimental reactor and the relating equipment.

I would also like to thank the Industrial Research Chair on Cellulosic Ethanol and Biocommodities (CRIEC-B) as well as for MITACS for having economically supported my PhD project.

Lastly I would like to dedicate all of my gratitude to a very special person, Jelena, for having thoroughly worked with me on the translation of the French parts of this work.

TABLE OF CONTENT

Figures list

Tables list

1. INTRODUCTION

The increasing interest in renewable energies and related technologies is due to the increasing demand for energy as well as concern for global warming effects caused by the massive exploitation of fossil fuels resources. While depleting, fossil fuels represent a non-renewable source of energy whose uneven distribution around the globe entails economic and geo-political tensions for many countries [1].

Biomass guarantees a renewable source of energy because of its carbon neutral life cycle and rapid growing rate. Solar energy absorption and carbon dioxide are fixed (in form of chemical energy) by plants into biomass via photosynthesis for a total amount of 4000 EJ/year [2]. On the other hand the total global energy demand is estimated in about 470 EJ/year [1]. When thermo-chemically decomposed, biomass releases this quantity of carbon dioxide closing a carbon-neutral cycle. Comprehensively speaking, biomass includes agricultural and forestry residues, wood, by-products from processing of biological materials, and organic parts of municipal and sludge wastes [1]. However, in literature, there is a not clear convergence on the bio-energetic potential because of the different types of biomass considered and methods of estimation. So for example, Fischer and Schrattenholzer [3] evaluated the global biomass potential to be 91 to 675 EJ/year for the years 1990 to 2060. In their study they considered the biomass deriving from crop and forestry residues, energy crops, and animal and municipal wastes. Hoogwijk et al. [4] estimated this potential to be in between 33 to 1135 EJ/year by including energy crops on marginal and degraded lands, agricultural and forestry residues, animal manure and organic wastes. According to Kumar et al. [1] only about 40% of potential biomass energy is exploited worldwide with the only exception of Asia where the biomass usage slightly exceed the sustainable biomass potential. Considering one of the biggest worldwide energy consumer such as United States, it was estimated [5] that, without many changes in land use and without interfering with the production of food grains, 1.3 billion tons of biomass can be harvested every year on a sustainable basis for biofuel production. The total energy content of this amount of biomass would cover more than 50 % of the USA total oil consumption [6]. Despite these numbers, there are other aspects such as harvesting, collecting and storage of biomass which limit the profitability of using lignocellulosic biomass for production of fuels, chemicals and bio-power [7]. Moreover this type of biomass presents a significant bulkiness which, combined

to a low energy density represents an important barrier to a quick transition from fossil fuels to biomass fuels [8]. Alternatively dedicated crops can be used to enhance the production of (conventional) bio-fuels, which however can result in a serious competition in the use of lands for food production as well as contributing to deforestation. In order to cope with these limitations, there is a growing interest in the exploitation of other types of carbon based materials which may help to develop a more sustainable supply of energy (advanced bio-fuels).

There are two principle and conceptually very different strategies which can be used in the energy conversion of biomass (Figure 1.1).

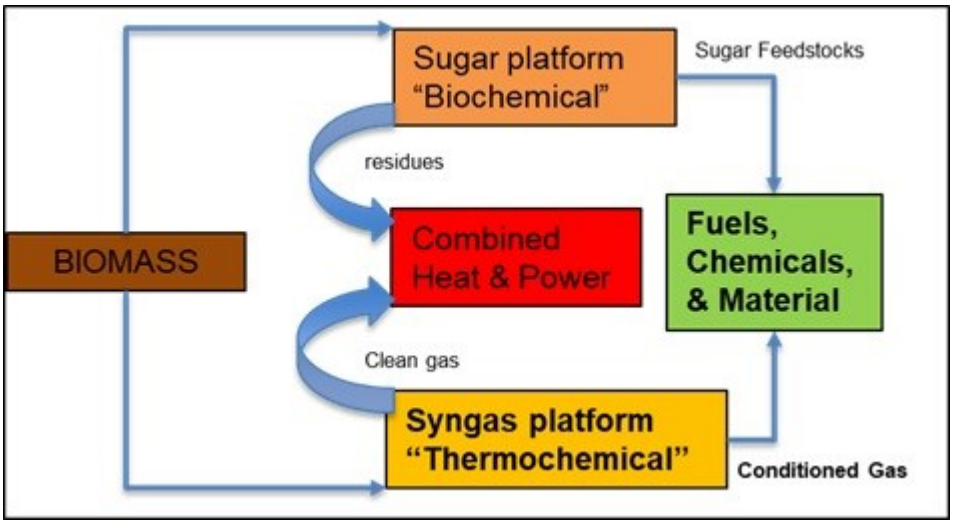

Figure 1.1- Main pathways for the conversion of biomass into heat, power, fuels and/or chemicals

The first one is the biochemical platform which in turn can be divided in fermentation and anaerobic digestion producing ethanol and methane (not reported in Figure 1.1) respectively. Since it is not an objective of this work, this first pathway will not be further discussed here.

A second pathway is the thermochemical biomass conversion that embraces a series of different transformations (not reported in Figure 1.1), ultimately leading either to the production of electricity or other forms of fuels (solid, liquid, gas). Among these possible thermochemical energy conversions combustions, pyrolysis and gasification are quite extensively considered or used in industrial application.

Combustion, one of the most common thermochemical processes, is carried out though high-temperature exothermic oxidation in an oxygen-rich environment. Pyrolysis can be either

fast or slow. The former involves rapid heating in the total absence of oxygen, aiming to maximize the conversion of biomass toward liquid fuels while slow pyrolysis (torrefaction) can be used alternatively to optimize the chars fraction. Differently from combustion, gasification usually operates at lower temperature under sub stoichiometric oxygen condition with the final aim of producing a mixture of gas compounds (mainly CO and H_2) known as synthetic gas.
Among the various types of biomass, the biogenic carbon feedstock, such as refuse derived fuels (RDF) generated from municipal solid waste (MSW), has a great potential for contributing to biofuels production as well as green chemicals for industrial applications [8].

The increasing world population, combined with the massive economic growth in developing countries such as India, China and Brazil, is making of municipal solid wastes an increasing concern at a planetary level. In this context, the management of the MSW life cycle will require significant efforts to be tackled whilst also an utmost opportunity to valorize. The lack of suitable space for landfills combined to the hardly biodegradable nature of some of the materials found in MSW calls for supported measures in the upcoming years [9].

According to a 2012 World Bank report [10], production of MSW is estimated to be approximately 1.3 billion tonnes yearly and is supposed to increase to 2.2 billion tonnes yearly by 2025. Most of it is landfilled or ultimately incinerated. The former solution presents several economically and environmentally drawbacks such as:

- The considerable production of CH_4, CO, CO_2 (high GHG impact).
- Potential contamination of groundwater by leachate
- Unpleasant odors
- The massive use of land that could be used for other purposes
- The intrinsic negative cost deriving by a proper management of wastes and respect of safety regulations.

Alternatively to landfilling, MSW can be burnt directly to generate heat and electricity. This technique has been used extensively in many developed countries mainly because of its high potential for energy recovery. Over the last decades incineration has been proposed as the most convenient technology to reduce MSW volume since it is a relatively simple technology, well known and mastered, that can reduce the initial volume of waste by as much as 85% whilst offering solutions for problems such as waste odor and leachate. However, in

the last decades, the incineration primary objective of reducing the generated volume of urban waste was edged by new environmental requirements. In fact, new and more restricting policies (Kyoto Protocol, the deliberations at Copenhagen in 2009 and the Landfill Directive of the European Union) were approved, aiming to minimize the environmental impact of atmospheric emissions, risks for human health and to accomplish national/international mandates for energy process recovery. Despite the consistent development of Municipal Solid Waste Incineration (MSWI) technologies as well as Air Pollution Control (APC), some drawbacks and negative impacts still remain, as shown by several recent studies and scientific reports [11]. MSWI exhaust gas produces a multitude of pollutants which are difficult and very costly to keep under control due to the large variability of chemical compounds originally present inside urban feedstock. Moreover, production of MSW is highly subjected to the specific demography of each country which, in addition to other factors, can further impact on its final composition. A concern shared by most of MSWI technologies is that very harmful compounds can be trapped inside micro flying ashes. This can have possible environmental and health consequences on the surrounding area. Besides, other technical issues such as corrosion of the incineration systems have led to a relatively low economic and energy efficiency.

In this context, *gasification* represents a very promising technology which, so far, has been widely applied to coal but more rarely to biomass and even less to MSW [12]. Lately, the application of this technology to MSW attracted a strong interest as a consequence of recent policies to tackle climate change and natural resources conservation [13]. As a "novel" waste-to-energy technology, gasification has several potential benefits over traditional incineration, mainly related to lower emissions and more flexible and efficient utilization of MSW chemical energy. The first and probably greatest strength of gasification is its environmental performance, since emission tests indicate that gasification meets the existing pollutants limits while having an important role in the reduction of landfill disposal [8]. The second and huge strength of this thermochemical pathway relies in the numerous downstream possible technologies converting syngas and allowing a broad diversity of end products (Figure 1.2).

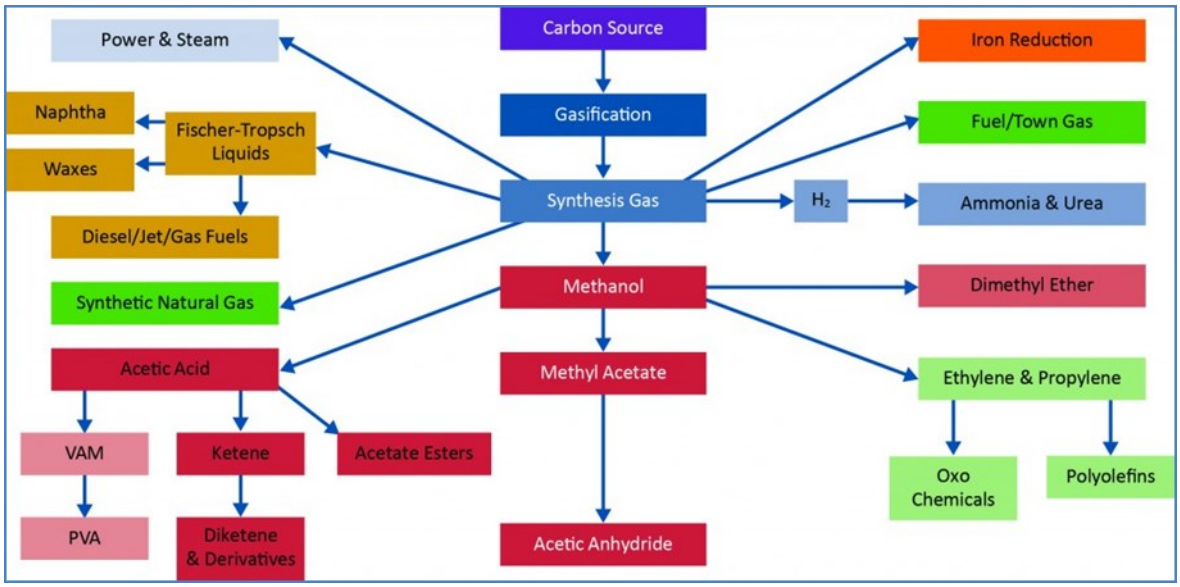

Figure 1.2 - Downstream gasification products and opportunities [102]

Besides the aforementioned advantages, gasification also presents other key aspects over combustion technologies. In fact, gasification can use low-value feedstocks and convert them not only into electricity, but also into liquid and gaseous fuels that can be easily handled and transported, with low operational costs [1]. The syngas generated from gasification can also be used in advanced technologies such as gas turbines and fuel cells, with high energy efficiency [14]. When used in combined cycles for heat and power generation, the use of syngas allows for a more efficient removal of species such as sulfur and nitrogen which ultimately results in much lower emissions [15].

Nevertheless, economics must be considered as a fundamental aspect affecting the profitability at commercial scale and ultimately the possibility for a concrete market penetration. This validity has to be proven for MSW gasification [16]. The main economical drawbacks are linked to the operational and capital costs estimated to about 10% higher than those of conventional combustion-based plants [13]. This is mostly due to the ash melting system and the overall higher complexity of the technology.

The gasification process takes place in the gasifier unit where the thermochemical decomposition stages of carbon-based feedstock occurs. Gasifiers are classified mainly on the basis of their gas-solid contacting mode and gasifying medium, ultimately resulting in different architectural and functioning concepts (Figure 1.3). More details about these type of concepts are reported in the next chapter of this work.

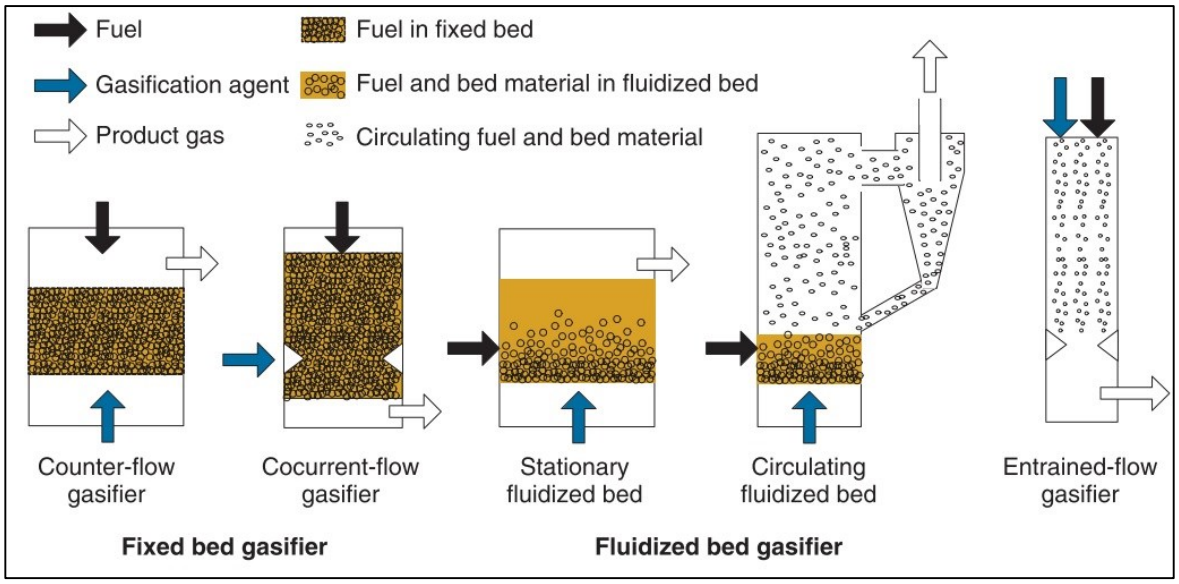

Figure 1.3 – Various concepts of gasifier units based on different gas-solid contact modes [17]

In this work, we focused on fluidized beds, being the one operated by the industrial partner (Enerkem)* for biofuels production. More specifically, among various types of fluidization regimes (Figure 1.3), Enerkem adopts the bubbling fluidized bed technology. Based on this hydrodynamic regime, the gasifier unit presents two contiguous regions which can be distinguished based upon different multiphase properties and reactions involved. More specifically:

- The "bubbling bed", located at the bottom part of the gasifier involves a multiphase environment with reactions between the carbon based feedstock, the inert bed material (heat carrier) and the gasifying agent (steam, and/or air, and/or oxygen);
- The "free-board", located up above the bubbling bed, where the primary syngas (permanent gas plus tars) are present along with a low concentration of fine particles (char, flying ashes). Part of present tars undergo a process of thermal reforming inside this vessel, ultimately leading to more permanent gas.

The gasifier unit is part of a broader technology (Figure 1.4) and it is used to produce a syngas that is downstream converted to biofuels and green chemicals.

* " Enerkem's disruptive technology converts non-recyclable municipal solid waste (i.e. garbage) into cellulosic ethanol, methanol and other renewable chemicals, with better economics and greater sustainability than other technologies relying on fossil sources. Enerkem operates a full-scale commercial facility in Edmonton, Canada as well as both a demonstration plant and a pilot facility in Quebec. The company is developing several cellulosic ethanol and methanol production facilities in North America and globally, based on its modular manufacturing approach." [18]

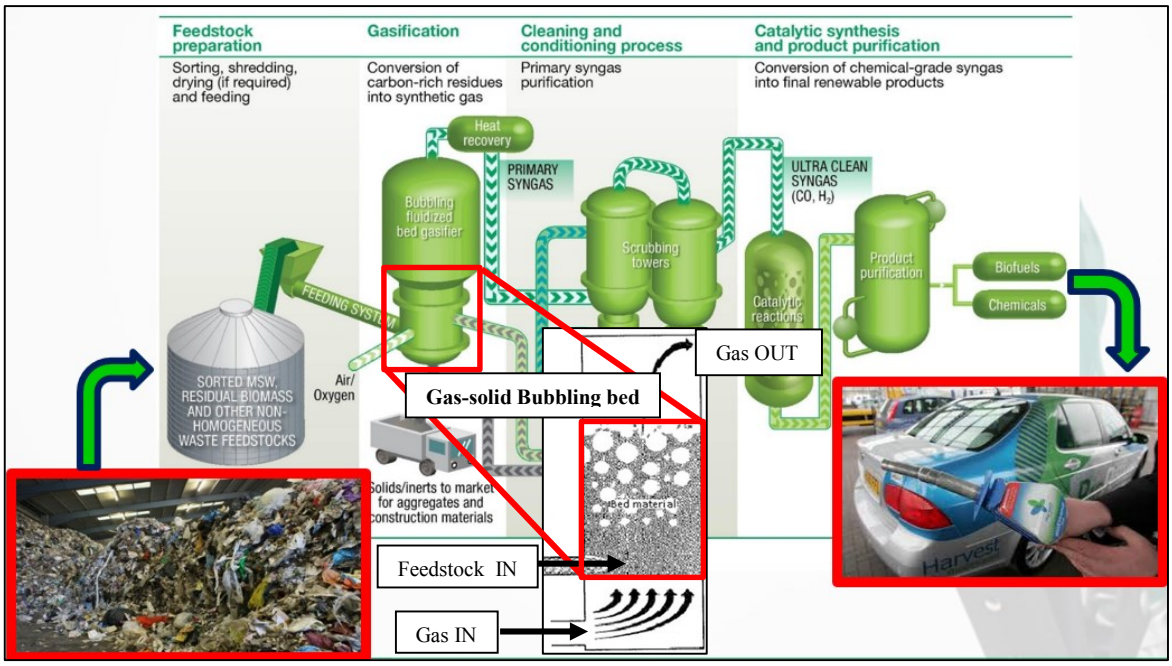

Figure 1.4 From MSW to Biofuels - Enerkem overall technology scheme [18]**. In the spotlight the first technology stage called fluidized bubbling bed gasifier**

The optimization of this type of process at industrial scale is fairly challenging since it involves a complex chemistry as well as mass and energy transfer phenomena in a multi-phase fluid-dynamic environment [19]. In order to limit expensive iterative hands-on experimental work, Computational Fluid Dynamic (CFD) modeling represents a very valuable tool to predict the evolution of fluid-dynamics and thermochemical variables resulting from various design configurations and variations [20]. The possibility of relying on numerical predictions can be very important in a context of technological optimization.

Gasification is a well-known process in literature since it has a long tradition of applications in various fields [21]. However, reliable and comprehensive CFD characterization of this process is very challenging and still to be reached. The lack of numerical modeling of gasification is due to the difficulty of accounting for the several thermochemical and fluid dynamic aspects involved in the process combined with the limited computational power which is still representing a major constraint. Despite these limitations, CFD can potentially provide essential information about syngas composition and sensitivity with regard to operating conditions and feedstock properties. The contribution that could be given by simulation analysis may help designing new efficient generation units with significant save of time and money (Figure 1.5).

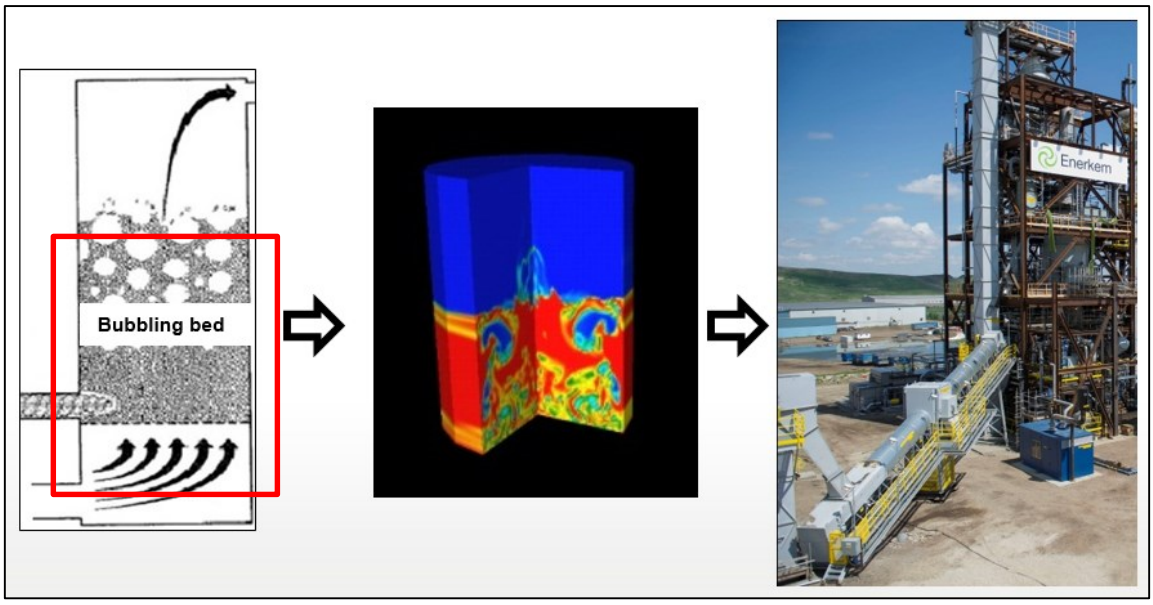

Figure 1.5 - CFD simulations to investigate bubbling fluidized bed and support technology advancement of industrial units

It has been proven that fluid dynamics impacts significantly on the overall efficiency of gasification [20]. This consideration highlights the importance of understanding gasification fluid-dynamics over a continuous space-time thus motivating the objective of this work.

In light of this last considerations a "cold" laboratory scale bench reactor was used to reproduce and investigate the fluid dynamics of a gas-solid fluidized bubbling bed. Based upon this lab-scale setup, different CFD models were then implemented and studied. The final target is to apply these CFD models to production scale using them as supporting tools for the designing process and optimization to ultimately improve the overall gasification efficiency. Such improvement may derive from CFD simulations of different design configurations for the gasifier and its operating conditions.

The research was carried out aiming to achieve a reliable numerical description of fluidized bubbling bed technology while finding the advantages and disadvantages specific to each type of numerical model in the perspective of their possible application to industrial scale. Is there a model that could be more efficient to simulate a full industrial scale gasifier and eventually at which cost?

2. STATE OF THE ART

2.1 GASIFICATION TECHNOLOGY OVERVIEW

Gasification systems present the coexistence of different biomass thermochemical conversion stages such as combustion, pyrolysis and gasification (Figure 2.1). Among various factors, the oxygen availability within the bed is of a primary importance in determining which and where each of these stages takes place. These stages, accordingly to the specific type of technology, may occur separately in the different zones of gasifiers or more spatially homogenized throughout the whole bed.

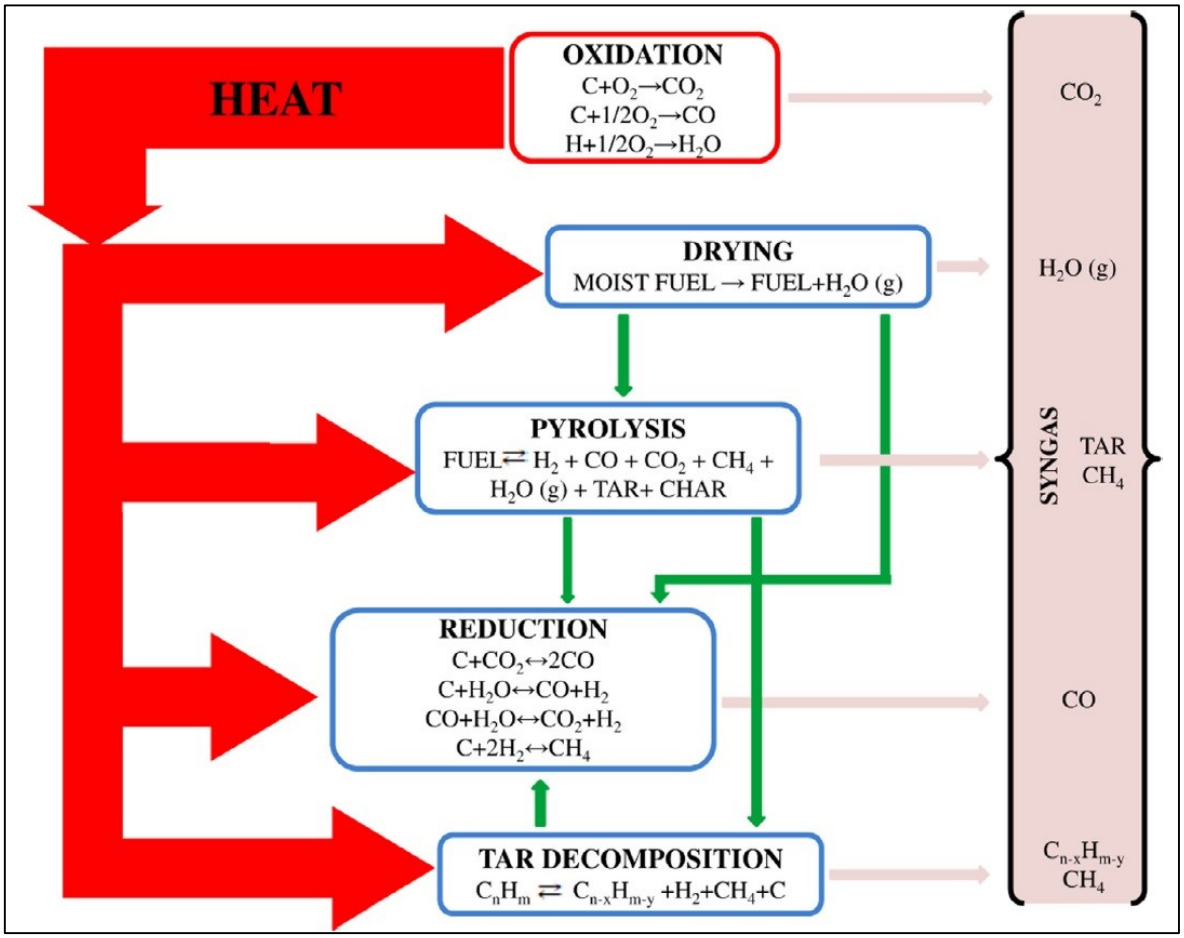

Figure 2.1 - Gasification of biomass: principal steps and products involved in the thermo-chemical decomposition of biogenic carbon from MSW [22]

Based upon the type of contact between solid material (either biomass, char or inert material) and gas phases (gasification agents and gas released from thermochemical decomposition of

feedstock) different reactor concepts have been developed and applied to gasification of carbon based feedstock [8]. Among several different possibilities in terms of reactor architectures and functioning a significant distinction can be found in moving bed on one side and fluidized bed technology on the other.

In the moving (packed) bed, the feedstock occupies between 30% and 80% of the reactor volume and is supported on a grate. The biomass is fed from the top and it decomposes while it slowly moving downwards the reactor. The ash extraction is made at the base of the bed. Biomass residence times are quite long, usually 2-10 hours. Fairly distinct zones are established in the bed corresponding to the different stages of the gasification process, each at different temperatures. While biomass moves downward, the gasifying agent can flow through the bed concurrently, counter-currently, or cross-wise, which ultimately defines three corresponding types of moving bed concepts namely downdraft, updraft and cross draft beds (Figure 2.2). More details about constructions technology, operating conditions and features of these various fixed beds configurations can be found in [8].

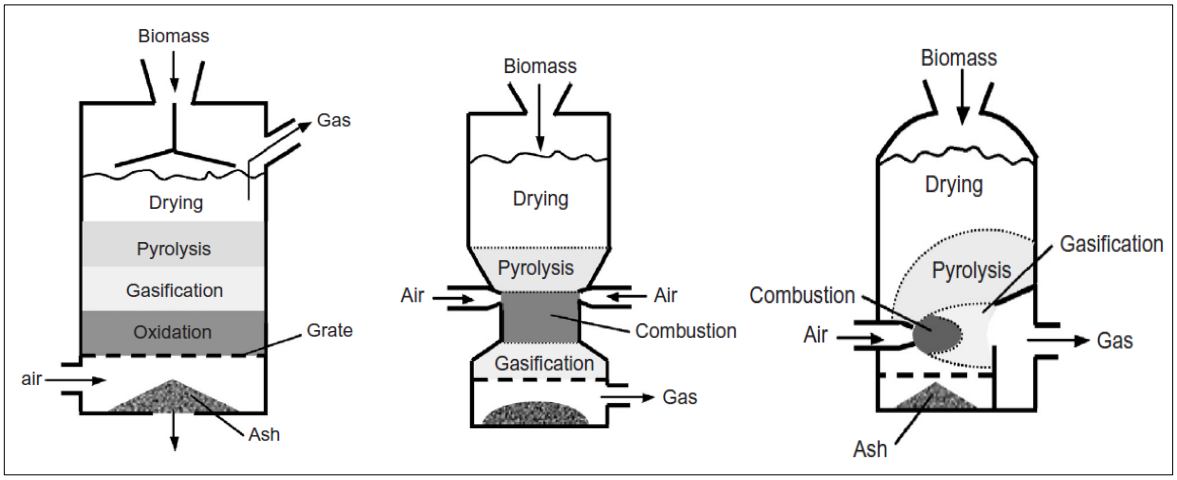

Figure 2.2 – Packed bed gasifiers: a) updraft, b) downdraft, c) cross-draft [8]

In the second type of concept (fluidized systems) the solid particles are kept in a semi-suspended condition (fluidized state) by the flow of the gasifying medium through them at the appropriate velocities [8], which is obviously considerably higher than in packed beds. Biomass is fed usually from the side and near the base of the reactor while the gasifying agent (air, oxygen, steam or CO_2) flows upwards (Figure 2.3). The biomass residence times are short, usually seconds or minutes with an extremely efficient mixing due to the high turbulence, so that distinct zones are not established in the bed. All gasification stages occur

simultaneously throughout the bed. Temperatures are highly uniform, typically at 800-1000°C.

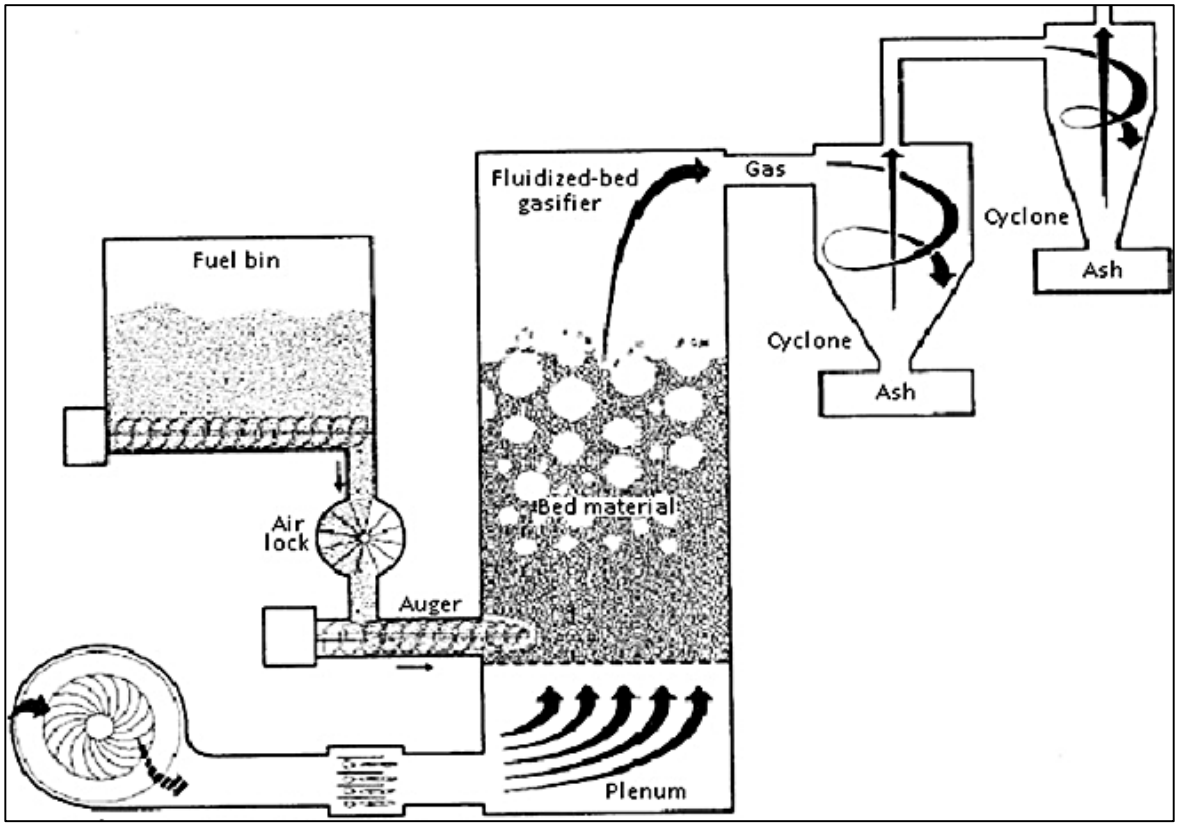

Figure 2.3 - Schematic of a fluidized bed gasifier [23]

2.2 FLUIDIZED BUBBLING BED DYNAMICS

There are actually many possible fluid dynamics regimes that could take place inside a fluidized bed gasifier reactor (Figure 2.4). These regimes mainly depend upon the superficial velocity at which the gasifying agent is operated. The actual Enerkem technology is based on an intermediate regime, which is bubbling fluidization (marked in red in Figure 2.4). In this regime, the multiphase system includes regions with very low solids density (called bubble phase), and other regions with a higher solid concentration (called emulsion phase). Bubbles tend to rise through the bed increasing turbulence and increasing the mixing inside the reactor. This ultimately helps to enhance the overall efficiency. For this reason, it is essential to understand bubble fluid dynamics in order to optimize the whole process.

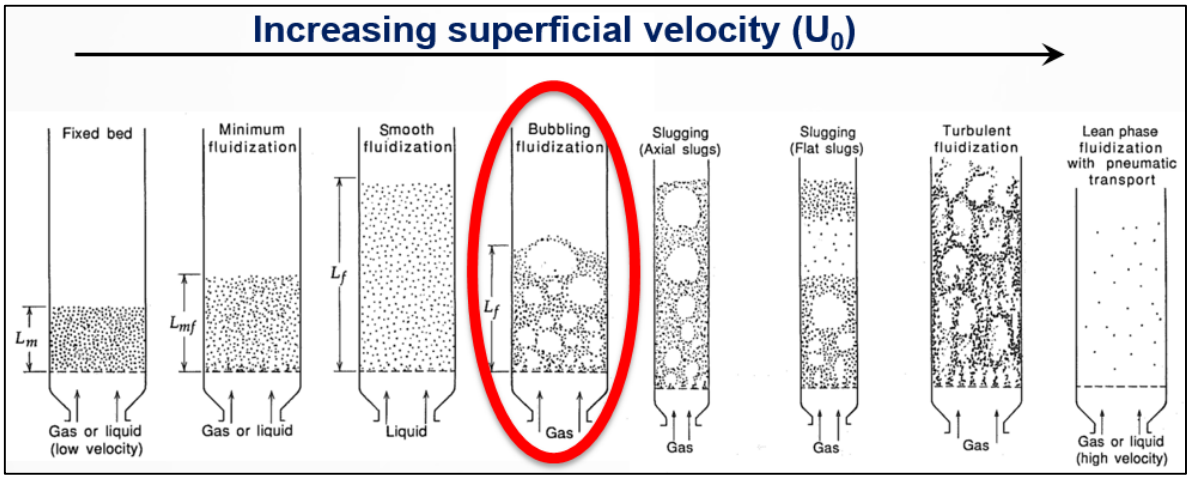

Figure 2.4 - Different fluid-dynamic regime taking place inside a gasifier as function of increasing superficial velocity [24]

Fluidized bed reactors are extensively used both in combustion and gasification systems to thermo chemically convert the solid fuel (and the intermediate pyrolysis products, char and tars) using oxidizing agents and inert bed material. The experience built over decades in this field has shown that bubbling fluidization regime is one of the best ones to guarantee optimal mixing between various phases, ultimately allowing efficient heat and mass transfer [20], [25].

The hydrodynamic behavior of a bubbling fluidized bed results from the balance of forces established between the fluidization agent and the solid particles as well as the mutual repulsive forces arising from particle collisions. In the fixed regime, the equilibrium between the drag force (exerted by the fluidization medium), the constraint reaction offered by the particles (which are packed) and the gravity (acting on the mass of solid particles) ensures a static condition for the bed. In this circumstance, any increase of air velocity results in a linear increase of gas pressure drop until this latter equal the bed weight. A further increase in air velocity leads to a visible bed expansion and to macroscopic instabilities. The transition between the static and dynamic bed regime is marked by the minimum fluidization velocity (U_{mf}). Once this value is exceed, bubbles start forming in the proximity of the injection zone and then move upwards, contributing to phase mixing and turbulence.

In general, fluidization is significantly impacted by the properties of solid particles, which have been classified according to Geldart [26]. This classification, widely accepted in

fluidized bed modeling, divides particles in four groups according to their physical properties and behavior in fluidization system (Figure 2.5).

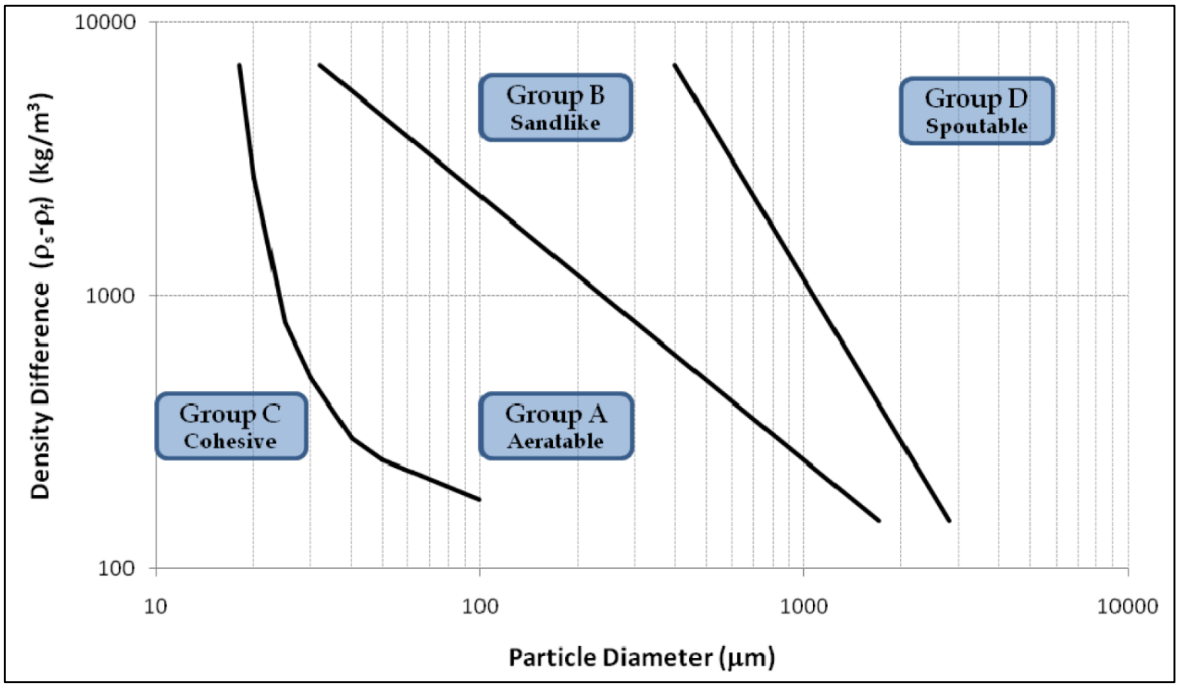

Figure 2.5 – Graphical representation of Geldart classification, showing the particles behaviors in fluidized systems according to their physical properties [27]

As far as this study is concerned, particles belonging to Group B (namely having a medium diameter in the 40-500 µm range, and density between 1400 and 4000 kg/m^3) will be the center of experimental interest. The use of these particles allows reaching good fluidization when operating at high flow rates, while also ensuring bubbles generation on fluidization onset and coalescing during the motion.

All transfer phenomena involved in bubbling fluidized beds, especially in their application to thermochemical processes (such as gasification), are conditioned by the particular type of contact between the various phases [28]. In order to maximize the contact between phases and consequently their mass and heat transfer, a vigorous and turbulent mixing is highly desirable. This mixing is mainly promoted by bubbles motion which, moving inside an emulsion of solid and gas phase [29], enhances their contact and ultimately the transfer phenomena efficiency. Consequently, over the last few decades, significant efforts were invested to cope with a lack of understanding that led to difficulties in design and scale-up of gas-fluidized bed systems [28].

2.3 NUMERICAL MODELING AND MULTI-LEVEL SCALES IN GAS-SOLID FLOWS

Along with the increasing computational power of the new computers generation, numerical simulations became a very useful tool to investigate fluidized beds. As explained by Van der Hoef et al [28], simulations can be used in two different manners. First they can contribute to bring an insight into the fundamentals of the complex dynamics of particles-gas systems, unveiling the effect of physical principles such as drag, friction, dissipation etc. In addition, they can be used as a predictive tool for supporting the scale-up design of bubbling fluidized beds. As reported by the authors, it is not possible to achieve all of this with one single simulation method but rather with a family of approaches, working on different scales and time lengths, which will be presented in the following of this chapter.

Nowadays Computational Fluid Dynamics (CFD) is the most widespread numerical analysis for such applications and current limitations to their validity are related to theoretical issues as well as CPU performances. In this sense, major constraints are shown very clearly when attempting to simulate real systems, involving complex geometries and physical phenomena, at full industrial scale [20]. Moreover, the time required for CFD simulations increases exponentially with the complexity of the real system under investigation, which represents an additional limitation. In spite of these intrinsic barriers, reliable CFD models are essential for the optimization of fluidized beds. Several information can be derived from post-processing of CFD results, such as the local inert material concentration in bed, fuel mixing efficiency, temperature profiles of solids and gas phases present in the bed, heat flux etc. It would be otherwise impossible to gain a full detailed map (in time and space) of all these variables from the experiments.

Modern CFD is a combination of fluid dynamics models, solved with numerical methods and algorithms applied to fluid flows [20] (or multiphase flows like in the current case of study). The framework within which CFD modeling attempts to describe thermochemical processes, such as gasification, comprises a wide range of physical and chemical interconnections as shown in Figure 2.6.

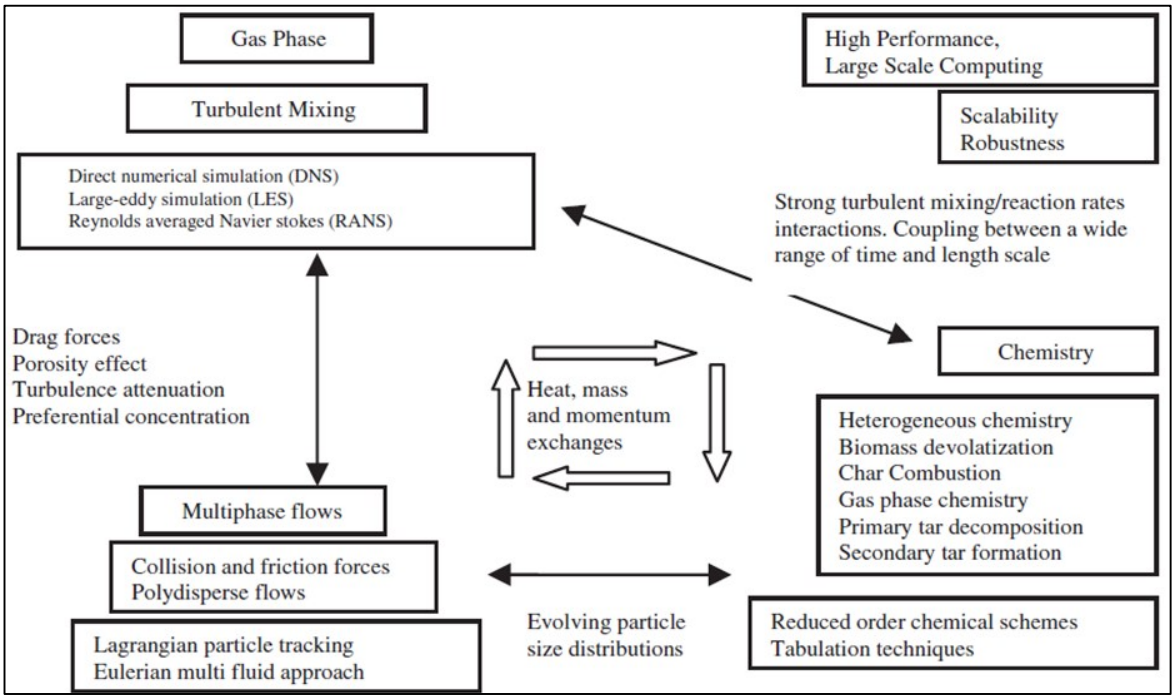

Figure 2.6 - Modeling of physical and chemical processes interaction in thermochemical conversion of fuels [19]

This complexity derives from the contingent need to account for several aspects involved in multiphase systems and related thermochemical processes, resulting in a fully coupled system of equations. Equations coupling derives, for instance, from several "source terms" which account for the connections between various phases both in terms of exchange of momentum, mass and energy. Another example of equations coupling comes from the phase densities, used in the continuity and momentum equations, in general linked to the system temperature which is retrieved from the energy balance equations.

The theoretical knowledge of the specific type of applications/problems is absolutely fundamental to choose the most appropriate modeling strategy in order to possibly simplify this great complexity. This is also the reason why CFD literature [20] of fluidized bed applications is divided in three main branches based upon the specific part of the reactor under investigation (where the concentration of secondary phase is significantly different) which are principally:

- The bubbling bed
- The splash zone
- The free board/riser

As far as the actual work is concerned, the focus will be on the first part of the gasifier (the bubbling fluidized bed), whose modeling approaches and inherent literature review will be presented in the rest of this chapter.

The term “bubbling” refers to the specific type of fluid dynamics taking place inside the reactor (Figure 2.4). The choice of this particular system, as mentioned previously, is related to turbulent mixing and high efficiency in term of heat and mass transfer, which justifies its extensive use in the industry. Moreover, when compared to more vigorous regimes (Figure 2.4), the risk of an excessive entrainment of solid particles in the free board and ultimately out of the reactor itself is significantly reduced.

In the industrial bubbling gasifiers, there is always a coexistence of several phases involving both gases (gasification medium combined with the one produced from the thermochemical decomposition of feedstock) and solid particles. A vast majority of these particles are forming the so called “inert bed material” that served the purpose of transferring heat to the fuel particles (in mass less than 10 % of the bed) acting as a thermal buffer.

In cold bubbling applications (usually not employed for industrial purposes) this distinction remains, even though the multiphase system is quite simplified since only two phases can be theoretically involved. Here, ambient air or nitrogen are usually chosen to fluidize the bed, and are considered as primary phase, while the secondary phase involves the solid inert particles. The concentration of the two phases cannot be predicted a priori, being the result of a random event brought by the turbulent mixing caused by bubbles. Solid phase concentration can reach high values in the lower and lateral (close to the wall) areas of the bed, depending on the particle distribution and shape, and low values in the presence of bubbles or close to the bed surface (where bubble explosions occur).

The gas phase is usually modeled according to micro- to macro-scales where a scale length is characterized by the local Knudsen (Kn) number. This number defines the ratio between the mean free path of molecules and a characteristic length scale of the flow. Depending on this number, three regimes and corresponding transitions may be possible. The lowest Knudsen numbers (smaller than 0.01) are representative of incompressible flows that can dynamically be described by the Navier Stokes equations. At the opposite, a Kn higher than 10 would be representative of a free path system where molecules would move freely and colliding only with the system boundaries. These two extreme situations for the gas phase

find a modeling correspondence in the continuum and molecular models. While this latter can apply only to micro-scale (despite being theoretically applicable to any length scale, its use is limited by computing capacity) the former is used to wider scale systems (in the order of meters) investigation. The gap between the two models is filled by the kinetic theory based on the Boltzman equation [28].

As for the solids there is a possibility to define various types of models accordingly to the scale of simulations and particles density magnitude. Some of the methods used to describe granular systems are taken from the molecular gas theory and extended for analogy to fit the need to describe particles properties that are obviously quite different. Solid particles and gas molecules do not share the same mechanical properties. Specifically, it happens that while molecules can be assumed to collide elastically (with no loss of kinetic energy during the collision), real particles collisions involve a surface friction and elastic-plastic deformations, which generate a loss in the kinetic energy of solid system. These two last aspects can distance the granular flow behaviour from ideal gas one quite significantly making the description of the solid particles system not straight forward. From this point of view, the granular flows description and modeling is quite complex but at the same time presents also a significant margin of improvement towards reliable hydro-dynamic models development [28]. When choosing the proper model for a multiphase system, a very important aspect to consider is the degree of particle packing inside the bed. Depending on this value, various interphase coupling possibilities are available, as reported by Elgobashi [30] and shown in Figure 2.7.

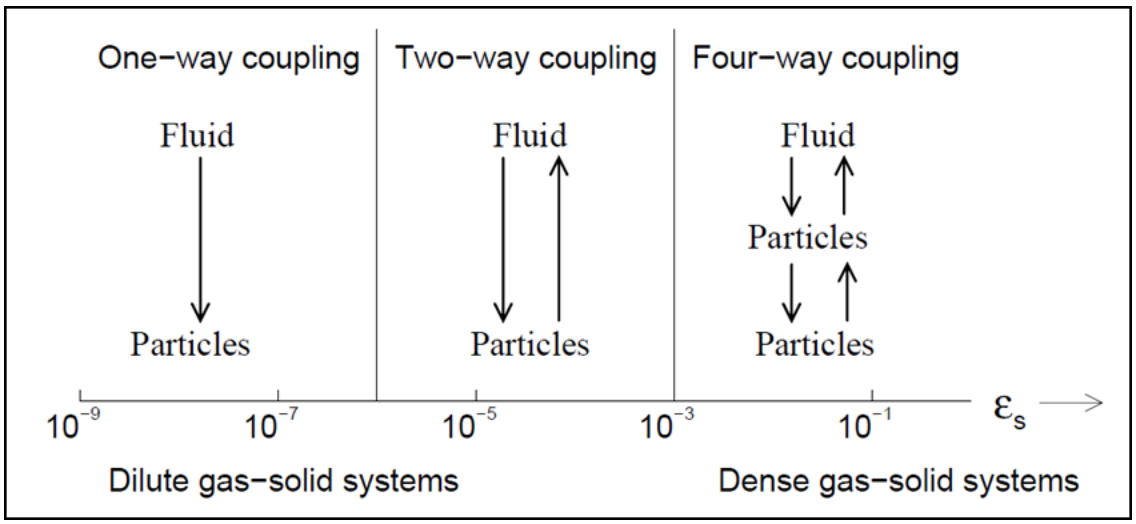

Figure 2.7 – Interphase fluid-particles coupling (based on [30]**)**

Given the high density of solids involved, the four-way coupling (Figure 2.7) was considered for current thesis work. In fact, in bubbling fluidized beds, the solid fraction ranges from 0 (in presence of pure gas bubbles) to a maximum packing limit that in case of irregular shape particles is a phase fraction ranging between 0.5-0.6. In such circumstances, the solid concentration can drastically affect the gas pattern and structure while particles are interacting with each other (and with the boundaries of the physical domain) exchanging momentum throughout collisions and surface friction.

In bubbling fluidized beds with no chemical reactions, the two main protagonists driving the fluid dynamic of the overall system are the fluid-particles drag forces and the particle-particle interactions.

In the last decades, despite the technological advancement in computing science, the construction of reliable models for large-scale systems has been seriously hindered by the lack of understanding of the fundamentals of dense gas-particle flows [31]. As remarked by Van der Hoef et al. [28], one very big challenge, studying multiphase systems, is represented by the definition of spatial scales involved. In general the accepted concept is that larger flow structures (in the order of meters) might be affected by smaller scales where particle-particles interactions take place. This considerations can explain why many efforts have been put forward over the years to search for proper micro to meso-scale modeling equations of gas-particle and particle-particle interactions. These interactions at small scale are of utmost importance since they allow developing proper closure laws which, once applied at macroscopic scale, provides better modeling of macroscopic flow structures, which are usually of major industrial interest. Open literature [20] reports that there are currently three main techniques to investigate the multiphase fluidized systems whose multi-level scheme and inter-connections are depicted in Figure 2.8.

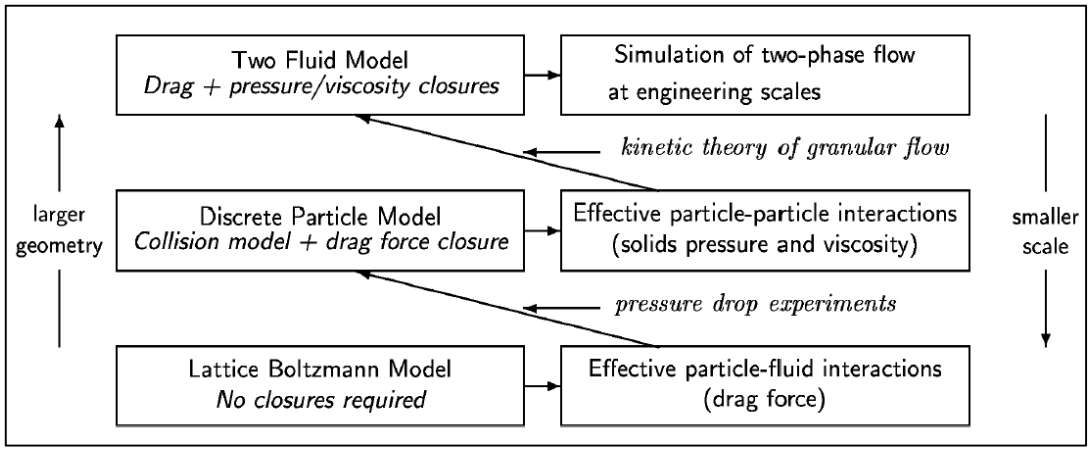

Figure 2.8 - Multi-level modeling scheme [28]

From the smaller to the larger scale we can find:

1. Lattice Boltzman Model (LBM) or alternatively the Discrete Numerical Simulations (DNS) (which represent a broad family of methods despite being not reported in Figure 2.8).

2. Eulerian-Lagrangian Discrete Particle Model (DPM). Belonging to this family are the Kinetic Theory of Granular Flow (KTGF) model (used in this work), the hard/soft sphere models and the MPIC approach.

3. Eulerian-Eulerian Two Fluid Model (TFM).

2.3.1 Principle features of different numerical approach to solid-gas flows

At the smallest applicability scale (Figure 2.8) is the Lattice Boltzman Model (LBM) which in the last two decades, has emerged as a promising tool for modelling the Navier-Stokes equations and simulating complex fluid flows [32]. The fundamental idea is that gases/fluids can be imagined as consisting of a large number of small particles moving with random motions. The exchange of momentum and energy is achieved through particle streaming and billiard-like particle collisions. More details about the mathematical derivation and formulation of this method can be found in works of Bao and Meskas [32] as well as in Van der Hoef et al [28]. Alternatively to LBM there is another class of methods called Direct Numerical Simulation (DNS). This family of methods are the most detailed approach, fully resolving the flow around each single particle (Figure 2.9) by solving the Navier Stokes

(N.S) equations without turbulence models. The solid-fluid interaction is based on a "stick" boundary conditions at the particle surface site enabling to describe a fully resolved momentum exchange between phases. In such type of simulations, turbulence swirls and their effects are accounted in the whole range of time and space scale length making this approach highly computationally demanding. In turbulent flows, the total energy is consumed according to a macro to micro scale of vortex (also known as Kolmogorov scale) induced by turbulence and their correct numerical resolution would require to account and solve for the whole scale of these vortex. Specifically, it can be proved that the ratio between the Kolmogorov micro-viscosity scale (for which N.S equations have to be solved) and the macro scale (comparable to the length of the flow field) is scaling up with 1/Re, ultimately resulting in extremely fine numerical mesh required to study flow field at high Reynold numbers.

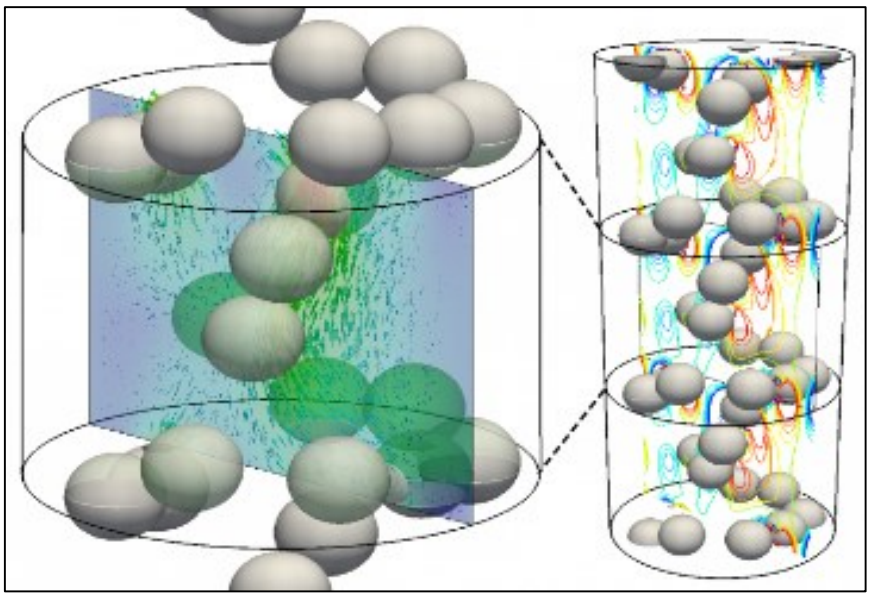

Figure 2.9 – Example of a Direct Numerical Simulation (DNS) where the gas flow is numerically resolved around each single particle in a system [33]**,** [34], [35]

As an example, a simulation of a flow with a Re$\sim 10^6$ in a field of ~1 m would require to work on a numerical grid in the order of 10^{-5} m. For this reason DNS has been used to describe only very small scale systems (around 1 cm max) comprising few thousand particles [28]. Even with the most powerful new generation computers, this method is not reported in literature among those potential techniques used to study multiphase applications at pilot or

industrial scale [20]. The goal of these simulations is rather to develop and tune drag laws that might possibly be employed in larger scale applicability models (DPM , TFM etc..).

In their recent work Tang et al. [36] used a DNS approach to study the fluidization of 5000 particles in a pseudo-2D gas-fluidized of $3.75 \cdot 10^{-4}$ m^3. Using Particle Image Velocimetry (PIV) they were able to obtain detailed information on the gas flow and motion of individual particles, with specific focus on comparing the empirical and numerical particle granular temperature (as key characteristics of particle velocity fluctuations).

The empirical system investigated in the present thesis work, comprises a total volume of approximately $1.85 \cdot 10^{-2}$ m^3 with around 680 million particles. It is here clearly evident how a DNS approach would not be possible to characterize such a dense particle system.

The other two modeling approaches, namely the TFM and DPM (DDPM)-KTGF, were used in this work to investigate bubbling bed fluidization. The decision of investigating these two models was motivated by their conceptual difference in the numerical treatment of the solid phase. From here, the motivation in exploring the main features of these two CFD models to ultimately determine and compare the advantages and drawbacks of each of them in the perspective of their potential application to industrial scale. The most significant features of these two methods and related applications to multiphase systems (as reported in open literature) are presented in the rest of this chapter while their proper equations will be shown in Chapter 3.

The DPM (DDPM)-KTGF represents only one of the possible options in the Eulerian-Lagrangian description of gas-solid systems (where the hard or soft sphere approaches may also be used). The reasons behind the choice of this particular Lagrangian approach will be discussed at the end of section 3.3.

The two selected modeling approaches share a very important aspect, which is the Kinetic Theory of Granular Flow (KTGF) [37], [38] used to define the granular properties of the solid phase. According to this theory, the particles behavior is approached in a similar manner to the one of a molecular gas. The use of this theory allows to bring important closure relations ultimately bridging the micro-scale description of granular flows (DNS) to a macro scale approach. According to the KTGF theory, two granular flow variables such as the solid pressure and the solid shear stress tensor (both including kinetic, frictional and collisional components) are introduced to account for repulsive forces between colliding particles.

These two variables are in turn computed as a function of the local granular temperature (for which an extra conservation equation is solved) which is defined from the fluctuations in the velocity of the solid particles. More explanation of each of these term can be found in the next chapter (section 3.3).

The *Euler-Lagrangian Discrete Particle Model (DPM)* represents a class of methods occupying an intermediate place in the applicability scale shown in Figure 2.8. In DPM methods, the primary phase (gas/fluid phase) is described as a continuum (fluid) by solving the Navier Stokes equations, while to the secondary (solid) phase is modeled a system of spheres according to a discrete approach. Differently from the DNS approach, the cell size over which the gas field is resolved contains many particles and the flow properties are averaged within each cell resulting in the impossibility to detail the gas flow around each particle. However the advantage of this method is the possibility to provide a detailed description of the overall solid phase distribution inside the domain (thanks to the Lagrangian particles tracking) without confining the study to only few particles (as for the DNS approach). In this context the trajectory of each sphere results from a double integration of the Newton's second law which expresses a force balance applied to each of them within the Lagrangian framework. Consequently this class of methods allows detailing the motion and evolution of feed stock solid particles in the bed (for hot model applications) as well as simply investigating cold segregation phenomena (shown as an example in Figure 2.10) when particles of different size are used.

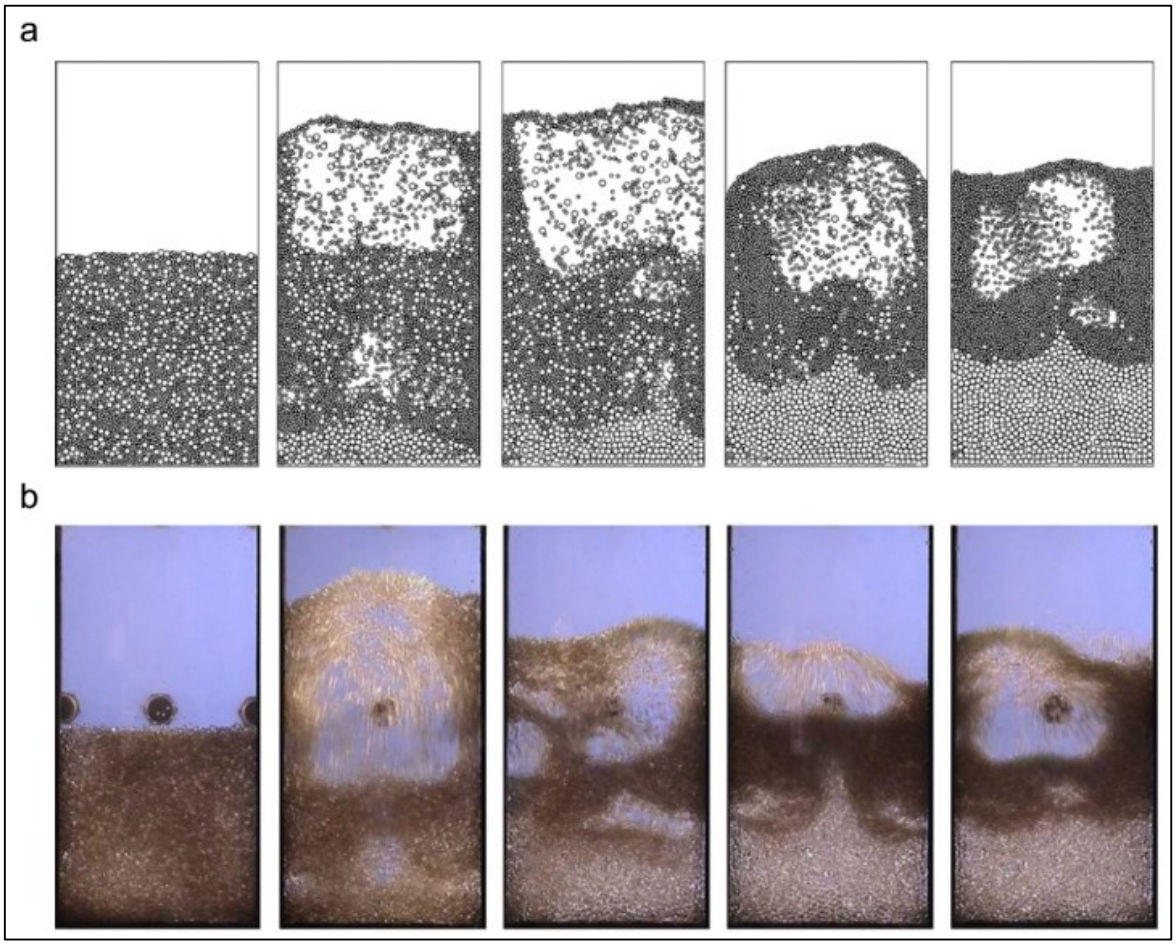

Figure 2.10 -Snapshots of size segregation in fluidized bed: (a) simulated and (b) experimental binary mixture mixing [39]

In order to avoid any possible confusion about the nomenclature (acronym) of the Lagrangian model used in this work (where DDPM-KTGF will be used in place of DPM-KTGF), it is important to highlight some aspects which strictly relate to the definition of this type of model within the software used here (Fluent). According to the present software, the DPM approach will only be valid when the solid fraction of the dispersed phase (solid particles) is below 10-12% of the fluid (gas) domain [40]. In such a circumstance the volume fraction of the discrete phase is sufficiently low and it is not taken into account when assembling the continuous phase equations. Moreover the low volume fraction of particles allows neglecting the particle-particle interactions (collisions), which represent a significant simplification. However the respect of this solid load threshold limits the exploitation of the DPM approach (so conceived) to bubbling fluidized bed application. In such a type of system, particles can accumulate very easily (in some part of the bed even exceeding the 50

% of the total volume) requiring to both account for the volume exclusion effect in the primary phase (considering a gas fraction coefficient in both the continuity and momentum equations) and particle-particle collisions. For these reasons a Dense Discrete Phase Model (DDPM) was used in this work and coupled with the Kinetic Theory of Granular Flow (KTGF) to account for particle-particle interaction forces. While the DPM represents a class of Lagrangian approaches to multiphase flows (well known in open literature and independent from any software nomenclature), this DDPM approach comes as an extension of the DPM to high density granular systems according to the definitions specific of the present software. Therefore in the rest of this work, the acronym DDPM will be used instead of DPM, which will also allow to be consistent with other works found in open literature where authors used the same software and referred to the DDPM approach.

In the DDPM-KTGF model, particles contact forces (collisions) are estimated by solving the gradients of granular flow variables (solid pressure term and shear stress tensor), which are derived from an averaging process involving the position and velocities of particle over the Eulerian grid (where the primary phase is solved). Conversely, in fully resolved collisional methods (such as the Eulerian-Lagrangian soft sphere model briefly introduced at the end of section 3.3) collisions are independent of Eulerian variables but are rather computed as a function of particles mechanical properties (elasticity coefficient, particle stiffness, damping coefficient etc..). This motivates the reference to this DDPM-KTGF as an Euler-Lagrangian hybrid approach to multiphase system [41].

At a larger applicability scale (see Figure 2.8) there is the *Eulerian-Eulerian Two Fluid model (TFM)* which considers a simplified description of both gas and solid phases. These are both described as inter-penetrating fluids, thus introducing phasic volume fraction as continuous function of space and time. The summation of all phasic volume fraction is obviously equal to one. The application of this method to multiphase granular systems allows observing the concentration of different phases within the domain thus without recognizing the single particles distribution (Figure 2.11). Despite the apparent simplicity in the representation of various phases, this one of the most complex approach to multiphase granular systems since it requires the definition of several constitutive relations (derived from the application of the KTGF theory) to close the set of governing equations. These latter are represented by the mass and momentum conservation equations, which are solved

per each phase. The resolution of these equations allows to recover the motion field (velocity and pressure) for both phases together with the distribution of phasic fractions.

This method proved to be computationally cost-effective when the volume fractions of gas and solid phases are comparable and the interaction between these phases is significantly impacting on the overall fluid dynamic behavior such as in bubbling fluidized beds [20]

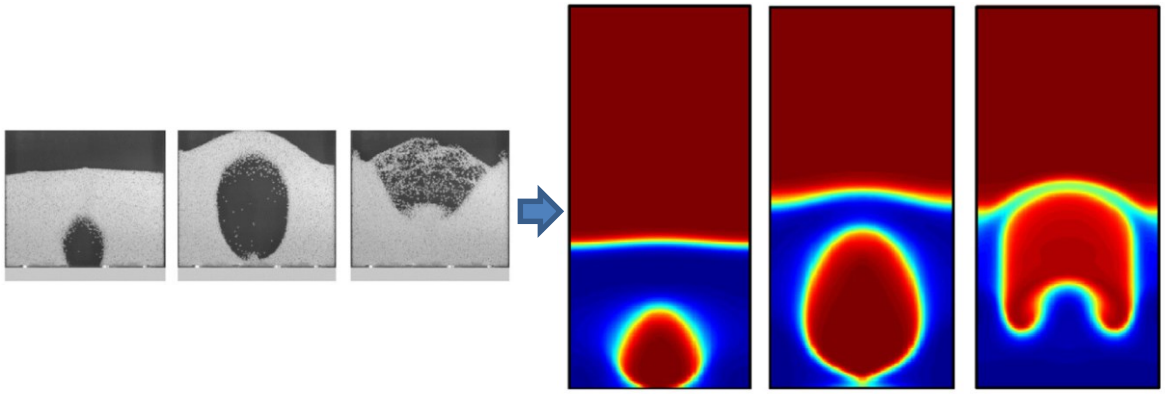

Figure 2.11 - Injection of a single bubble into the center of a mono-disperse fluidized bed consisting of spherical glass beads of 2.5mm diameter at incipient fluidization conditions. Comparison of experimental data (left) with TFM (right) [103]

As a sum up of these three different class of methods, namely the DNS simulations, the DPM approach and the TFM, Figure 2.12 schematically reports the main differences and scales of applicability. Here is provided an example of multi-level modeling application to the study of a life-scale fluidized bed (left). The arrows represent a change of model. In first place the TFM (see enlargement) can be used to simulate large sections of the unit providing overall information about phase concentrations (see the shade of gray cell by cell). On the right, a part of the same section is modeled using discrete particles (DPM). The gas-phase is solved on the same grid as in the two-fluid model which is containing a certain number of particles whose shape or size is not relevant in capturing the gas flow patterns and features. The bottom graph shows the most detailed level, where the gas-phase is solved on a grid much smaller than the size of the particles (DNS) which allows to account for the specific particles properties (size, shape etc..) and their effect on the gas flow.

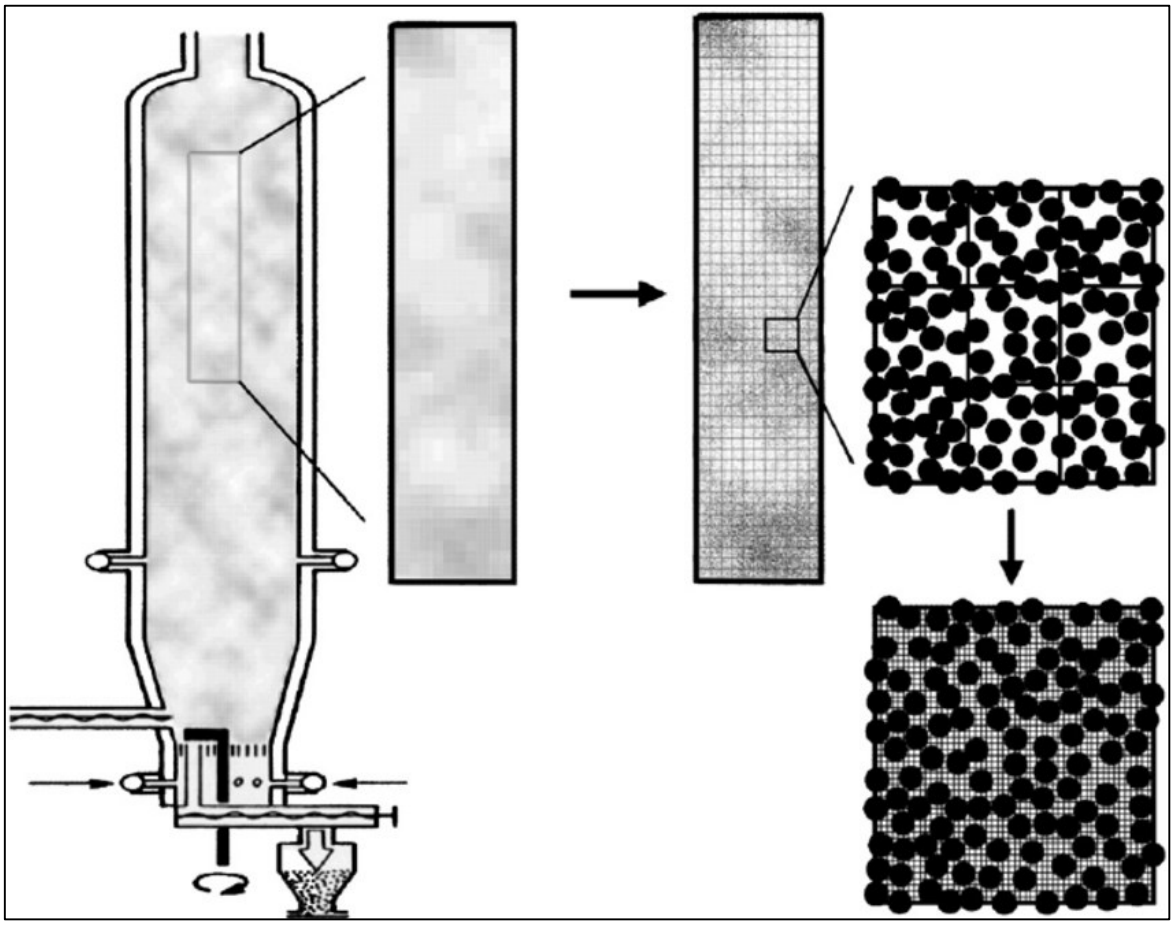

Figure 2.12 - Graphic representation of the multi-level modeling scheme [28]**.**

2.3.2 CFD models: TFM and DDPM-KTGF applications in open literature

TFM

Different versions of the TFM approach have been proposed over the years, mainly differing for the type of closure used for approximating the solid shear stress tensor and more specifically the solid viscosity being an important part of it. Here, in the early stage of this hydrodynamic model development, authors such as Anderson and Jackson [42], Sundaresan et al. [43], Kuipers et al. [44] and Tsuo et al. [45] proposed the use of an empirical constant viscosity along with an empirical correlation, linking the solid pressure term with solid fraction volume. However, these simplifications presented as major limitations the absence of a fundamental link between the solid viscosity and pressure with the particles phase rheology. Another class of TFM was developed for dilute systems, relying on the extension of turbulent viscosity approach for the gas to solid phase. Nevertheless, these models,

developed initially by Elgobashi et al. [46] and Chen et al. [47], and later extended by Zhou and Huang [48], did not include the effect of particle-particle collisions on the solid viscosity. Consequently these models were not suitable to investigate dense multiphase system (such the one object of this work) even though useful for studying dilute granular flows.

In this work the closure for the shear stress tensor derives from the application of the kinetic theory of granular flows (KTGF) to the continuum description of the solid phase. Major contributions to this modeling approach is owed to the works of Gidaspow et al. [49], [50].

Following Gidaspow et al. findings, Sinclair and Jackson [51] used the TFM-KTGF model to predict the core-annular regime for steady developed flow in a riser. Samuelsberg and Hjertager [52] performed transient simulation of gas-particle flow in a riser comparing it to empirical data while Nieuwland et al. [53] applied this model to investigate a circulating fluidized bed. Detamore et al. [54] exploited the model to perform a scale-up analysis of a similar fluidized system. In more recent works, Peirano et al. [55] conducted a CFD study of a bubbling fluidized bed (BFB) using an Eulerian TFM approach both in 2D and 3D to assess its numerical accuracy and suitability to catch the dynamic behavior of bubbles. Syamlal and O'Brien [56] used a TFM-KTGF model to investigate the contacting behavior of catalytic reactors by catalytic decomposition of ozone (O_3). After having obtained a verified model, they also found a good quantitative agreement with experimental data. McKeen and Pugsley [57] showed that a freely bubbling bed of fluid catalytic cracking (FCC) catalyst can be simulated for superficial gas velocities in the range of 0.05 to 0.2 m/s with reasonable accuracy, using the two-fluid CFD code. In this work, they compared numerical and empirical data based on the bed expansion, and bubble diameters and rise velocities. Zimmerman and Taghipour [58] exploited a TFM-KTGF model to simulate the hydrodynamics and reaction kinetics of gas-solid fluidized beds containing catalytic cracking (FCC) particles (Geldart group A). Specifically in their study the authors focused on the the effect of different drag formulations on the overall bed expansion, solid-gas momentum exchange and conversion of ozone. The authors proved that the effect of the drag model was significantly impacting the result predicted by the TFM and specifically that the Gidaspow [59] and the Syamlal-O'Brien [60] drag were not applicable in their original forms for simulating their empirical test case. These two models were found over predicting the bed expansion and the momentum exchange between the gas and the solid phase. However

the modification of the Syamlal-O'Brien drag law based on the minimum fluidization conditions, as a generalized method to decrease the drag, was found to provide modeling predictions in reasonable agreement with the experimental data. Vega et al. [61] used a full 3D TFM-KTGF approach to investigate a cylindrical bed filled with Geldart-B particles and fluidized with air in the bubbling regime comparing numerical results with experimental data obtained from pressure and optical probe measurements in the real bed. The TFM description of bubbles motion (within the solid bed) was found accurate enough to provide a link between the local effect (monitored between two very close points in the bed) of these bubbles and the local pressure drop fluctuations (Figure 2.13). Thus the TFM was considered satisfactory to prove the connection between the spectrum of the local pressure drop fluctuations and the one the solid phase fluctuations.

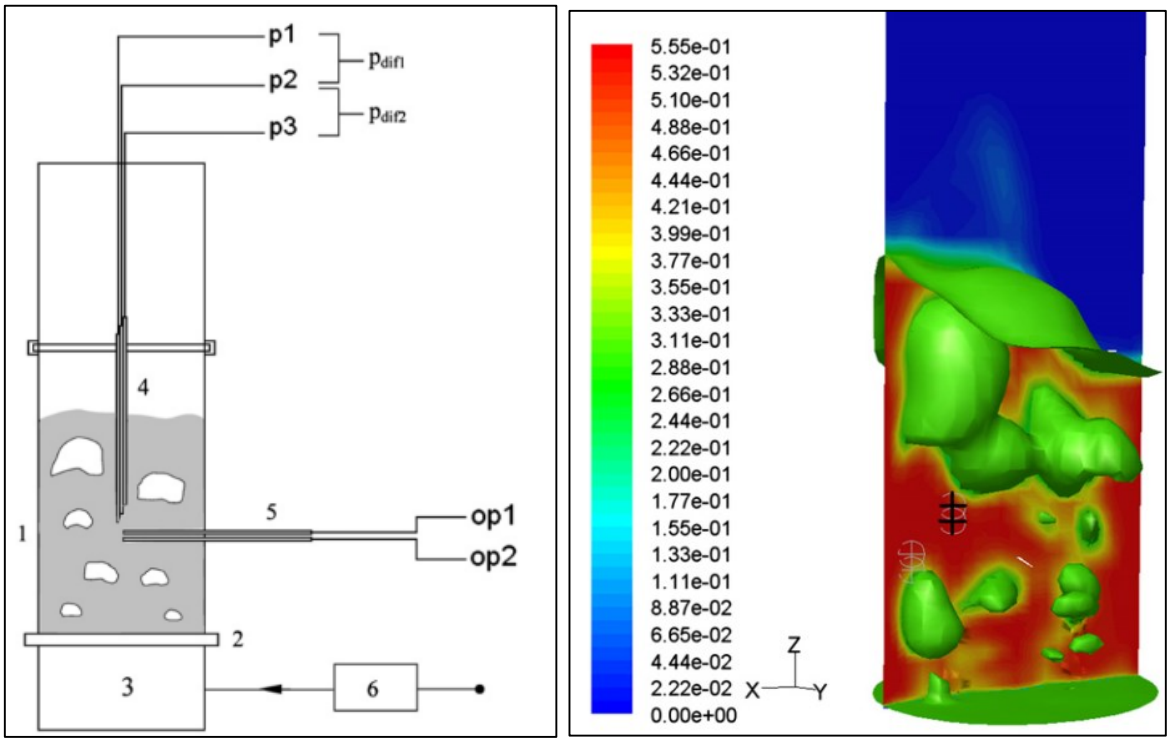

Figure 2.13 Experimental vs 3D-TFM applied to bubbling fluidized bed to investigate the effect of local pressure drop fluctuations induced by local variation of solid load [61]

Esmaili and Mahinpey [62] compared the results of their 3D-TFM to empirical data (testing them over a wide range of superficial velocities), using time-averaged pressure drop at different locations as well as bed expansion ratio. In particular, they highlighted the importance of drag formulations (Figure 2.14) on the correct numerical prediction of these two indicators.

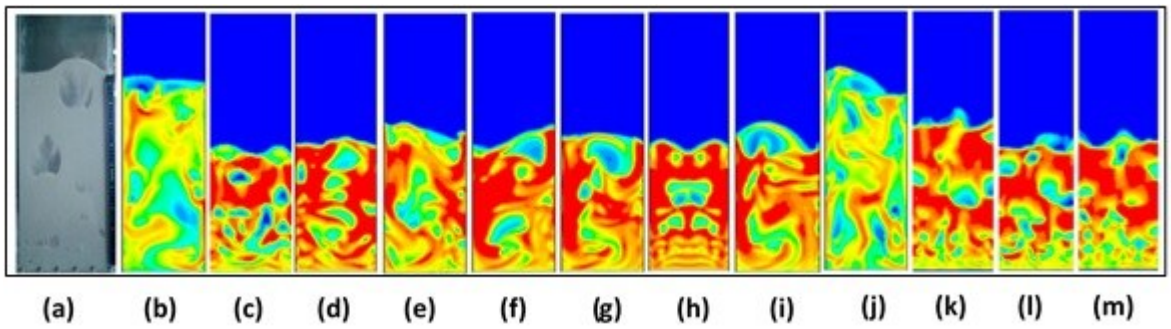

Figure 2.14 –Effect of drag law formulation on bubbling fluidized bed dynamics; from the left to the right the experimental fluidized bed (a) and the CFD simulations obtained using the following drag law formulations : (b) Syamlal–O'Brien adjusted; (c) Syamlal–O'Brien; (d) Arastoopour; (e) Gibilaro; (f) Hill Koch Ladd; (g) Zhang–Reese; (h) Richardson–Zaki; (i) RUC; (j) Di Felice adjusted; (k) Di Felice; (l) Wen–Yu and (m) Gidaspow [62]

Also in this case, the TFM showed a significant sensitivity to the particular choice of drag law and only two formulations were found to provide a good match with the empirical time-averaged pressure drop and bed expansion (pictures b and j in Figure 2.14). Min et al. [63] validated their 2D and 3D TFM-KTGF throughout gas hold-up measurements (using X-ray imaging system) as well as by the time-averaged pressure drop data. They also focused on the effect brought by different formulations of the drag law prediction on the gas holdup variation through the bed height. Jang and Arastoopour [64] used a 3-D TFM-KTGF model to simulate the gas-solid flow patterns both in a small and a large-scale bubbling fluidized beds. The TFM was found to provide very good match with some of the empirical gas-solid hydrodynamics indicators such as mixing, pressure drop, solid void fraction distribution inside the bed, and bed height expansion. The authors concluded that TFM approach could ultimately be considered as a promising tool in the design and scale-up of bubbling fluidized bed systems. Tagliaferri et al. [65] simulated the dynamics of a fluidized bed of a binary solid mixture using TFM-KTGF model, focusing on the role of both the restitution coefficient and the accuracy of different time and spatial discretization methods (used to discretize the governing equations) on the bed dynamics. In their work, the authors found as main result that the TFM approach is greatly impacted by the numerical diffusion induced by the first order spatial discretization schemes, which is ultimately limiting its ability to correctly predict the bubble fraction in the bed and in turn the solid mixing rates.

DDPM-KTGF

When compared to other numerical models (TFM or DPM-DEM), the literature available on the DDPM-KTGF model appears quite limited. Only a few authors have tried to investigate this approach while benchmarking his performance and accuracy against the two aforementioned methods.

Chen and Wang [66] used all three possible approaches to model an impinging gas-solid flows phenomena. In order to test the accuracy and limit of applicability of these models, Chen varied the solid load of jets as well as their velocity and observed the predicted numerical behavior in the impinging zone. In this work, the use of a DDPM-KTGF model allowed correctly predicting the dynamics of solid jets in most of the operating conditions in agreement with the more sophisticated DPM-DEM method. However it failed in predicting the dynamics of two colliding jets, whose solid fraction load of 0.1 was expected to result in a merging phenomenon. In such a circumstance, both the TFM and DEM model correctly predicted the merging of these two jets, while the DDPM-KTGF predicted these two jets crossing each other most likely (as explained by the authors) because of the simplified particle-particle interactions treatments leading to an unreliable overlapping of solid particles. The over-simplified treatment of particles collision and resulting unreliable overlapping were found to be the main drawbacks of this numerical approach.

Major contributions on the exploitation of the DDPM-KTGF approach came from Cloete at al. [67]–[70] who employed this model at different scales and for different applications (always for gas-solid systems). In a first study [70], they compared the TFM and DDPM-KTGF to dilute granular systems to investigate the capability of the 2 models in predicting the evolution of granular temperature, momentum coupling between the two phases and standard deviation of volume fraction field. They found a pretty good agreement between the two models even if the DDPM approach was able to resolve very fine structures and clusters, which were not caught by the TFM (where only wider clusters where predicted). One possible reason, claimed by the authors, was due to the absent numerical diffusion in the DDPM approach. Oppositely, the TFM approach (despite a very fine grid employed) still showed some numerical diffusion causing the time-averaged flow variable to keep changing with any further mesh refinement. In addition, using a dedicated experiment, the authors where able to explain the higher clustering effect predicted by the TFM. The DDPM model was found able to correctly predict the interaction of impinging solid jets while the TFM

always resulted in delta shock (merging effect) each time some solids jets would cross each other's trajectories, resulting in the formation of higher solid density regions (clusters).

Cloete et al. [69] showed the superior capability of DDPM-KTGF model in an industrial-scale fluidized bed application on coarse meshes. This model was able to provide the same structures resolution on a four time coarser mesh size (as compared to the TFM) while allowing 4 times greater time step. This combined effect contributed to a massive simulations speed-up.

Quite similar results were obtained and shown later by the same authors [68], who applied this model to a pseudo-2D fluidized bed. Here the DDPM-KTGF model was found able to reach the same level of structures resolution as the TFM on 8x fewer grid cells (Figure 2.15).

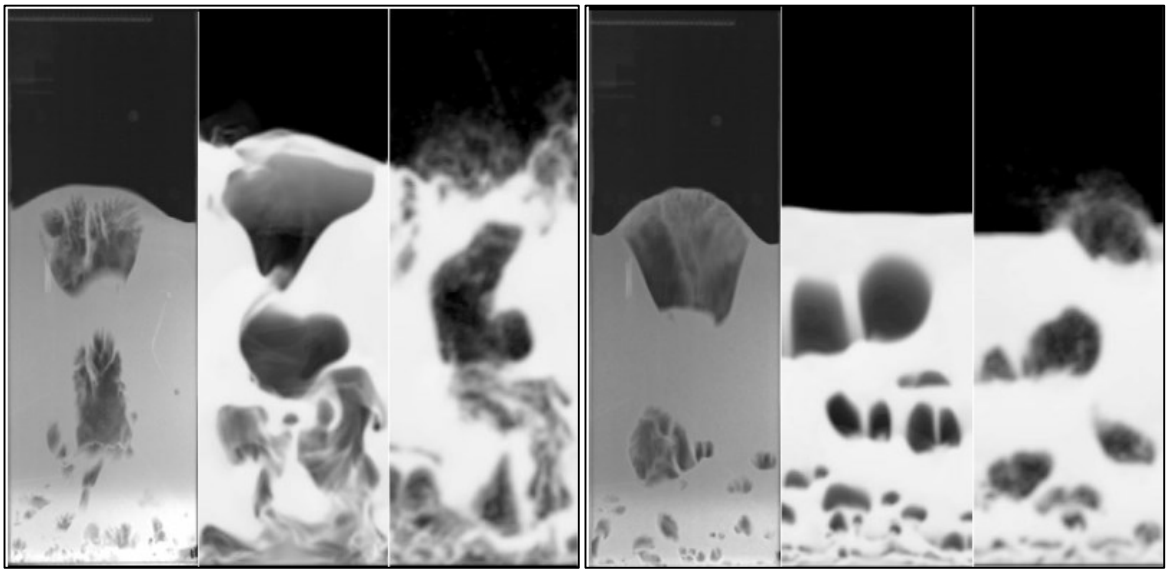

Figure 2.15 - Snapshots of the experiments (left) and volume fraction distribution as predicted by the TFM (centre) and DDPM (right) for 150 µm (first group on the left) and 350 µm particle size (second group on the right) [68]**.**

With this work, Cloete et al. concluded that the DDPM accurately predicts the flow dynamics in bubbling fluidized beds, pointing out how this method can achieve a superior grid independence behavior, ultimately holding great promises for large-scale 3D simulations of bubbling fluidized systems.

Adamczyk et al. [41] also used the DDPM-KTGF approach to model a dense gas-solid flow that was combined with a combustion process in a large-scale industrial CFB boiler whilst comparing its results to TFM predictions (Figure 2.16). Using these two models, the authors

found a similar time-averaged map of solid distribution, which compared fairly well in both cases with empirical data. However the use of DDPM approach was found significantly advantageous to include the particle size distribution (PSD) in their system, which conversely strongly limited the performance of the TFM approach.

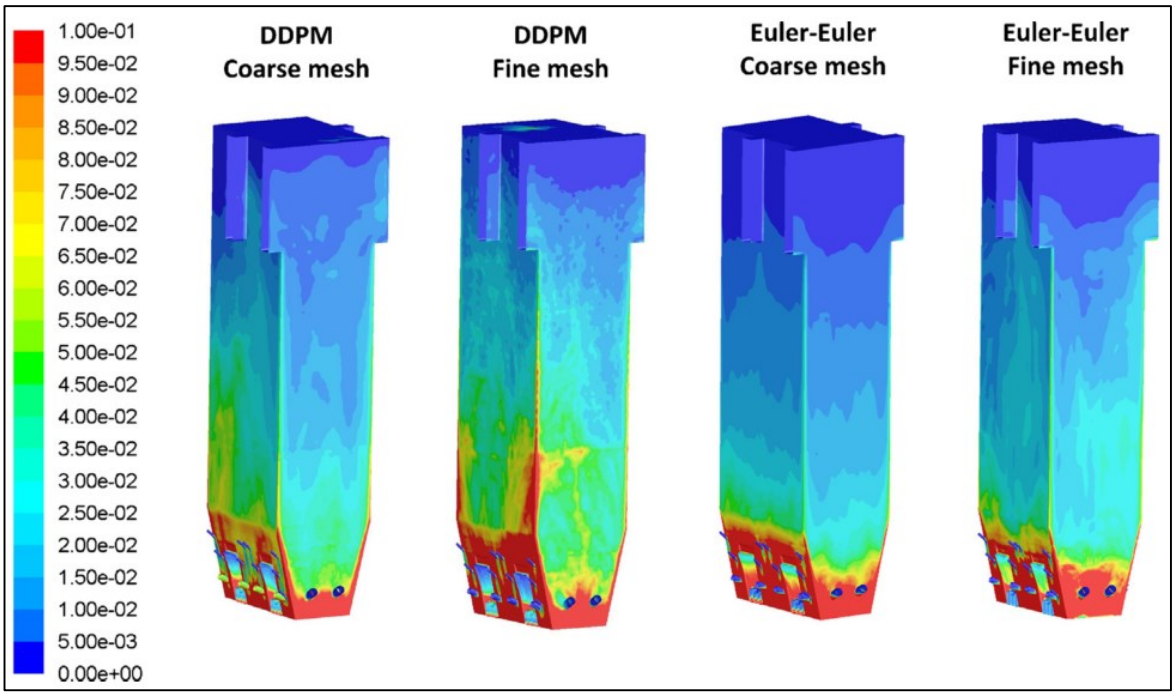

Figure 2.16 – Distribution of solid fraction on external boiler walls using the DDPM and TFM methods for two different mesh size [41]

As it emerges from the literature examples reported in this section, the validation of a CFD model can be very complex since there are several features that can be compared between the real and virtual systems. In many cases, authors focused on the observation of the volume fraction distribution inside the bed, the gas displacement, bubbles shape (etc…). The latter can be achieved using various type of tomography analysis such as virtual imaging reconstruction throughout penetrating x-ray waves. However, such high tech equipment may not always be available, especially at industrial scale. In this work a simpler strategy was employed to validate CFD models (such as pressure drop data) allowing to significantly reduce the costs of the experimental apparatus while using a method which could be easily extended to investigate industrial units.

3. METHODOLOGY

3.1 MODELING APPROACH

In the present work, a methodological procedure was put in place and followed in order to implement numerical tools which could provide an accurate representation of a real bubbling fluidized bed. When modeling a real problem, there are three main steps to follow:

- The choice of the *conceptual model* (following the observation of the experimental problem)
- The *model verification* (convergence of numerical solutions)
- The *model validation*

This approach, explicitly drawn in Figure.3.1, has to be accomplished in all of its steps and in the same order to ensure the robustness of the CFD results. This will affect the CFD ability to reproduce empirical data but also, and most importantly, its reliable predictions of the effect of the change of operating conditions and geometry on the system behaviour.

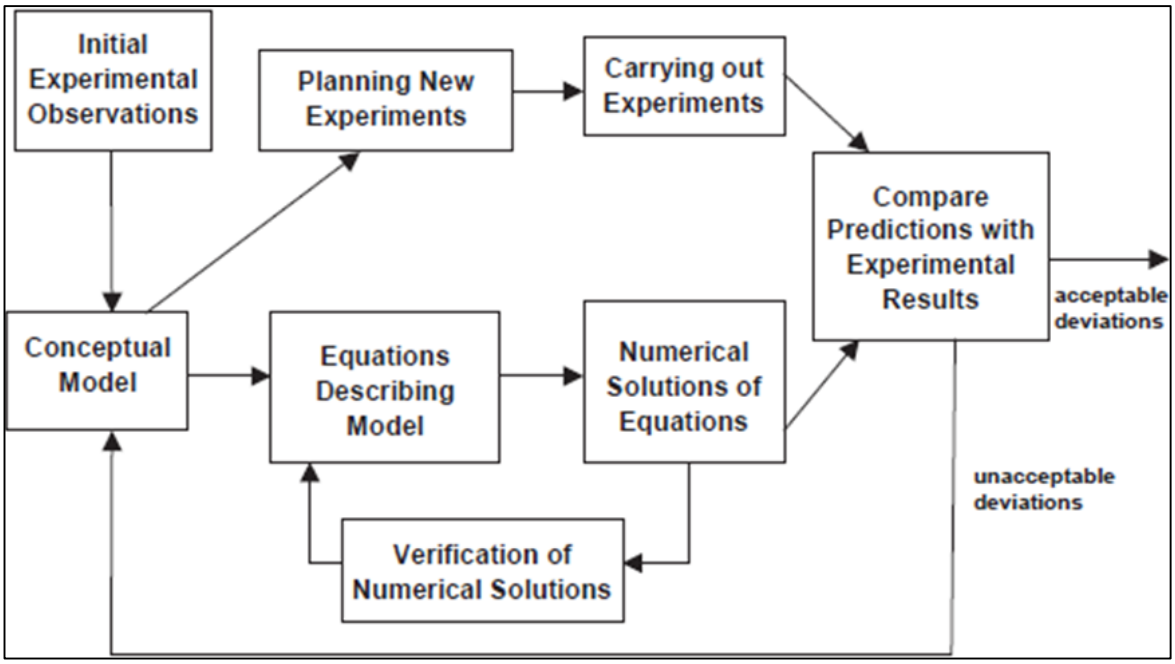

Figure 3.1 - Numerical modeling methodology [71]

The conceptual model is the starting point and represents the translation of the mechanisms (physics) specific of the real problem into mathematical formulation.

Obviously this first step of the modeling framework, requires the prior definition of the empirical problem to investigate and the characterization of its physics. The choice of the conceptual model is a crucial step since a mistake here would lead to a wrong simulated model of the real problem, even in case of a perfect execution of the further stages. Such a situation may occur due to an erroneous definition of the equations used to describe the physical problem. However this contingency is quite rare when using commercial CFD software where all the equations have already been properly selected for the specific type of problem. More likely, some terms might be neglected in the equations or, if not, their formulation may not be accurate to capture the nature of the real phenomena inside the system. Thus, beside the main equations defining the conceptual model, there are also specific terms and functions to be modeled in order to properly catch the physical phenomena involved. Consequently, at this stage, it is important to have a solid understanding of the physical phenomena in order to properly select and solve its governing equations together with all significant terms. As a rule of thumb, discarding terms (representative, inside the equations, of physical mechanisms) whose importance is known to be negligible can reduce the computational demand of the CFD models. However, the correct and accurate modeling of certain mechanisms (drag, friction, collisions etc…) is vital to correctly predict the behaviour of the physical system.

The definition and the importance of the second and third steps of this modeling path (verification and validation) was very effectively described by Grace and Taghipour in their work [71]. After the proper choice and description of the mathematical model (throughout its equations and related terms), the numerical verification stage takes place. This part of modeling is not related to the physics of the real problem under investigation, but rather relates to the study of convergence of numerical solutions as derived from the resolution of governing equations. CFD analysis involves in fact the discretization of these equations over a space-time grid to ultimately obtain a set of non-linear algebraic equations in which the unknown variables can be solved according to a certain space-time accuracy determined by the specific numerical method used. This investigation is aimed to: a) correctly assess the importance of the numerical setup, mostly mesh grid and numerical schemes (temporal and spatial discretization of variables), on the numerical solutions convergence and b) finding a numerical setup such as to ensure this convergence, namely the numerical solution independency from any further accuracy refinement. Consequently, the most significant challenge is to find the coarsest possible mesh size and least accurate discretization scheme

ensuring the convergence of numerical solutions. Finding this limit can significantly benefit the simulation performances once the model is properly set.

The (numerical) solution found at this stage may still be distant from the empirical data measurements. This is easily comprehensible since, at this stage, the choice of physical parameters and/or their proper modeling inside the equations may still not be accurate enough to give the best match with the empirical data.

Moreover, to ensure the reliability of the numerical solution convergence, the most accurate set of discretization schemes should be chosen. This is highly desirable to limit numerical diffusion and thus the change of numerical solution with grid refinement. Even though performing simulation with higher order schemes is translating in longer simulations, this choice can prevent further loss of time which may result from a lower order scheme. In fact switching from first order to second order scheme might change the numerical solution again putting the user in a situation where it is necessary to rethink about the grid refinement process a second time.

As a general approach, in order to speed up this stage, a "base case" set of simulations can be chosen. Practically the values/formulations of all the solid/gas parameters (and operating conditions) are identical while the mesh is refined in order to assess the variation into numerical solution behavior. Figure 3.2 reports an example of grid refinement whose effect reflects a more detailed distribution of solids and bubbles inside the bubbling bed.

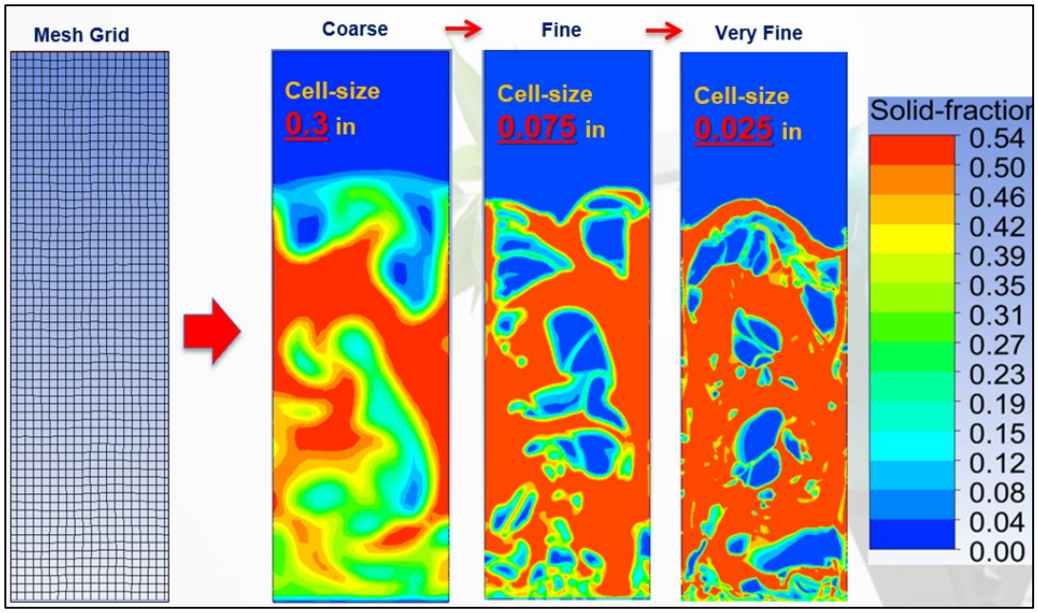

Figure 3.2 - Example of mesh refinement approach: very fine mesh the model allows catching micro structures not visible at coarser level but at very high computational costs

Thus, ideally, one should first decide a “reasonable” set of values (for constant parameters such as restitution coefficient etc.) and proper functions (describing the intrinsic physical properties and behavior of solid phases) and afterwards move forward refining the grid until a convergence trend is achieved. The concept of “reasonable set” is essential at this stage, since numerical instabilities could result from the wrong choice of some of them, causing the entire simulation to crash. This occurrence is quite common in the early stage of model development.

The last stage in numerical modeling procedure is the so called *model validation*. Among the possible definition of validation one widely accepted [72] defines it as “the process of determining the degree to which a model is an accurate representation of the real world from the perspective of the intended uses of the model”. According to this definition, validation involves not a single test but rather a process to be carried out. It also requires an accuracy assessment on both the experimental and modeling sides to define the uncertainties and ultimately the level of confidence in corresponding results. Another implication is that the context in which the model is to be applied has its own relevance and different applications may lead to different requirements to be met in order to claim the model validated. In any case, the validation represents the sum of all prior steps of simulations work and is aimed at showing the intrinsic robustness of the overall model. At this stage the user “challenges” the CFD model, testing its own ability to reproduce experimental data obtained under different operating conditions (such as air velocity, type of inert, bed height for the present study). As remarked by Grace and Taghipour [71] both model predictions and experimental data are needed, preferably covering a broad range of conditions while also using multiple independent and dependent variables for the model validation assessment.

Practically, during model validation, all sensitive parameters undergo a tuning or fitting process in order to minimize the error between the models and empirical data. Whereas the verification can be achieved without physical evidence, validation requires the model predictions to meet the experimental data.

3.2 EXPERIMENTAL: METHODOLOGY APPROACH AND SETUP DESCRIPTION

The experimental observation and measurements represent an essential part in the definition of the first and third steps of the modeling approach previously presented. In fact the conceptual model (first step) is built upon the knowledge of the experimental system and its physics whereas the model validation (third step) arises from comparison between the empirical measurements made on this system and the model predictions.

In order to accurately simulate the real bubbling fluidized system (Figure 3.3, left), that embeds and couples the multiphase fluid dynamics with a set of complex chemical reactions, various simplifications and assumptions were made. The need to simplify both the geometrical and physical aspects was justified both by the computational power requirements and the intrinsic complexity involved. Moreover it can be a good practise to separate the reactive part of the problem from its fluid dynamics side in order to lower down the complexity of parameters fitting. For instance if kinetic parameters are specific of certain type of reactions, their fitting could take place in a different and more simple reactor, rather than fluidized beds, and applied to it in a second moment. After all kinetic and transport phenomena may interfere with each other which would result in a highly complex system to be numerically characterized. Besides, very little literature is available about the application of CFD modeling to full industrial scale hot-model [20]. For these reasons, the very first step was to assemble a down-scale bench reactor of a bubbling bed, which could still be representative of the fluid dynamic behavior of real units. This down-scale bench reactor was assembled to experimentally observe the hydrodynamics of cold bubbling bed, its characterization throughout proper measurements and ultimately for CFD modeling validation. It was decided to discard the reactive part of the model in order to focus only on the cold fluid-dynamic behavior of the bed. The second step was to rely on a simplified air injection system in order to ease the numerical modeling of the gas distributor. This allowed for the implementation and use of a planar-2D model of the bed which conversely would have not been possible using a more complicated feeding geometry (Figure 3.3, left), such as the one used at industrial scale [73]. In this last case, only a 3D model would have been able to correctly represent the injector system architecture and the dynamic of the gas flow at the reactor inlet, resulting in costly simulations in the very early stage of model development. Moreover the idea of simplifying the air distributor in order to study a 2D

problem was justified by the primary need of catching the overall behaviour of the bed, with no need, at first, to have a precise prediction of the fluid dynamics in the proximity of the air injection zone.

Figure 3.3 - From a "hot" industrial unit [74] **to a cold laboratory scale bench**

Further considerations related to the link between the industrial and laboratory scale system

In order to support the first type of simplification (namely studying a cold model as representative of a hot one) and such as to guarantee the validity of future model extension to industrial application, an additional in-depth explanation is required. In fact one while the cold model experiment are carried out at ambient temperature, in real systems, such as industrial gasifiers, temperature can reach values in the order of 600 °. The effect of high temperature on the gas properties can be significant, leading to an increase of viscosity and a decrease of density. Among these two effects, the increase of gas viscosity shows to be the

predominant effect leading to a lower value of the experimental minimum fluidization velocity ($U_{mf)}$. Such a discrepancy would lead to an unacceptable divergence between the cold and the hot model predictions for the system fluid dynamic in a given set of equal operating conditions and material properties. Despite that, one strength of this work lies in the choice of a particular drag law which, as explained in the section 3.3.4, computes a drag coefficient based upon the experimental value of the minimum fluidization velocity. Consequently, despite the important difference between a hot and a cold system linked to temperature, the CFD models here implemented are flexible enough to take into account this change. Another potential difference between the industrial and the laboratory system concerns the choice of inert particles diameter forming the bubbling bed. In this case such a variation would result in a different value of U_{mf}. For the aforementioned reasons (and also in this case) the CFD models implemented here would easily take into account this aspect adapting the drag coefficient based upon a different value of U_{mf}.

Experimental setup description

The experimental setup used in this work (Figure 3.3 on the right) was chosen following the assembling method discussed by Conshohocken [75]. A scheme of this setup and its principle components can be observed in Figure 3.4. The setup comprises of a lab-scale fluidized bed and specific instrumentation measuring and monitoring both the gas flow discharge and the pressure drop along the bed. The reactor body is made of clear PVC, which allows a dynamic visual analysis of the process. The body of this system is a 6" i.d. over a 40" height cylinder. The bottom flange allows stabilization of the base of the PVC cylinder wall while embedding the porous gas distributor plate. This latter is stainless 316L-made and presents a micro-porosity of 1.3 μm such as to ensure an optimal homogenization of the gas prior to the reactor inlet. The choice of such a distributor typology is dual, first contributing to generate small bubbles all over the cross section while ultimately helping avoiding some experimental drawbacks like dead spaces and the back-sitting of solids. Secondly, as previously explained, it allows for an easier numerical schematization of the inlet boundary condition that can be accounted easily into a 2D geometry. Moreover the very fine porosity is such to guarantee a local pressure drop (induced by its own intrinsic porosity) comparable to the one along the bed in the fluidization regime. Despite being highly conservative, this precaution is always considered when designing a proper gas distributor

in order to avoid a potential and persistent gas channeling inside the bed induced by a too low pressure drop. A filter is placed on top of the upper flange to prevent solid particles from being entrained out of the bed during fluidization regime and, right next to it, a relief valve allowing to avoid any dangerous overpressures. For the tests, the reactor was operated under ambient conditions. The key device, for validation purposes, was a differential pressure gauge (Kistler 4264A), capable of recording up to 1000 pressure-drop data per second. These were then transferred to a Labview acquisition system for data saving and real time pressure drop monitoring. The pressure drop was measured between two points at the extremities of the cylinder's body. The bottom probe was positioned at 2.5 inches over the porous plate and the upper one was at the proximity of the top flange. Two small meshed screens were put inside the two pipes of the differential pressure gauge to avoid particles entrainment and therefore potential damages to the instrument. Two flow meters were included in the setup, one manual (rotameter) potentially available to measure high air flows, and the other was an electronic unit operating in the range 0-300 SLPM. Experiments were performed at 22 °C (room temperature) and 1 atm, conditions that remained constant during the tests. Finally a small light bulb was located in the upper interior section of the reactor flange, lighting up the bed surface hence allowing to take better quality pictures and videos.

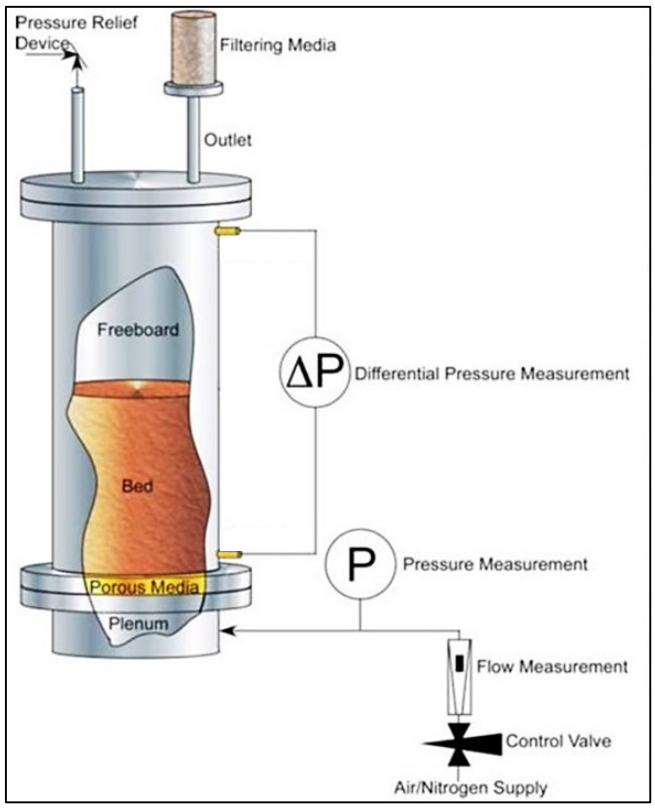

Figure 3.4 - Schematic drawing of the experimental setup used in this work [75]

The bed material used for this study is an alumina powder (190 µm Sauter diameter) belonging to the Geldart Group B (Figure 2.5). Alumina was selected since it is a material often used in industrial-scale gasifiers (where this inert represents by far the major part of the total solid bed mass). The particular size allowed covering a good range of hydrodynamic conditions (from fixed bed to vigorous bubbling condition) since the minimum fluidization velocity is strongly linked to the diameter of solid particle. By doing so, the system could be operated without the need for a manual flow-meter, whose reading accuracy, could be considerably lower than the electronic unit.

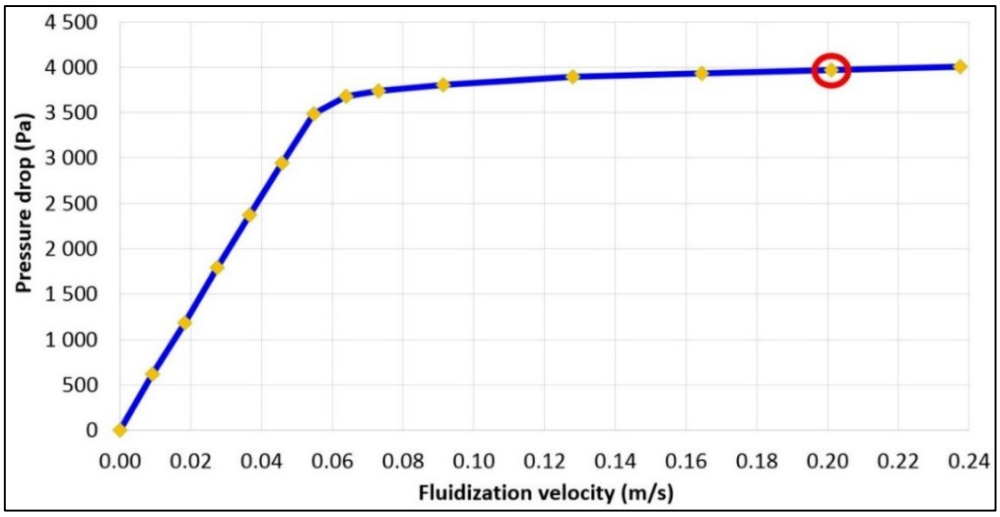

Figure 3.5 Experimental fluidization curve (Uo=0.2 m/s) where the red circle shows the value of superficial velocity (equal to 0.2 m/s namely around 3.5 times the minim fluidization velocity) used for the bubbling regime study

The bench reactor was filled with alumina up to a bed height of approximately 260 mm, corresponding to a total mass of approximately 9.5 kg. Figure 3.5 shows the experimental fluidization curve where the time-averaged values of pressure drop is plotted with regards to the superficial gas velocity. These values were calculated as a ratio between the flow discharge (measured by the electronic flow meter) and the cross sectional area of the cylinder. All the velocity values below the minimum fluidization one were exploited for the CFD validation (of TFM) in the fixed regime, whereas only the one circled in red (corresponding to 240 SLPM and 3.5 times the minimum fluidization velocity) was used for validating the CFD models in the "bubbling" regime. This value was selected in order to guarantee a vigorous fluidization regime while respecting a margin of accuracy for the electronic air flow reading.

3.3 CFD MODELS

In Chapter 2, an overall description of numerical CFD models and their application to similar studies (as found in open literature) is provided. Their main features, relative advantages and limitations as well as some glimpses on their progressive development are also discussed. Here both the upstream numerical setup and the model equations are presented, highlighting the importance of various terms involved and their possible formulations.

3.3.1 Domain design, mesh generation and numerical setup

The very first step in the implementation of a CFD model is the design of the numerical geometry representing the physical domain under investigation. In this study the model design is not a complex task because of the intrinsic geometrical simplicity of the experimental bench reactor to model. Consequently, using the design modeller of Fluent, a rectangular (for 2D planar simulations) or cylindrical (for 3D simulations) geometry was created based upon the dimensions of the real system. The only difference in this sense came

the domain together with the definition of the boundary condition (B.C) types. To this regard, a velocity inlet of 0.2 m/s was set on the bottom of the domain (namely equal to 3.5 times the U_{mf} of the system), a pressure outlet was selected as B.C on the top of the system (ambient pressure) and walls (including a no slip conditions for both phases) completed the boundaries of the numerical domain (Figure 3.6).

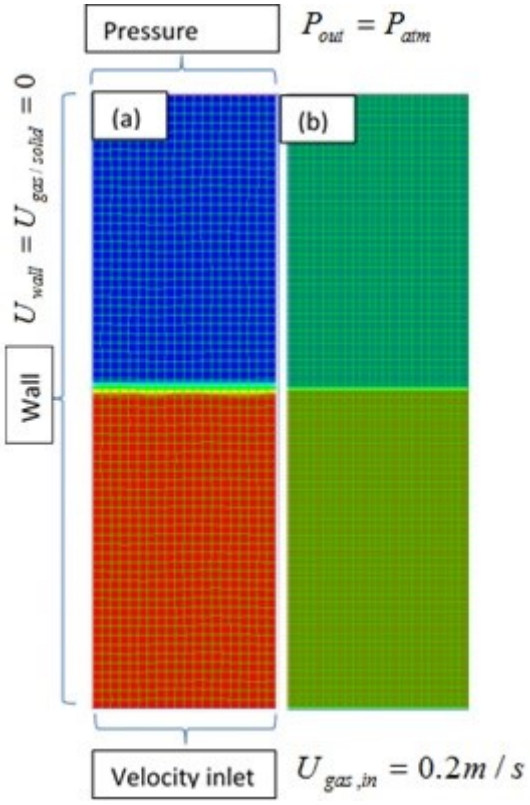

Figure 3.6 – Example of the numerical setup in the TFM approach showing the boundary conditions, the initial condition (solid patch in red) and the mesh size discretization, coarse (a) and fine (b)

Once that model geometry and mesh have been created the next step requires the definition of the type of multiphase approach to use. For the reasons explained in the previous chapter, here both the Eulerian-Eulerian (TFM) and Eulerian-Lagrangian (DPM-KTGF) models were considered. More details about the equations used for these two different type of multiphase approaches can be found in the following sections. The choice of a specific type of model comes along with the definition of a proper set of parameters, which identifies major functions used in the description of granular flows. The choice of these functions and parameters has been summed up in specific tables included in the two models-dedicated papers. To be consistent a set of operating conditions is to be set accordingly to the experimental ones (setup description in Chapter 3.2). The initialization of simulations required the definition of initial conditions (I.C) for both phases, together with the patch of the solid phase or the particles injection accordingly to the type of model used and in any case consistently with the empirical height and porosity of the bed at rest. Finally the numerical settings was defined, which requires the definition of solution methods and

controls to discretize and solve the governing system equations. The solution method was defined using a Phase Coupled SIMPLE scheme along with second order accurate schemes for both spatial and time discretization to enforce and ensure the validity of the model verification (as explained previously). The solution controls involved the definition of the so called "relaxation factors" which affect the stability and convergence speed of numerical solutions. In this work, default values were used for these factors.

3.3.2 Eulerian-Eulerian Two Fluid Model (TFM)

The model considers both the gas and the solid phase as two inter-penetrating fluids for which conservation equations are derived. However these equations require a proper closure, which can be provided by the constitutive/rheological laws. The latter are obtained from the application of the kinetic theory of granular flows (KTGF).

The general form of the TFM equations are the following:

Conservation of mass

$$\frac{\partial}{\partial t}\alpha_g \rho_g + \nabla \cdot \alpha_g \rho_g \vec{u}_g = 0 \tag{3.1}$$

$$\frac{\partial}{\partial t}\alpha_s \rho_s + \nabla \cdot \alpha_s \rho_s \vec{u}_s = 0 \tag{3.2}$$

The first term (in both the equations 3.1 and 3.2) represents the mass time derivative while the second term is the mass convection term. α_s and α_g represent the solid and gas volume fraction, respectively, and ρ_s and ρ_g their densities while $\vec{u}_s$ and $\vec{u}_g$ their cell-averaged velocities.

Conservation of Momentum

$$\frac{\partial}{\partial t}\alpha_g \rho_g \vec{u}_g + \nabla \cdot (\alpha_g \rho_g \vec{u}_g \vec{u}_g) = -\alpha_g \nabla P + \nabla \cdot \alpha_g \bar{\bar{\tau}}_g + \alpha_g \rho_g \vec{g} + K_{gs}(\vec{u}_s - \vec{u}_g) \tag{3.3}$$

$$\frac{\partial}{\partial t}\alpha_s \rho_s \vec{u}_s + \nabla \cdot (\alpha_s \rho_s \vec{u}_s \vec{u}_s) = -\alpha_s \nabla P - \nabla P_s + \nabla \cdot \alpha_s \bar{\bar{\tau}}_s + \alpha_s \rho_s \vec{g} + K_{gs}(\vec{u}_g - \vec{u}_s) \tag{3.4}$$

The first two terms (in both 3.3 and 3.4) of the left hand side (LHS) are the momentum time derivative and convection term respectively. The first term of the right hand side (RHS) is the pressure gradient (the equation 3.4 includes also the solid pressure gradient as specific term of solid phase). The second term on the RHS is the gradient of the stress tensor, the third term (on the RHS) accounts for the gravity effect while the last term is related to the momentum exchange due to the fluid-solid drag effects.

The formulation for the phase stress-strain tensors are:

$$\bar{\bar{\tau}}_g = \mu_g(\nabla\vec{u}_g + (\nabla\vec{u}_g)^T) + (\lambda_g - \frac{2}{3}\mu_g)\nabla\cdot\vec{u}_g \cdot I \tag{3.5}$$

$$\bar{\bar{\tau}}_s = \mu_{s,tot}(\nabla\vec{u}_s + (\nabla\vec{u}_s)^T) + (\lambda_s - \frac{2}{3}\mu_s)\nabla\cdot\vec{u}_s \cdot I \tag{3.6}$$

Where λs and λg are respectively the solid and gas bulk viscosities.

The stress tensor formulation for the solid phase is formally identical to the one used for the gas due the conceptual mathematical treatment of various phases in the TFM approach. However, an important difference comes from the viscosity coefficient, which for the solid phase is not constant but embeds the combination of three variable components according to the use of the KTGF [38], [40] to granular phase modeling:

$$\mu_{s,tot} = \mu_{s,col} + \mu_{s,kin} + \mu_{s,frict} \tag{3.7}$$

The latter are described below and are correspondingly the collisional [59], kinetic [76] and frictional [77] components of the total sheer stress. The relating importance of each of these viscosity components is directly linked to the specific dynamics of the bed in the different regions of the domain (Figure 3.7).

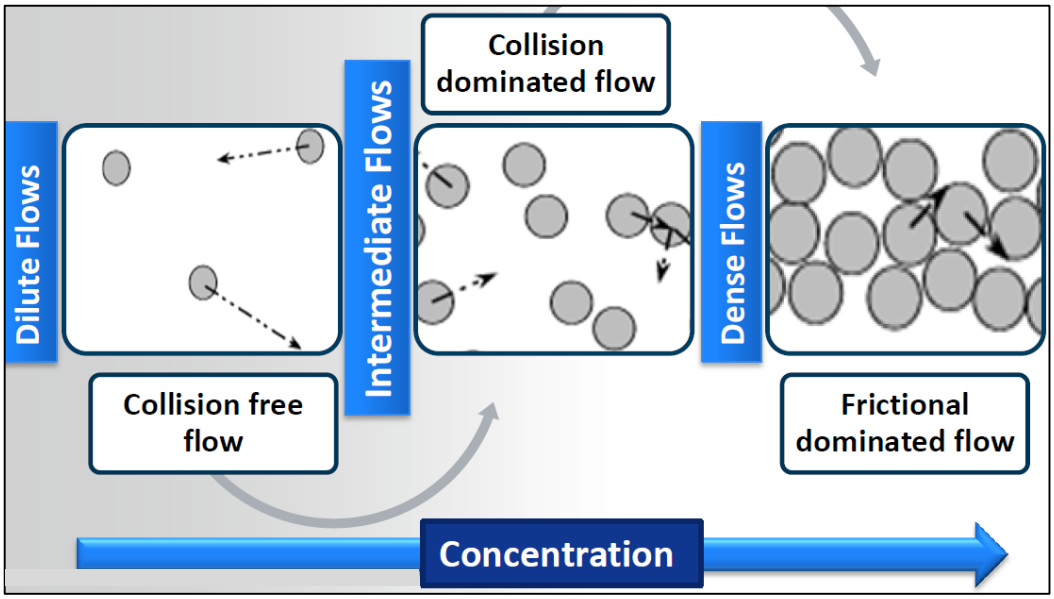

Figure 3.7- Different regime which may occur during in a multiphase granular system during bubbling fluidization [78]

Where collisions are more likely to occur, such as in the surface proximity where bubbles explode, the collisional term is more significant whereas in the denser regions (for example along the walls) where the frictional term tends to be predominant. In this last situation, for example, the solid phase approaches its own packing limit and the generation of stress is mainly due to the friction between particles while collisional stress tends to zero. In any case the relative importance of these shear stress components is linked to the aforementioned granular flow parameters, which vary inside the bed according to the particular local solid distribution.

$$\mu_{s,col} = \frac{4}{5}\rho_s d_s g_{o,ss}(1+e_{ss})\left(\frac{\Theta_s}{\pi}\right)^{1/2}\alpha_s{}^2 \tag{3.8}$$

$$\mu_{s,kin} = \frac{10\rho_s d_s\sqrt{\Theta_s\pi}}{96(1+e_{ss})g_{o,ss}}\left[1+\frac{4}{5}g_{o,ss}\alpha_s(1+e_{ss})\right]^2 \tag{3.9}$$

$$\mu_{s,frict} = \frac{P_{frict}\sin\beta}{2\sqrt{I_{2D}}} \tag{3.10}$$

Where P_{frict} is the frictional component of the solid pressure [79], Θ_s (m^2s^{-2}) represents the granular temperature of the solid system, $g_{o,ss}$ the radial distribution function [80], $d_s(m)$ the mean solid particle diameter, and e_{ss} the restitution coefficient expressing the ratio between the particle speed after and before collisions.

The mathematical description of these granular flow variables, is given by the following expressions:

$$\Theta_s = \frac{1}{3}\left\langle \vec{u}_s{}' \cdot \vec{u}_s{}' \right\rangle \tag{3.11}$$

$$g_{o,ss} = \left[1 - \left(\frac{\alpha_s}{\alpha_{s,\max}}\right)^{1/3}\right]^{-1} + \frac{1}{2}\alpha_s \tag{3.12}$$

$$\lambda_s = \frac{4}{3}\rho_s d_s g_s (1+e_{ss})\left(\frac{\Theta_s}{\pi}\right)^{1/2} \alpha_s{}^2 \tag{3.13}$$

$$P_{frict} = Fr\frac{(\alpha_s - \alpha_{s,\min})^2}{(\alpha_s - \alpha_{s,\max})^5} \tag{3.14}$$

$$P_s = \alpha_s \rho_s \Theta_s + 2\rho_s (1+e_{ss})\alpha_s{}^2 g_{o,ss}\Theta_s + P_{frict} \tag{3.15}$$

Where P_s is the granular pressure derived from the kinetic theory of granular flow [81], λ_s is the solid bulk viscosity [81] accounting for the resistance of the granular flow to compression and expansion. Equation 3.15 (similarly to equation 3.7) also accounts for three different components related to the kinetic, collision and friction effects of the solid phase respectively. This parameter is specific of the momentum conservation equation for the solid phase and its gradient (equation 3.4) works as a closure in the definition of the solid interaction forces. Equation 3.12 modifies the probability of collisions between grains when the solid granular phase becomes dense. Equation 3.11 defines the theoretical concept of granular temperature, in analogy to molecular gas system, as a quantity which varies proportionally to the fluctuations of solid particle velocity. This variable is in general found as a solution of the following (simplified) conservation equation:

$$\frac{3}{2}\frac{\partial}{\partial t}(\alpha_s \rho_s \Theta_s) = (-p_s I + \bar{\bar{\tau}}_s) : \nabla \vec{u}_s - \gamma_{\Theta_s} + \Phi_{gs} \tag{3.16}$$

The equation here presented was obtained by neglecting both the convection and diffusion terms. This assumption is fair considering that in dense bubbling bed, the local generation and dissipation are predominant as compared to convection and diffusion and granular temperature is varying mainly as a result of friction and inelastic collisions [68]. The first term on RHS represents the energy generation due to the solid shear stress, the second term

on the RHS is the collisional dissipation of energy while the last term on the RHS represents the transfer of kinetic energy between the particles and the fluid phase. More details about mathematical formulation of each of these terms can be found in [40].

3.3.3 DDPM-KTGF

The mass and momentum conservation equations for the gas phase are identical to the one previously described in the TFM approach (equation 3.1 and 3.3). Also, all the granular parameters and their formulations (equations 3.8 - 3.16) are identical in the DDPM-KTGF method. The main difference in this second approach (but the same consideration stays for any other DPM models) is the description of the solid particles, no longer described as a fluid but rather tracked as spheres (see Fig. 3.8) within the fluid domain. The description of particles trajectories is possible by solving a force balance equation (Newton's equation) which accounts for fluid-solid drag, gravity force and particle-particle collisional forces.

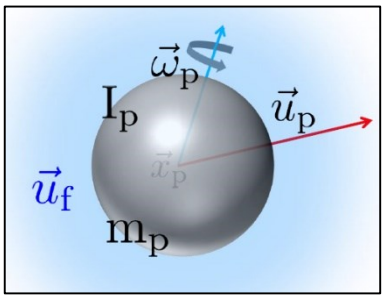

Figure 3.8 - Single particle surrounded by a fluid [104]

Since the time to perform simulations is linked to the size of the numerical problem to solve, and this latter is made up of the total number of equations to solve, a numerical artifice was used in order to reduce the size of this problem. In fact, despite the lab-scale size of the empirical system, the total number of particles constituting the bed was estimated in the region of 600 million. Since in the Lagrangian DPM each particle motion is associated with an equation to solve, the size of the numerical problem would be prohibitive to be dealt with.

At this purpose the "parcels" concept was used allowing regrouping many single particles in one sphere (see Figure 3.9), which is tracked inside the system as if it was a point with a mass equal to the total mass of all the particles contained inside.

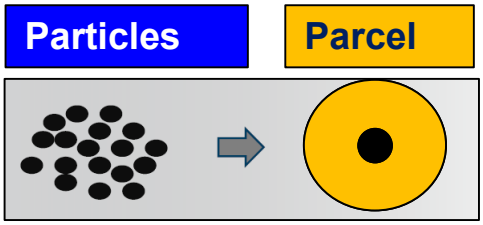

Figure 3.9 - From single particles to "parcels" system [78]

This simplification was used inside the CFD model to reduce the size of the numerical system to be solved. In order to introduce this simplification a proper Matlab code was implemented to generate an injection of a certain amount of parcels in the interior of the numerical domain. Thanks to this code, the number of parcels targeted was controlled by changing their size and consequently, the number of particles per parcel as explained in the following.

Particles (parcels) motion and collisional model

The DDPM-KTGF approach allows describing the single particle motion by solving the following Newton's equation:

$$\frac{d}{dt}\vec{u}_p = \frac{K_{gp}(\vec{u}_g - \vec{u}_p)}{\rho_p} - \frac{g(\rho_p - \rho_g)}{\rho_p} + \frac{\nabla \bar{\bar{\tau}}_s}{\alpha_s \rho_p} - \frac{\nabla P_s}{\alpha_s \rho_p} \tag{3.17}$$

Where α_s is the volume fraction of the solid phase calculated from the particles concentration volume within each cell and $\vec{u}_p$ (m/s) is the particle velocity.

In the CFD model here implemented, because of the aforementioned reasons, the equation 3.17 is not used to track a single particle but rather applied to the parcel level (see Figure 3.9) throughout a scaling factor. This latter accounts for the number of particles per parcel as shown below:

$$\frac{N_{particles}}{parcel} = \frac{M_{parcel}}{M_{particle}} = \frac{4/3\pi R^3 \rho_s}{4/3\pi r^3 \rho_s} = \left(\frac{R}{r}\right)^3 \tag{3.18}$$

The number resulting from this ratio (equation 3.18) ensures the respect of two important aspects. Firstly it prevents the risk of having any empty spaces inside parcels (whose space is totally occupied by particles) which otherwise would lead to an overestimation of the simulated bed height at rest. Secondly, this coefficient allows for a perfect scale up of the

gas-solid drag force (from the particle scale to the parcel scale) and consequently a reliable dynamic behaviour of the parcels system, which in spite of their mass are fluidized equally to single particles.

According to the KTGF approach the parcel repulsive forces (due to collisions) are modeled throughout the last two terms of eq. (3.17). These two terms represent the solid shear stress tensor and the solid pressure (respectively) whose mathematical formulation can be found in equations 3.6 and 3.15. So collisions are not accurately solved, based upon the mechanical properties of particles (as accounted by other Lagrangian methods such as the DEM approach), but are rather borrowed from terms computed onto Eulerian frame. This procedure makes of the DDPM-KTGF a hybrid approach to solid particles modeling.

3.3.4 Drag law formulations

The last term on the RHS of both the equations 3.3 and 3.4 and the first on the RHS of the equation 3.17, represent the drag force causing the interphase momentum exchange between the gas and solid phases. This term is one of the predominant ones (especially in cold systems) because it represents the only fluid mechanic link between phases (considering the absence of any thermochemical reactions) and consequently, its formulation can significantly affect the CFD outputs [62] .

In general, the interphase momentum coefficient K_{gs}, can be derived from two different types of empirical data. For high values of the solid fraction, this coefficient can be estimated from the Ergun drag model for pressure drop in packed beds [82]. However, this type of correlation necessitate to be extended using other drag formulations, such as the Gidaspow drag law [47,79], to account for low values of solid fraction, which may occur inside the bubbling fluidized bed. Alternatively, the terminal velocity of particles in fluidized or settling beds can be estimated and used to derive a formulation for the drag coefficient depending on the void fraction and Reynolds number. An example of this last category is the Richardons and Zaki model [84].

Among the possible choices suitable for dense particle systems, the Gidaspow and the parametric Syamlal O'Brien drag laws have been investigated as representative of these two different classes of empirical data used for drag law derivation. While only the latter was

used in the TFM study, both of them have been employed and compared in the DDPM-KTGF model.

The Gidaspow model [59] is a combination of the Ergun equation [82] and the Wen and Yu model [85] accounting for different solid concentrations. Specifically:

When $\alpha_g > 0.8$, the fluid-solid exchange coefficient K_{gs} is derived from the Wen and Yu model expressed as follows:

$$K_{gs} = \frac{3}{4} C_D \frac{\alpha_s \alpha_g \rho_g \left|\vec{u}_s - \vec{u}_g\right|}{d_s} \alpha_g^{-2.65} \tag{3.19}$$

Where

$$C_D = \frac{24}{\mathrm{Re}_s \alpha_g} \left[1 + 0.15(\mathrm{Re}_s \alpha_g)^{0.687}\right] \tag{3.20}$$

When $\alpha_g \leq 0.8$ the fluid-solid exchange coefficient K_{gs} is derived from the Ergun equation taking the following form:

$$K_{gs} = 150 \frac{\alpha_s (1-\alpha_g)\mu_g}{\alpha_g d_s^2} + 1.75 \frac{\rho_g \alpha_s \left|\vec{u}_s - \vec{u}_g\right|}{d_s} \tag{3.21}$$

The drag force depends in general on the local relative velocity between phases and the void fraction but also on some other factors such as the particle size, particle shape, etc. The particle void fraction is however very difficult to determine other than in a packed bed or infinite dilution (single particle). Other factors such as particle shape, clustering and particle size distribution can also affect the local drag force but they have never been considered in deriving drag correlations [86]. Syamlal and O'Brien [60] derived a formula for the fluid-solids drag coefficient for multiparticle system using a Richardson-Zaki type velocity-voidage correlation [84]. Based on the terminal velocity of particles in fluidized or settling beds, the authors proposed the following drag correlation:

$$K_{gs} = \frac{3}{4} \frac{C_D}{v_{r,s}^2} \frac{\rho_g \left|\vec{u}_s - \vec{u}_g\right|}{d_s} \alpha_g \alpha_s \tag{3.22}$$

Where

$$C_D = \left(0.63 + \frac{4.8}{\sqrt{\mathrm{Re}_s / v_{r,s}}} \right)^2 \tag{3.23}$$

$$\mathrm{Re}_s = \frac{\rho_g d_s \left| \vec{u}_s - \vec{u}_g \right|}{\mu_g} \tag{3.24}$$

$$v_{r,s} = 0.5 \left[A - 0.06\,\mathrm{Re} + \sqrt{0.0036\,\mathrm{Re}^2 + 0.12\,\mathrm{Re}(2B - A) + A^2} \right] \tag{3.25}$$

With

$$A = \alpha_g^{4.14} \tag{3.26}$$

$$B = \begin{cases} \alpha_g^{C_1} & \text{if } \alpha_g \geq 0.85 \\ C_2 \alpha_g^{1.28} & \text{if } \alpha_g < 0.85 \\ C_1 = 2.65 \text{ and } C_2 = 0.8 \end{cases} \tag{3.27}$$

However, the Syamlal O'Brien drag model presented above (with constant coefficients C_1 and C_2) can result in the under/over prediction of the minimum fluidization velocity and consequently in a too high/low bed expansion [40]. In order to cope with this drawback, a parametric version of the Syamlal O'Brien drag model was used. This parametric drag model exploits the minimum fluidization velocity and void fraction (on the fluidization onset) as a calibration point to adjust the drag force. In order to compute an accurate estimation of the inter-phase momentum exchange coefficient, these two parameters should be experimentally measured and provided to the drag model inner algorithm, which performs an iteration process to minimize the following objective function:

$$\left\{ U_{mf}^{\mathrm{exp}eriment} - \mathrm{Re}_t \frac{\alpha_g \mu_g}{d_s \rho_g} \right\}^{Min} \rightarrow 0 \tag{3.28}$$

Where

$$\mathrm{Re}_t = v_{r,s}\,\mathrm{Re}_{ts} \tag{3.29}$$

$$v_{r,s} = \frac{A + 0.06B\,\mathrm{Re}_{ts}}{1 + 0.06\,\mathrm{Re}_{ts}} \tag{3.30}$$

$$\mathrm{Re}_{ts} = \left(\frac{\sqrt{4.8^2 + 2.52\sqrt{4Ar/3}} - 4.8}{1.26} \right)^2 \tag{3.31}$$

$$Ar = \frac{(\rho_s - \rho_g) d_s^3 \rho_g \vec{g}}{\mu_g^2} \tag{3.32}$$

With

$$A = \alpha_g^{4.14} \tag{3.33}$$

$$B = \begin{cases} \alpha_g^{d_1} & \text{if } \alpha_g \geq 0.85 \\ C_2 \alpha_g^{1.28} & \text{if } \alpha_g < 0.85 \\ d_1 = 1.28 + \dfrac{\log(C_2)}{\log(0.85)} \end{cases} \tag{3.34}$$

$$C_D(\mathrm{Re}, \alpha_g) = \left(0.63 + \frac{4.8}{\sqrt{\mathrm{Re}/v_{r,s}}} \right)^2 \tag{3.35}$$

Where Re_t represents the Reynolds number of a multi-particle system at the fluidization onset (minimum fluidization velocity or settling condition), Re_{ts} is the corresponding number for one single particle, *Ar* the Archimedes number, $C_D(\mathrm{Re},\alpha_g)$ an analytical expression for the multi-particle drag coefficient and v_r is the terminal velocity for the solid phase as derived by the velocity-void correlation proposed by Garside and Al-Dibouni [87].

According to an algorithm, the parameter C_2 (and consequently d_1) is changed until the objective function (objective function 3.28) is minimized. Hence a new set of two parameters is obtained, which gives a more accurate estimation of the drag coefficient for any dynamic condition inside the bed (Re and α_g) as by the equation 3.35.

Further considerations related to the choice of the DDPM-KTGF model

Besides the application of the KTGF theory to account for particle collisions, another class of Eulerian-Lagrangian methods exists and classified based upon the mechanism of particle-particle interactions. According to the specific mechanism of particle-particle interaction, a granular system can be simulated either as "hard-spheres" or "soft-spheres". The latter, originally developed by Cundall and Strack [88], represented the first granular simulation technique published in open literature [28] and encountered a growing interest as far as the development of models to study gas-solid systems is concerned. This method allows computing the contact forces between colliding particles as a function of their local mechanical deformability and according to specific types of contact force scheme. However this detailed description of particle interactions comes with at least two major drawbacks: a) the DEM model requires the definition and tuning of several parameters involved in the definition of the contact force scheme (which are mostly unknown and hardly assessable a priori); b) the DEM approach is well-known to be very computationally expensive since the particles tracking time needs to be considerably lower than the particle collisional time. So for instance, the higher is the particle stiffness (whose values can be very high especially when the solid phase is represented by alumina powders like in this study), the smaller the particle collisional time must be, which is ultimately constraining the particle tracking time within the solver. Time requirement, for simulations to perform, is a very important aspect to consider when selecting a model to be implemented and tuned. Often, the high number of model parameters to investigate results in a corresponding high number of simulations to perform ultimately leading to massive time requirement for the model development.

For the aforementioned reasons it was decided to first explore the Lagrangian DDPM-KTGF model to assess its accuracy, sensitivity and performance and to compare them to results obtained with the TFM. Nevertheless the possibility of using a "soft-sphere" model was not discarded and some numerical work, based on this type of approach, has been already carried out although they will not be presented in this work. However much more work is required to calibrate and validate the DEM model so that its use to investigate the bubbling bed and its granular properties will most likely come as a future extension of this project.

3.4 DATA PROCESSING FOR MODEL VALIDATION

A proper procedure was developed in order to process both the empirical and numerical data (Figure 3.10), aiming to achieve a convenient mathematical representation of the bubbling dynamic behaviour.

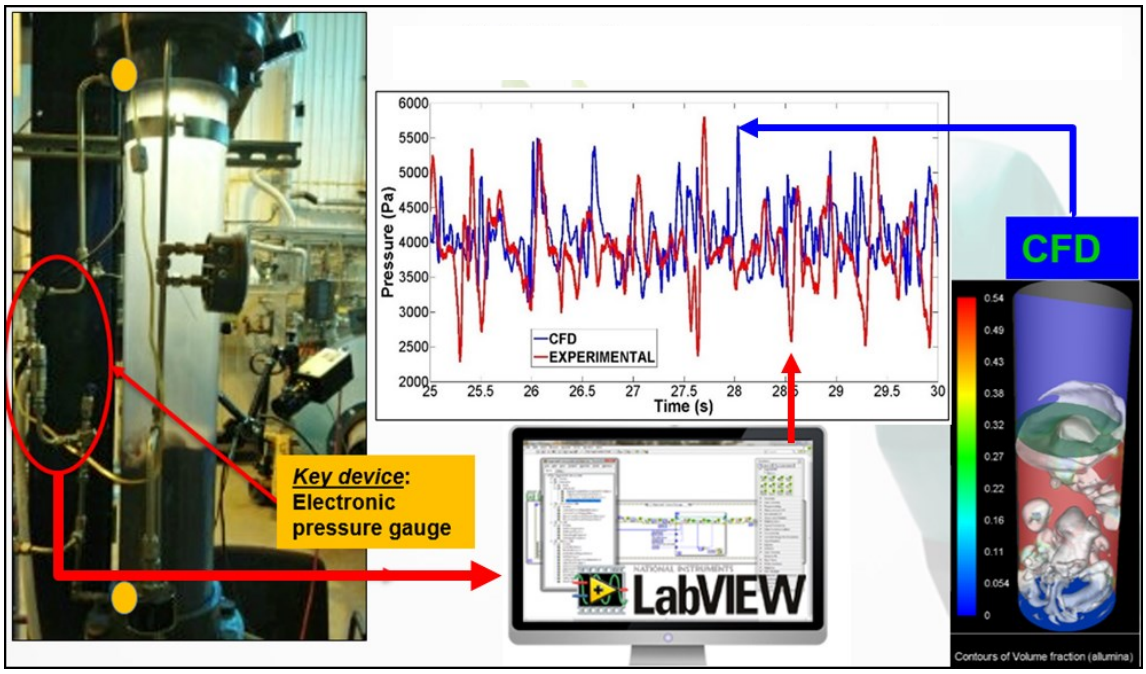

Figure 3.10 - Overall view on the experimental-CFD modeling process: on the left the empirical setup comprising of the cold bench, electronic differential pressure gauge and camera for video recording; on the right the comparison of pressure drop data coming from the empirical bench and the CFD modeling of it.

In order to understand the choice regarding the type of data and the corresponding analysis used this work, the following aspects were considered. Both the time-averaged pressure drop and the (continuous) time-pressure drop signal cannot fully and univocally characterize the dynamic behaviours of a bubbling multiphase system. Particularly important is this last aspect, which results in the impossibility to reproduce an identical time-pressure drop output under the same input conditions. From the empirical stand point this would strongly limit the chance to univocally characterize the fluid-dynamic behavior of the bed to ultimately obtain a representative set of empirical data for model validation.

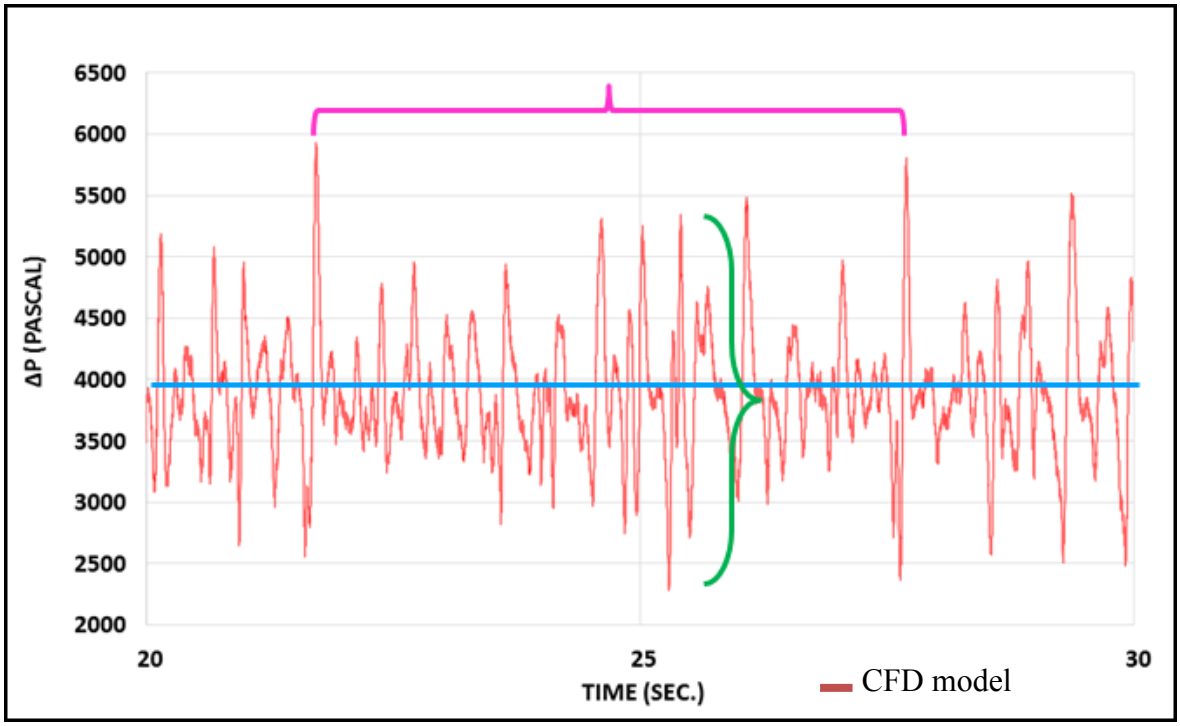

Figure 3.11 - Extract of a CFD simulation showing the time-pressure drop signal and his principle indicators in the time domain: frequency (pink), amplitude (in green), time-averaged pressure value (in blue)

Hence, the use of time-average pressure drop value and the continuous time-pressure drop signal can still be useful to verify the physical consistency of the CFD model predictions with real physics (i.e checking that the time averaged pressure drop matches the mass bed weight, see the blue line in Figure 3.11) and to have a qualitative assessment about the model prediction of time-pressure drop amplitude (green line in Figure 3.11). However, the observation and identification of pressure drop frequencies, associated to specific amplitudes, results almost impossible when time-pressure drop signal is used.

However, neither of these two types of data analysis can univocally characterize and quantify the dynamic behavior of the bubbling bed.

To overcome the aforementioned limitations, the Power Spectrum Density (PSD) analysis was used, attempting to quantify the observed fluctuations of the solid bed mass inside the system as well as linking it to the pressure drop signal. Spectral analysis is commonly used to reveal the periodic signal in a time-series. The PSD represents the frequency domain characteristic of a time series and is appropriate for the detection of frequency composition in a stochastic process [89].

In general the Power Spectral Density (PSD) is a measure of a signal's power intensity in the frequency domain. In practice, the PSD is computed from the Fast Fourier Transform (FFT) spectrum of a signal (in the time domain), resulting in a useful way to characterize its amplitude versus frequency contents. The FFT is based upon the idea of decomposing a random signal (in the time domain) into summation of an infinite sinusoidal functions of different frequencies as follows:

$$f(t) = a_0 + \sum_{k=1}^{\infty} a_k \cos(2\pi k v_1 t) + b_k \sin(2\pi k v_1 t) \tag{3.36}$$

Where v_1 is the fundamental frequency which defines the fundamental period $T = 1/v_1$. The coefficient of the the series are determined by the following equations:

$$a_k = \frac{2}{T}\int_0^T f(t)\cos(2\pi k v_1 t)dt \tag{3.37}$$

$$b_k = \frac{2}{T}\int_0^T f(t)\sin(2\pi k v_1 t)dt \tag{3.38}$$

The Fourier Transform is defined as the integral function:

$$F(\omega) = \int_{-\infty}^{+\infty} f(t)\mathrm{e}^{-\mathrm{j}\omega t}\,dt \tag{3.39}$$

And it represents a transformation from the time function *f(t)* in the frequency function $F(\omega)$ which is defined as its own image in the frequency domain. Practically the Fourier transform is obtained as the integral between t=0 and T, namely:

$$F(\omega) = \int_{-\infty}^{+\infty} f(t)\mathrm{e}^{-\mathrm{j}\omega t}\,dt = \int_0^T f(t)\cos(\omega t)dt + j\int_0^T f(t)\sin(\omega t)dt \tag{3.40}$$

In practice a continuous function f(t) is usually described by a discrete function of time (analog signal) since the there is only a limited number of time steps along which the function can be sampled. Consequently the Fourier Transform of a discrete function becomes:

$$F(u) = \frac{1}{N}\sum_{i=0}^{N-1} f(i)\exp(-\mathrm{j}\omega_u \mathrm{t}_i) = \frac{1}{N}\sum_{i=0}^{N-1} f(i)\exp\left(\frac{-\mathrm{j}2\pi \mathrm{u}i}{N}\right) \tag{3.41}$$

Where N is the number of data sampled in the period T. By definition $\omega_u t_i = 2\pi v_u t_i = \frac{2\pi u}{T} i\Delta t = \frac{2\pi u i \Delta t}{N\Delta t} = \frac{2\pi u i}{N}$, Δt the sampling interval (sec), $j = \sqrt{-1}$ and $u = 0, 1, 2, \ldots N-1$. The exponential term can be represented as:

$$\exp\left(\frac{-j2\pi ui}{N}\right) = \cos\left(\frac{2\pi ui}{N}\right) - jsin\left(\frac{2\pi ui}{N}\right) \quad (3.42)$$

Where v_1 is still the fundamental frequency defined as the inverse of the fundamental period $v_1 = 1/T = 1/(N\Delta t)$ while all the other frequency are called harmonics which are generally defined as $v_u = u/(N\Delta t)$. The DFT contains information for all the frequencies until $u = N/2$ namely $F_{N/2} = N/(2N\Delta t) = 1/(2\Delta t)$. The Fast Fourier Transform (FFT) used in this work is a faster version of the DFT which can reduce the number of operations from N*N (required by the DFT) down to N * log2(N) operations. In general, the FFT is a complex quantity units (according to the equations 3.40 and 3.41) having real and imaginary values for every frequency point. For the the present purpose, only the amplitude of the spectrum (PSD) is required [89]. To obtain the PSD each FFT is multiplied by its complex conjugate with the result being a real number with a squared unit of measure of the original signal (in this case Pa^2 being the pressure drop the original signal). The PSD so obtained captures both the power (or intensity) of the input signal and its frequency content distribution. Mathematically, the area under a PSD-versus-frequency curve is equal to the variance (square of the standard deviation) of the input signal.

Kage et al. [90], [91] revealed the presence of three different peaks (Figure 3.12) in the spectrum of pressure oscillation and above all he was able to experimentally link them to the bubble generation, eruption and natural oscillation of the fluidizing bed (as a whole).

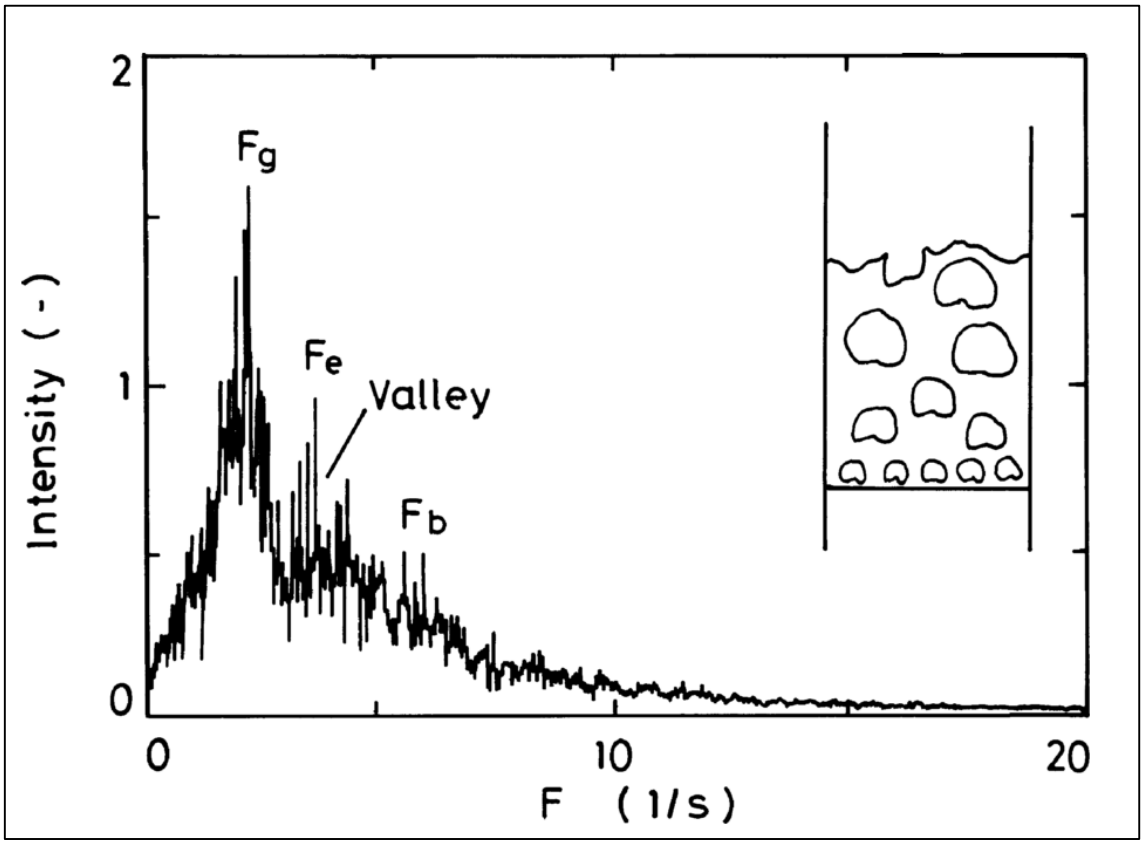

Figure 3.12 - Empirical power spectrum density (PSD) function obtained in fluidized beds formed by Group B particles in the Geldart classification [91]

The location of these three main peaks (as well as the minor ones) together with their intensity, are contributing to the shape the growth of the integral PSD function. The PSD (both in its frequency distribution and integral form) summarize the whole history of the pressure fluctuations inside the bed. Moreover, given a certain set of operating conditions, it is also representative of the specific bubbling bed dynamics, resulting in a key point to compare the empirical and numerical outputs.

Consequently both the model sensitivity analysis and validation were based on the spectrum analysis of pressure drop fluctuations which, for a sufficient time scale (sub-section 4.5.1), provides a scientific characterization of the bed dynamics.

Once the CFD and the empirical time-pressure drop signals were obtained (Figure 3.13 -a), the power spectral density (PSD) of the signal was calculated to show the frequency distributions of these oscillations (Figure 3.13-b).

To this purpose the Fast Fourier Transform (FFT) was applied to the original signal cutting the first two seconds of each simulation in order to exclude the transitory behaviour of the system. This data processing allows transporting the pressure fluctuation from the time domain to the frequency domain. This operation was carried out exploiting the FFT algorithm as already implemented in the software Fluent.

After this first step, an integral calculation of the PSD distributions was computed, showing the cumulative frequency growth. This step was carried out in Matlab, to increase the readability and the PSDs which indeed are clearer (Figure 3.13-c). Moreover, according to the physical meaning of this integral (asymptotic value reached by the integral curves), it was also possible to obtain a complementary information about the total "energy" specific of the original signal (in time). This value represents a useful indicator of the bubbling vigor since it relates to the peaks in the frequency spectrum, which in their turn are affected by the fluctuations amplitudes in the time domain. Figure 3.13 depicts the main chronological steps of data processing as discussed above.

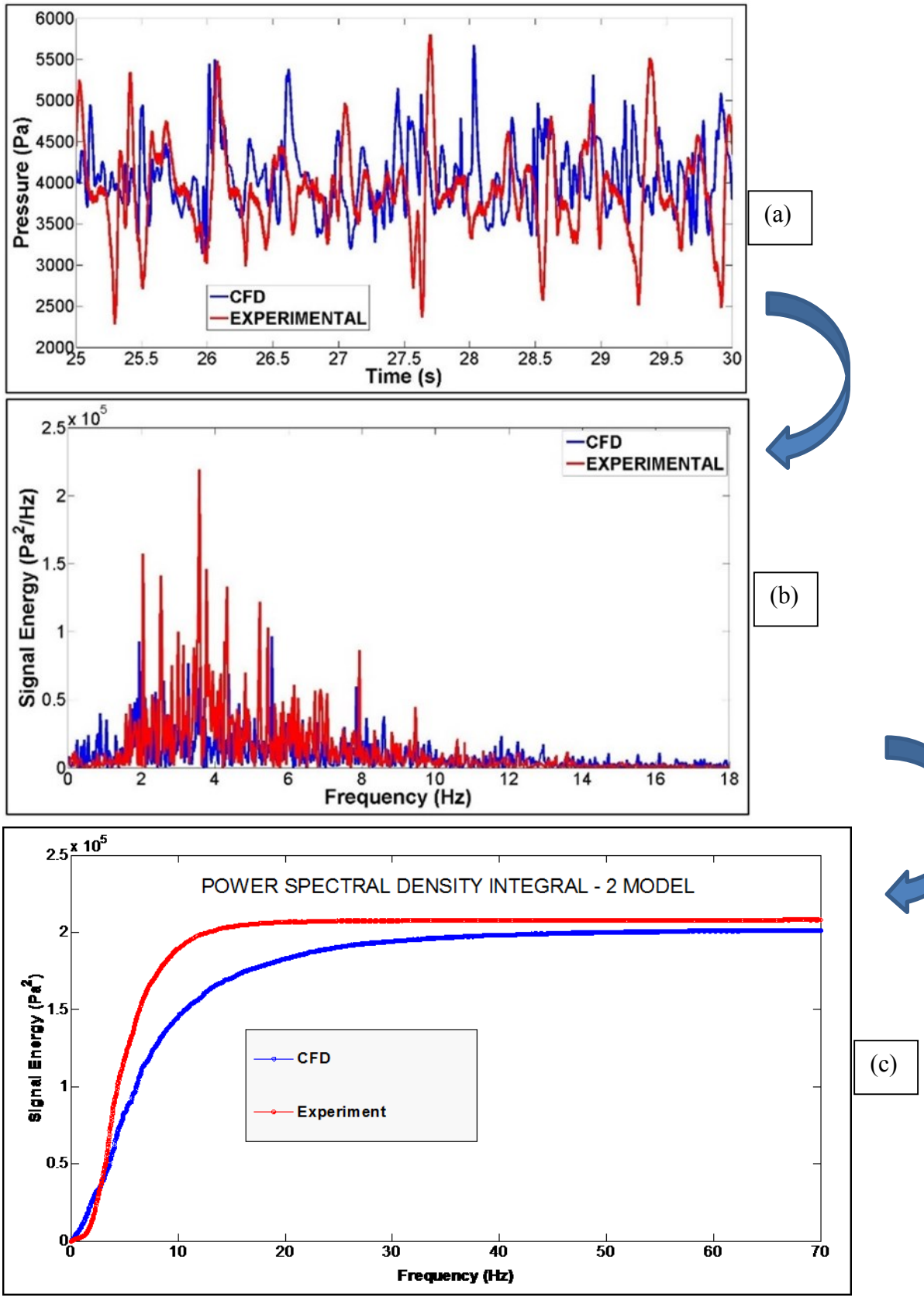

Figure 3.13 - Processing data procedure: the "raw" time-pressure drop signal (a), the PSD frequency distribution (b) obtained from the application of the FFT to the signal in time, and lastly the PSD integral curve (c) that allows (this latter) to better quantify the dynamic behavior of the system

3.4.1 Supporting model validation: video analysis

The distribution of the phase volume fractions inside the bed is crucial and is also often used as a key validation point [62],[65]. However, the visual observation of the stochastic evolution of flow patterns (bubble, cluster, channeling phenomenon etc...) inside the experimental bench is rather challenging. This is also limited to wall proximity without any chance to evaluate what occurs deeper inside the system body. Moreover, under fluidization regime, the bubbles move really fast and their presence close to the wall is unpredictable. The presence of a thin layer of dust between bubbles approaching the reactor wall and the PVC wall itself further complicates the visual analysis. Despite these limitations, the use of a commercial video camera revealed to be helpful for a basic and overall assessment of the real system hydrodynamics to be compared to CFD outputs. In order to perform such comparison, 100 frames (pictures) per second were saved during simulations and afterwards put together to form a video whose speed was tuned to match the real flow time.

Despite being a pure qualitative assessment, the video comparison between CFD and experiments revealed some interesting points showing similar hydrodynamic behavior of bubbles eruptions and mass oscillations (Figure 3.14).

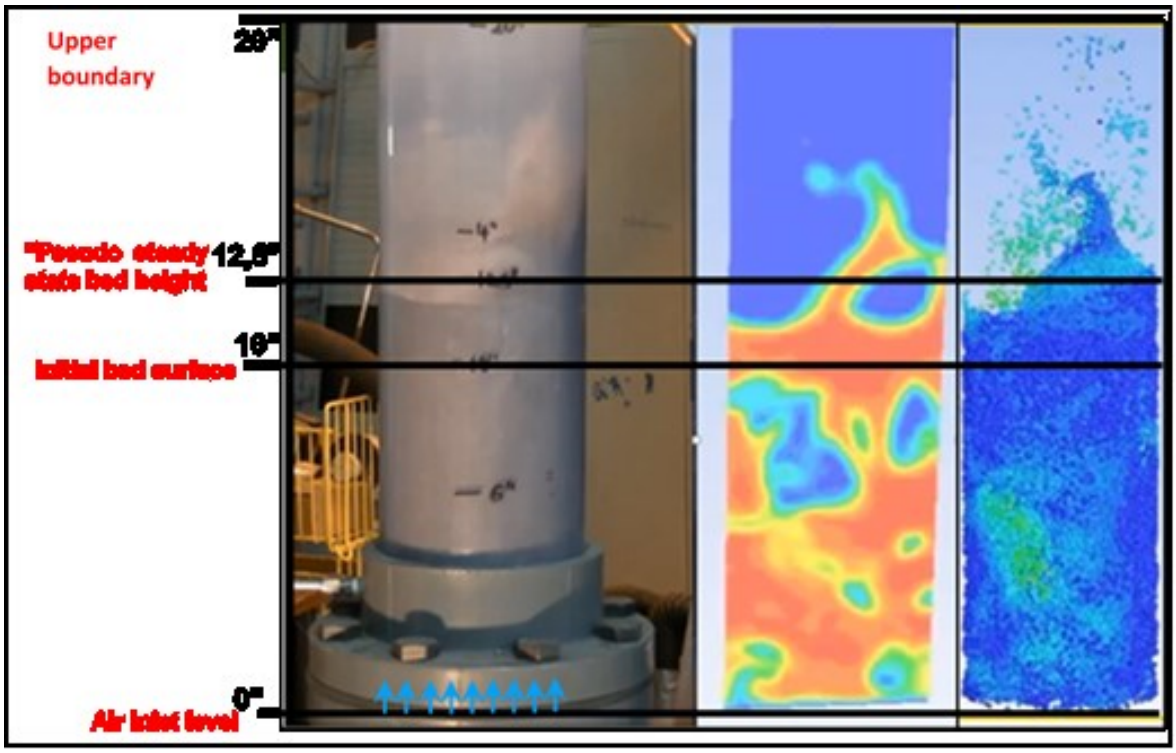

Figure 3.14- Dynamic visual analysis of the bubbling regime: an example showing the comparison between the experimental bench reactor (left), the 2D cross section of the 3D-DDPM-KTGF model (solid fraction map, middle) and the 3D parcels distribution (right).

This video analysis was often used as a support to assess the accuracy of the CFD models in predicting the dynamic behavior as observed in the experiments.

3.5 FURTHER CONSIDERATIONS AND INTRODUCTION TO PAPER WORKS

Despite the simplicity of the physics involved at this stage of models development (cold models), both the TFM and DDPM models were found computational demanding mainly as a result of the very fine mesh required for the model verification. Aiming to limit the long simulation time (flow time) some empirical tests were carried out to find the minimum time scale such to ensure the convergence of empirical data (processed data such as PSD distributions) namely to be fully representative of the dynamic behavior of the bubbling bed. In order to do that, the empirical PSD (corresponding to the different time duration of these tests) were compared to pinpoint the optimum time scale. This latter was later used as flow time for numerical simulations (real time that simulations will perform) to make sure to have also on the numerical side a representative amount of data to characterize the bubbling bed process. In spite of this strategy both these models required several days in order to perform.

Almost all simulations, whose results are presented in the following of this work, were run on high performance computing (HPC) machines at the University of Sherbrooke (*Mammoth Parallel 2*) which is deemed to be among the fastest computer all over the world. However an important aspect relates to the total number of cores which could reasonably used for simulations in consideration of a maximum number of 88 units available for the whole group of research. The contingent need of sharing these cores (among the three members of the group) resulted in the possibility of using not more than 32 units per time. For the 2D model simulations (which represented the vast majority in this PhD) 16 cores were found as the best compromise between performances and cores usage. Consequently for the 2D model the limited number of cores only translated in a limited number of simulations which may possibly be performed in parallel. Conversely, when running the 3D model, the high number of cells (equations to solve) requires a superior number of cores which could not always be available. The increasing performance with an increasing number of cores is linked to the actual size of numerical problem to be solved. So while a high number of cores (for example

more than 16) would not benefit 2D simulations, this would instead be highly beneficial for 3D model performances.

The numerical verification of the models (mesh study) and numerical sensitivity analysis (to various granular flow parameters) both combined with testing different numerical concepts to solid phase descriptions (Eulerian and Lagrangian models) resulted in a massive number of simulations. For this reason it was preferred to limit the experimental work to only one set of operating condition and used the relating empirical data as a reference to judge the numerical accuracy.

The next two chapters are dedicated to show the results obtained by the application of TFM and DDPM-KTGF approaches to the cold bubbling bed, which have been gathered and summarized separately in two dedicated papers. The two different models have been applied to study the experimental cold bench reactor operated using the same solid particles type, bed height and superficial velocity. The focus (in both papers) was on showing the comparison between the experiments and CFD model outputs to investigate and assess the ability of these models in matching the overall PSD of empirical data. In both these two works, major efforts were invested on the numerical sensitivity analysis with regard to several parameters to understand where and how it was eventually possible to improve the accuracy of model predictions as well as assessing the possibility of their scale up to industrial application.

4. CFD modeling and validation of a bubbling fluidized bed throughout pressure drop fluctuations

Auteurs et affiliation :

- **Leonardo Tricomi :** Département de génie chimique et de génie biotechnologique, Faculté de Génie, Université de Sherbrooke. La Chaire de Recherche Industrielle sur l'Éthanol Cellulosique et les biocommodités (CRIEC-B).
- **Jean-Michel Lavoie :** Département de génie chimique et de génie biotechnologique, Faculté de Génie, Université de Sherbrooke. La Chaire de Recherche Industrielle sur l'Éthanol Cellulosique et les biocommodités (CRIEC-B).
- **Tommaso Melchiori :** Département de génie chimique et de génie biotechnologique, Faculté de Génie, Université de Sherbrooke. La Chaire de Recherche Industrielle sur l'Éthanol Cellulosique et les biocommodités (CRIEC-B).
- **Micael Boulet :** Enerkem Inc., Sherbrooke, Québec, Canada
- **David Chiaramonti :** RE-CORD/Dept.of Industrial Engineering, University of Florence, Florence, Italy

Date de soumission : 10 March 2017

Revue : Frontiers in chemical engineering

Titre en français :
"Modélisation CFD et validation d'un lit fluidisé bouillonnant à travers les fluctuations de la chute de pression"

Résumé

D'après la théorie du modèle bi-fluide (TFM), un modèle CFD a été mis en place pour l'étude d'un lit fluidisé d'échelle laboratoire et non réactif opérant en régime bullant. La variable clé utilisée pour caractériser la dynamique des fluides du système expérimental et pour la comparer aux prédictions du modèle, était la chute de pression en temps induite par le mouvement des bulles à travers le lit. Ce signal temporel a ensuite été traité pour obtenir la répartition de la densité spectrale de puissance (PSD) des fluctuations de pression. Un aspect important de ce travail a été l'étude de l'effet de l'échelle du temps d'échantillonnage sur la densité spectrale de puissance empirique (PSD). Une échelle de temps de 40 secondes a été considérée comme un bon compromis, assurant à la fois la performance des simulations et la cohérence de la validation numérique. Le modèle CFD a d'abord été vérifié numériquement par un processus de raffinage du maillage, après quoi, il a servi à l'étude de la sensibilité en ce qui concerne la vitesse de fluidisation minimale (comme point d'étalonnage pour la loi de traînée), le coefficient de restitution et le terme de pression solide, tout en évaluant la précision de sa concordance avec la PSD empirique. Le modèle 2D a fourni une correspondance semblable avec la chute de pression empirique moyenne en temps, l'amplitude des fluctuations liées et l'énergie du signal calculée en tant que l'intégrale de la PSD. Une version 3-D du TFM a également été utilisée et a amélioré la correspondance avec la PSD empirique dans la première partie du spectre de fréquence.

Sensitivity analysis and accuracy of a CFD-TFM approach to bubbling bed using pressure drop fluctuations

Leonardo Tricomi[a], Tommaso Melchiori[a], David Chiaramonti[b], Micael Boulet[c], Jean Michel Lavoie[a]

[a] Department of chemical engineering and biotechnology, University of Sherbrooke, Sherbrooke (Québec) CANADA J1K 2R1

[b] RE-CORD/Dept.of Industrial Engineering, Viale Morgagni 40, I-50134, University of Florence, Florence, Italy

[c] Enerkem Inc., 3375 King West St., Sherbrooke, QC J1L 1P8

Abstract

Based upon the Two Fluid Model (TFM) theory a CFD model was implemented to investigate a cold multiphase fluidized bubbling bed reactor. The key variable used to characterize the fluid dynamic of the experimental system, and compare it to model predictions, was the time-pressure drop induced by the bubble motion across the bed. This time signal was then processed to obtain the power spectral density (PSD) distribution of pressure fluctuations. As an important aspect of this work, the effect of the sampling time scale on the empirical power-spectral density (PSD) was investigated. A time scale of 40 seconds was found to be a good compromise ensuring both simulations performance and numerical validation consistency. The CFD model was first numerically verified by mesh refinement process, after what it was used to investigate the sensitivity with regards to minimum fluidization velocity (as a calibration point for drag law), restitution coefficient and solid pressure term while assessing his accuracy in matching the empirical PSD. The 2D model provided a fair match with the empirical time-averaged pressure, the relating fluctuations amplitude and the signal's energy computed as integral of the PSD. A 3-D version of the TFM was also used and it improved the match with the empirical PSD in the very first part of the frequency spectrum.

.

HIGHLIGHTS

- Analysis of pressure drop fluctuations in a cylindrical bench
- Implementation, verification and validation of a 2D and 3D TFM-CFD model
- CFD sensitivity analysis: effect of mesh size and geometry types
- CFD sensitivity analysis: Solid pressure, Restitution Coefficient, Parametric-U_{mf}-Drag
- Pressure drop and bubbles distribution from CFD post-processing

Keywords

Eulerian-Eulerian Two Fluid Model (TFM), Fluidized bed, Pressure drop oscillations, Power Spectral Density, Inter phase drag law

4.1. INTRODUCTION

Fluidized bubbling reactors are extensively employed in the industry, both for chemical and biochemical processes as well as for power generation, and one of the main reasons is due to their optimal level of heat and mass transfer induced by the bubbling turbulence [20]. Under this regime, bubbles are responsible for the overall mixing among phases and it is hence essential to understand their fluid dynamics in order to optimize the whole process. Improving reactors efficiency while at the same time reducing their CAPEX and OPEX is still a source of numerous investigation in literature [20]. Today, small to medium-scale fluidized bed and their applications are studied using CFD models throughout different numerical approaches offering different types of accuracy (as well as different computational costs). These latter represent a very important barrier when modeling complex systems such as bubbling fluidized beds and research is actively focusing on reducing the computational requirement of numerical models whilst improving their accuracy. In multiphase applications, where the solid phase involves a very high number of particles, the Eulerian-Eulerian Two Fluid Model (TFM) has been proven to be the most convenient investigation approach [20]. In addition to this method, two possible alternatives for describing the fluid dynamic of a multiphase granular system are the Eulerian-Lagrangian Discrete Particle Model (DPM) and the Direct Numerical Simulation (DNS). These two methods, and especially the latter, are well known for their accuracy in estimating the particles trajectories while providing a full detailed map of the fluid patterns inside the system. However, their application to dense particle systems is not an easy task since they require massive computational cost especially when describing a large amount of particles (in addition to their countless interactions). The TFM represents a convenient mathematical way to model

dense particles system because of its intrinsic quicker performance (when compared with the aforementioned approaches) in capturing and providing information about bubble shapes, motions as well as on the bed expansion.

Among the different experimental strategies that could be used to study and monitor the bubbling process, pressure fluctuation is one of the most convenient ones since it is easy to measure and can be directly linked to the bubbles dynamics. Numerous studies have investigated the coupling between bubbles dynamics and pressure fluctuations as a convenient way to characterize the transient behavior of a bubbling multiphase system, from the early works published by Davidson and Harrison [29] up to more recent studies [55], [61], [92].

Despite these advantages, the interpretation of pressure fluctuations is both complicated and challenging since there are various sources involved in generating this signal [93]. Qingcheng et al. [94] observed the physical phenomenon of a bubble formation and motion rising up through the solid particles bed and found in this process the main source of perturbation of the gas-solid system. While linking the local pressure fluctuations to the bubbles presence and movement, they also assessed the influence of the operating gas velocity on the overall amplitude of pressure drop as well as on their major frequency.

Peirano et al. [55] conducted a CFD study of a bubbling fluidized bed (BFB) using an Eulerian TFM approach. In their study, they highlighted the importance of pressure drop low frequencies because of their direct connection with the bubbling motion. Nevertheless a clear interpretation about the origin of the higher frequencies was not provided. Furthermore they assessed the suitability of a 2D model as far as the sensitivity analysis is regarded while recommending a full 3D modeling when attempting to catch the dynamic of the real system. A similar conclusion was also found by Vega et al. [61] who performed differential pressure spectrum analysis along with particle fraction spectrum. While showing the close relation of these two spectrums and consequently the local character of the information provided by differential pressure probes, they also advised the use of a full 3D simulation to catch the bubble coalescence and interaction with the surface of the bed.

The primary importance of the fluid-particle drag, as the main driving force in cold fluid dynamic systems, is often noticed in open literature and represents one of the key points to achieve a good prediction of bubbling bed hydrodynamic. In general, the drag law depends on a drag coefficient (*Cd*), which in its turn depends on the local relative velocity between phases and the void fraction. This coefficient depends as well on other factors such as particle

size distribution, particle shape, etc. However, it is difficult to characterize the void fraction dependency for any conditions other than for a packed bed or for infinite dilution (single particle model [86]. In order to bypass this lack of crucial data, some authors attempted to exploit the experimental minimum fluidization velocity of their own system as a calibration point. For example, *Syamlal and O'Brien* (1987) introduced a method to adjust the drag law using the U_{mf} value of their system [95]. This approach allows calibrating (before starting the simulations) a special correlation between a single and a multiple-particle systems under settling condition. Esmaili and Mahinpey [62] compared the results of their 3D-TFM to empirical data using time-averaged pressure drop at different locations as well as bed expansion ratio. They specifically focused on the effect brought by different drag formulations, finding the parametric Syamlal-O'Brien drag law [60] as one of the best for providing a correct prediction of these two indicators over the wide range of superficial velocities investigated. Min et al. [63] validated their 2D and 3D TFM throughout gas hold-up measurements (using X-ray imaging system) as well as by the time-averaged pressure drop data. They also focused on the effect brought by different formulations of the drag law. Both their 2D and 3D model correctly predicted the experimental time-averaged pressure drop and also, in this case, the Syamlal-O'Brien drag formulation showed a better prediction of the gas holdup variation through the bed height.

This drag law was used in this work because of its intrinsic superior capability to provide the best prediction for solid bed expansions, bubbling displacement and foremost, by matching the experimental pressure drop.

While it is clear that model validation cannot be achieved by means of mere time-averaged pressure drop (since no information related to the bed dynamic can be recovered out of it) the stochastic behavior of bubbles do not allow having an univocal time-signal that could be used as a validation point. However these limitations can be rounded up by performing spectrum analysis to obtain a frequency distribution, which is univocal of any specific operating condition set up (bed height, air velocity, particle size etc). Even though a few studies went through the analysis of pressure fluctuations (by performing spectrum analysis), information about the (sampling) time scale required to fully catch the "finger-prints" of pressure drop fluctuations through the bed has not being investigated in depth.

One major target of this work is to test the effect of sampling time on the empirical pressure drop oscillations spectra (PSD) in order to limit the duration of CFD simulations while ensuring the validation of CFD model with empirical data. This work will investigate the

numerical sensitivity of a TFM model applied to a bubbling fluidized bed reactor, in order to better understand the impact of certain parameters on the accuracy that such model can provide once compared to the empirical data. To this purpose the model was tested on a 2D geometry employing the parametric Syamlal-O'Brien drag law. For each parameter a specific set of simulations have been performed by varying its value or the related mathematical formulation. The results have been compared in terms of time-averaged pressure drop, variance and signal energy. Numerical verification was also carried out, prior to the model sensitivity analysis, identifying the maximum mesh size and therefore guaranteeing the convergence of the numerical solution. A full 3D model was also implemented and used to improve the numerical accuracy, ultimately resulting in a better fit with the first part of the empirical PSD.

4.2. EXPERIMENTAL SETUP

The experimental setup used in this work (shown in Figure 4.1) has been chosen following the assembling method discussed in [75]. The latter comprises of a lab-scale fluidized bed and specific instrumentation measuring and monitoring both the gas flow discharge and the pressure drop along the bed. In the actual work the reactor body is made of clear PVC, which has been selected to allow a dynamic visual analysis of the process. The body of this system is a 15 cm i.d. over a 1 m height cylinder. The bottom flange allows stabilisation of the base of the PVC cylinder wall while embedding the porous gas distributor plate. This latter is stainless 316L-made and presents a micro-porosity of 1.3 μm such as to ensure an optimal homogenization of the gas prior to the reactor inlet. The choice of such a distributor typology is dual, first contributing to generate small bubbles all over the cross section while ultimately helping avoiding some experimental drawbacks like dead spaces and the back-sitting of solids. Secondly it allows an easier numerical schematization of the inlet boundary condition that can be accounted easily into a 2D geometry, differently from what it would be required by other types of air injectors (such as nozzles) where the 3D model would be the only possible choice. This last aspect is crucial to perform CFD simulations with significant time economy in the early stages of model implementation and verification. Moreover the very fine porosity is such to guarantee a local pressure drop (induced by its own intrinsic porosity) comparable to the one along the bed in the fluidization regime. Despite being highly conservative, this precaution is always considered when designing a proper gas distributor

in order to avoid a potential and persistent gas channeling inside the bed induced by a too low pressure drop. However, at industrial scale, porous plates are not often employed hence avoiding the risks of clogging which could be induced by inert material (that does not fluidize) as well as other compounds that might melt on the distributor surface.

A filter is placed on top of the upper flange to prevent solid particles from being entrained out of the bed during fluidization regime and, right next to it, a relief valve allowing to avoid any dangerous overpressures. For the tests, the reactor was operated under ambient conditions. The key device, for validation purposes, was a differential pressure gauge (Kistler 4264A), capable of recording up to 1000 pressure-drop data per second. These latter were then transferred to a Labview acquisition system for data saving and real time pressure drop monitoring. The pressure drop was measured between two points at the extremities of the cylinder's body. The bottom probe was positioned at 2.5 inches over the porous plate and the upper one was at the proximity of the top flange. Two small meshed screens were put inside the two pipes of the differential pressure gauge to avoid particles entrainment and therefore potential damages to the instrument. Two flow meters were included in the setup, one manual (rotameter) potentially available to measure high air flows, and the other was an electronic unit operating in the range 0-300 SLPM. Experiments were performed at 22 °C (room temperature) and 1 atm, conditions that remained constant during the tests. Finally a small light bulb was located in the upper interior section of the reactor flange, lighting up the bed surface hence allowing to take better quality pictures and videos.

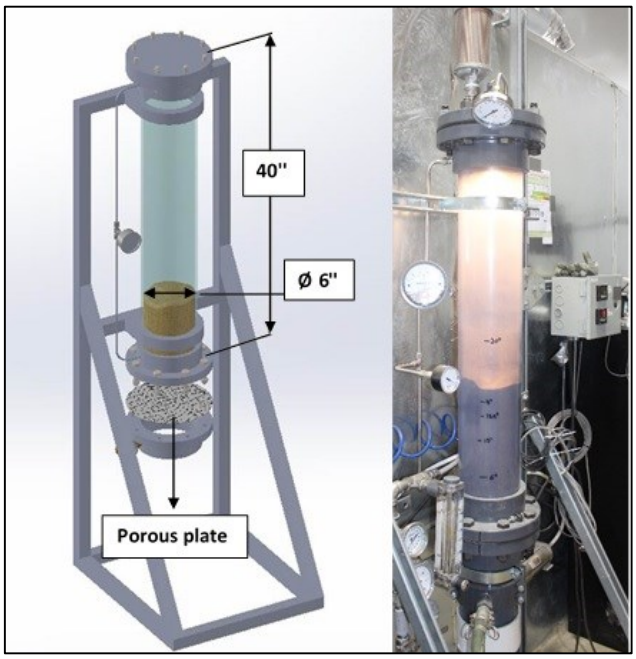

Figure 4.1 - Schematic of test apparatus and real laboratory scale bench (right) used in this work

The bed material used is alumina powder (190 µm Sauter diameter) belonging to the Geldart Group B. Alumina was selected since it is often used in industrial-scale gasifiers (where this inert represents by far the major part of the total solid bed mass). The particular size allowed covering a good range of hydrodynamic conditions (from fixed bed to vigorous bubbling condition) since the minimum fluidization velocity is strongly linked to the diameter of solid particle. By doing so, the system could be operated without the need for a manual flow-meter, whose reading accuracy, could be considerably lower than the electronic unit. Gas and solid properties used for both experiments and corresponding CFD simulations are listed in Table 4.1.

Material	Properties	Units	Value
Allumina	Particle Diameter	µm	190
	Particle density	kg/$\boldsymbol{m^3}$	3883
	Particle sphericity	-	0.6
	Coefficient of restitution	-	0.85
	Static bed height	mm	263
	Packing limit	-	0.54
	Friction packing limit	-	0.48
	Initial solid volume fraction	-	0.52
	Angle of internal friction	-	60°
Air	Density	kg/$\boldsymbol{m^3}$	2.417
	Viscosity	N s/$\boldsymbol{m^2}$	1.8 X $\boldsymbol{10^{-5}}$

Table 4-1 -. Materials physical properties for the experimental gas-solid system

The bench reactor was filled with alumina up to a bed height of 263 mm, corresponding to a total mass of approximately 9.5 kg. Different superficial velocity values below the minimum fluidization one were exploited for the CFD validation in the fixed regime, whereas only one value corresponding to 3.5 times the minimum fluidization velocity was used for validating the CFD model in the "bubbling" regime. This value was selected in order to guarantee a vigorous fluidization regime while respecting a margin of accuracy for the electronic air flow reading.

4.3. HYDRODYNAMIC AND NUMERICAL MODEL

This cold system includes gas and solid particles mixed together in an enclosed cylindrical vessel where the bubbles are generated at the very bottom of the reactor when the superficial velocity of the gasifying agents exceeds the minimum fluidization value. In this work, CFD

analysis is meant to predict the effect of bubble formation as well as their motion towards the bed surface. It should also allow predicting the pressure drop oscillations induced by bubble patterns and chaotic particles displacement. The model considers both the gas (generally air in cold fluid dynamic applications) and the solid phase as two inter-penetrating fluids for which conservation equations (mass and momentum) are derived. However these equations require a proper closure, which can be provided by the constitutive/rheological laws. The latter are obtained from empirical correlations and by application of the kinetic theory of granular flows (KTGF). The general form of the TFM equations are the following:

Continuity equation (valid for both gas and solid phase)

$$\frac{\partial}{\partial t}\alpha_q \rho_q + \nabla \cdot \alpha_q \rho_q \vec{u}_q = \sum_{p=1}^{n} \dot{m}_{pq} \tag{4.1}$$

Where α_q is the volume fraction of phase q (here representing either the gas or the solid phase), ρ_q its density and $\vec{u}_q$ the corresponding velocity vector. The term $\dot{m}_{pq}$ represents the mass transfer between phases ($kg\ m^{-3}s^{-1}$). By definition, the sum of the phase fractions α_q is equal to one.

Gas phase momentum equation

$$\frac{\partial}{\partial t}\alpha_g \rho_g \vec{u}_g + \nabla \cdot (\alpha_g \rho_g \vec{u}_g \otimes \vec{u}_g) = -\alpha_g \nabla P + \nabla \cdot \alpha_g \bar{\bar{\tau}}_g + \alpha_g \rho_g \vec{g} + K_{gs}(\vec{u}_s - \vec{u}_g) \tag{4.2}$$

P represents the operating pressure inside the system, g the gravity and K_{gs} the drag factor of phase s in phase g ($kg\ m^{-3}s^{-1}$).

The gas stress tensor is given by:

$$\bar{\bar{\tau}}_g = \mu_g(\nabla \vec{u}_g + (\nabla \vec{u}_g)^T) + (\lambda_g - \frac{2}{3}\mu_g)\nabla \vec{u}_g \cdot I \tag{4.3}$$

Solid phase momentum equation

$$\frac{\partial}{\partial t}\alpha_s \rho_s \vec{u}_s + \nabla \cdot (\alpha_s \rho_s \vec{u}_s \otimes \vec{u}_s) = -\alpha_s \nabla P - \nabla P_s + \nabla \cdot \alpha_s \bar{\bar{\tau}}_s + \alpha_s \rho_s g + K_{gs}(\vec{u}_g - \vec{u}_s) \tag{4.4}$$

Where α_s is the volume fraction of the solid phase s, $\vec{u}_s$ (*m/s*) is the corresponding velocity vector. All the other terms are explained in the following.

As for the gas also for the solid phase the total viscous stress tensor is expressed by the following expression:

$$\bar{\bar{\tau}}_s = \mu_{s,tot}(\nabla\vec{u}_s + (\nabla\vec{u}_s)^T) + (\lambda_s - \frac{2}{3}\mu_s)\nabla\vec{u}_s \cdot I \tag{4.5}$$

Where the viscosity coefficients include the combination of different terms:

$$\mu_{s,tot} = \mu_{s,col} + \mu_{s,kin} + \mu_{s,frict} \tag{4.6}$$

$\mu_{s,tot}$ is the total solid shear viscosity resulting from the summation of three different components, which are described below and are correspondingly the collisional [59], kinetic [76] and frictional [77] components of the total sheer stress .

$$\mu_{s,col} = \frac{4}{5}\alpha_s\rho_s d_s g_{o,ss}(1+e_{ss})(\frac{\Theta_s}{\pi})^{1/2}\alpha_s \tag{4.7}$$

$$\mu_{s,kin} = \frac{10\alpha_s\rho_s d_s\sqrt{\Theta_s\pi}}{96\alpha_s(1+e_{ss})g_{o,ss}}\left[1+\frac{4}{5}g_{o,ss}\alpha_s(1+e_{ss})\right]^2 \tag{4.8}$$

$$\mu_{s,frict} = \frac{P_s\sin\Phi}{2\sqrt{I_{2D}}} \tag{4.9}$$

Where α_s represents the solid volume fraction, Θ_s (m^2s^{-2}) the granular temperature, $g_{o,ss}$ the radial distribution [80], d_s (*m*) the solid particle diameter (Sauter), P_s the total solid pressure (below the expression from Lun et al [81]). P_{frict} is a frictional component [79], λ_s is the solid bulk viscosity [81] accounting for the resistance of the granular flow to compression and expansion and e_{ss} the restitution coefficient expressing the ratio between the particle speed after and before collisions. Mathematical description of these variables is given by the following:

$$\Theta_s = \frac{1}{3}\left\langle \vec{u}_s{}' \cdot \vec{u}_s{}' \right\rangle \tag{4.10}$$

$$g_{o,ss} = \left[1 - \left(\frac{\alpha_s}{\alpha_{s,\max}}\right)^{1/3}\right]^{-1} \tag{4.11}$$

$$\lambda_s = \frac{4}{3}\alpha_s \rho_s d_s g_s (1+e_{ss})\left(\frac{\Theta_s}{\pi}\right)^{1/2} \alpha_s \tag{4.12}$$

$$P_{frict} = Fr\frac{(\alpha_s - \alpha_{s,\min})^2}{(\alpha_s - \alpha_{s,\max})^5} \tag{4.13}$$

$$P_s = \alpha_s \rho_s \Theta_s + 2\rho_s (1+e_{ss})\alpha_s{}^2 g_{o,ss}\Theta_s \tag{4.14}$$

$$P_s = 2\rho_s (1+e_{ss})\alpha_s{}^2 g_{o,ss}\Theta_s \tag{4.15}$$

$$P_s = \alpha_s \rho_s \Theta_s \left[\left(1+4\alpha_s g_{o,ss}\right) + \frac{1}{2}\left[(1+e_{ss})\left(1-e_{ss}+2\mu_{fric}\right)\right]\right] \tag{4.16}$$

Drag law formulation

The last term on the RHS both for the equations 4.2 and 4.4 represents the drag force causing the interphase momentum exchange between the gas and solid phases. This term is by far the predominant one in cold systems and its formulation can significantly affect the CFD outputs [62].

The drag force depends in general of the local relative velocity between phases and the void fraction but also on some other factors such as the particle size distribution, particle shape etc. The particle void fraction is however very difficult to be determined other than in a packed bed or infinite dilution (single particle). Other factors such as particle shape, clustering and particle size distribution can also affect the local drag force but they have never been considered in deriving drag correlations [86]. Syamlal and O'Brien [60] derived a formula for the fluid-solids drag coefficient for multi-particle system using the Richardson-Zaki type velocity-voidage correlation [84]. Based on the terminal velocity of particles in fluidized or settling beds, the authors proposed the following drag correlation:

$$K_{gs} = \frac{3}{4}\frac{C_D}{v_{r,s}^2}\frac{\rho_g\left|\vec{u}_s - \vec{u}_g\right|}{d_s}\alpha_g\alpha_s \tag{4.17}$$

Where

$$C_D = \left(0.63 + \frac{4.8}{\sqrt{\mathrm{Re}_s / v_{r,s}}}\right)^2 \tag{4.18}$$

$$\mathrm{Re}_s = \frac{\rho_g d_s\left|\vec{u}_s - \vec{u}_g\right|}{\mu_g} \tag{4.19}$$

$$v_{r,s} = 0.5\left[A - 0.06\,\mathrm{Re} + \sqrt{0.0036\,\mathrm{Re}^2 + 0.12\,\mathrm{Re}(2B - A) + A^2}\right] \tag{4.20}$$

With

$$A = \alpha_g^{4.14} \tag{4.21}$$

$$B = \begin{cases} \alpha_g^{C_1} \text{ if } \alpha_g \geq 0.85 \\ C_2\alpha_g^{1.28} \text{ if } \alpha_g < 0.85 \\ C_1 = 2.65 \text{ and } C_2 = 0.8 \end{cases} \tag{4.22}$$

However, the Syamlal O'Brien drag model presented above (with constant coefficients C_1 and C_2) can result in the under/over prediction of the minimum fluidization velocity and consequently in a too high/low bed expansion [40]. In order to cope with this drawback, a parametric version of the Syamlal O'Brien drag model was used in this work. This parametric drag model exploits the minimum fluidization velocity and void fraction (on the fluidization onset) as a calibration point to adjust the drag force. Both these two parameters have to be experimentally measured and provided to the (drag model) inner algorithm which performs an iteration process to minimize the following objective function:

$$\left\{U_{mf}^{experiment} - \mathrm{Re}_t\frac{\alpha_g\mu_g}{d_s\rho_g}\right\}^{Min} \rightarrow 0 \tag{4.23}$$

Where

$$\mathrm{Re}_t = v_{r,s}\,\mathrm{Re}_{ts} \tag{4.24}$$

$$v_{r,s} = \frac{A + 0.06B\,\mathrm{Re}_{ts}}{1 + 0.06\,\mathrm{Re}_{ts}} \tag{4.25}$$

$$\mathrm{Re}_{ts} = \left(\frac{\sqrt{4.8^2 + 2.52\sqrt{4Ar/3}} - 4.8}{1.26} \right)^2 \tag{4.26}$$

$$Ar = \frac{(\rho_s - \rho_g) d_s^3 \rho_g g}{\mu_g^2} \tag{4.27}$$

With

$$A = \alpha_g^{4.14} \tag{4.28}$$

$$\mathrm{B} = \begin{cases} \alpha_g^{d_1} \text{ if } \alpha_g \geq 0.85 \\ C_2 \alpha_g^{1.28} \text{ if } \alpha_g < 0.85 \\ d_1 = 1.28 + \dfrac{\log(C_2)}{\log(0.85)} \end{cases} \tag{4.29}$$

$$C_D(\mathrm{Re}, \alpha_g) = \left(0.63 + \frac{4.8}{\sqrt{\mathrm{Re}/v_{r,s}}} \right)^2 \tag{4.30}$$

Where Re_t represents the Reynold number of a multi-particle system at the fluidization onset (minimum fluidization velocity or settling condition), Re_{ts} corresponding number for one single particle, *Ar* the Archimede number, $C_D(\mathrm{Re},\alpha_g)$ an analytical expression for the multi-particle drag coefficient and v_r is the terminal velocity for the solid phase as derived by the velocity-voidage correlation proposed by Garside and Al-Dibouni [87]. According to an algorithm, the parameter C_2 (and consequently d_1) is changed until the objective function (relation 4.23) is minimized. Hence a new set of 2 parameters is obtained, giving a more accurate estimation of the drag coefficient for any dynamic condition inside the bed (Re and

α_g) as shown by the equation 4.30. The main critical point of this parametric drag law is given by the necessity to provide a very precise values both for the minimum fluidization velocity and the air (void) volume fraction (since the CFD model is really sensitive to both). Thus these couple of values are to be provided to the CFD model according to the estimated experimental values on the onset of fluidization. However, especially regarding the determination of the U_{mf}, there is always a margin of uncertainty since from experiments, there is a not a clear limit of gas velocity marking the transition from fix regime to bubbling. In order to cope with this uncertainty, a series of simulations (as reported in section 4.5.2 and 4.5.3) were performed using different minimum fluidization velocities. The second parameter (bed void fraction) was determined univocally and according to the bed's weight and corresponding volume occupied inside the bed at the fluidization onset.

As shown above (equations 4.14 - 4.15 - 4.16), in this work three different formulation for the solid pressure term (Ps) have been considered to test the model sensitivity analysis with regards to this parameter as discussed in section 4.5.3. Based upon the kinetic theory of granular flow (KTGF), an algebraic formulation (obtained neglecting the convection and diffusion term) of the conservation of energy for the solid particles was used to work as a closure for the solid stress tensor (equation 4.5).

4.4. NUMERICAL SIMULATION

Numerical simulations were performed using Ansys-Fluent 16.2 and ran on high performance computers (HPC) at the University the Sherbrooke (*Mammoth Parallel 2*). The software adopted proper numerical methods for discretizing and solving the set of equations shown in section 3. The Eulerian-Eulerian TFM approach accounts for a set of conservation equations for each phase.

Based upon The Finite Volume approach, as the general framework for discretizing and integrating main equations, a Phase-Coupled Semi Implicit Method for Pressure Linked Equations (PC-SIMPLE) was used, thus extending the SIMPLE approach to multiphase cases. According to this method, the pressure values are computed for each time step in the cell centers while the velocities components are calculated at each cell interface. In this staggered scheme, velocities and pressure are first calculated and secondly corrected according to an iterative process in order to respect the continuity constraint. Because of the

transient formulation of the problem, an implicit second order scheme has been adopted for temporal discretization of time-derivate variables. A fixed time step of 10^{-4} s was chosen for all the simulations in order to ensure their stable convergence. The convergence criteria is based on the residual values of the solution (for each of the unknown variables) solved inside the numerical domain. The tolerances on residuals were set to 10^{-3} for continuity and 10^{-4} for the velocity components. For spatial discretization, the MUSCL method has been chosen in order to minimize numerical diffusion. In fact , as shown by Tagliaferri et al. [65], in the full fluidization regime, the First Order Upwind (FUS) scheme (provided inside the software as default option for spatial discretization) introduces a high numerical diffusion leading to the potential risk of smoothing out the solid volume fraction gradients at bubbles boundaries and ultimately failing to predict the correct bubble size and distribution.

4.4.1. Mesh grid sensitivity analysis (2D model)

Based upon the numerical set-up described in the previous section, a mesh grid sensitivity analysis was carried out to evaluate the convergence of numerical solutions. The performance of the CFD models (time required by the simulations to perform) are heavily affected by the choice of the mesh size. To this purpose, four simulations were carried out based on identical operating conditions (U_{gas} = 0.2 m/s) and material properties setup (Table 4.1) using four different square mesh sizes. The choice of the exact mesh size was made in order to obtain a precise discretization of the geometry thus avoiding any cut cells within the grid. For the 3D model only one mesh was investigated corresponding to 20 times the particles diameter. Related results and simulation performances are reported in terms of mathematical indicators in Table 4.2 and Table 4.3 respectively. The solid fraction distributions in Figure 4.2 shows the different accuracy of CFD models in displaying the bubbles shape and distribution. According to Vejahati et al. [86], the convergence of the numerical solution could be evaluated based upon macroscopic key indicators of the bubbling bed behaviour such as the time-averaged pressure drop (measured across the bed between two fixed points) and void fraction (computed as a surface time-averaged integral for a certain bed height, i.e 8 cm in this study). Finally, the variance of the pressure drop signal was compared and results were time-averaged in the 2-40 s. range thus excluding the initial unsteady state behaviour of the system (see Table 4.2). The observation of the pressure

drop and void fraction values (both time-averaged) along with the contours of solid fraction led to choose grid c (1.905 mm) as the one ensuring the convergence of the overall hydrodynamic behaviour. This result supports what was previously reported by van der Hoef [28], Syamlal and O'Brien [56] and Zimmermann and Taghipour [58], confirming the necessity to employ a mesh size less than or equal to 10 times the Sauter diameter of particles (0.19 mm) for solution grid-independency.

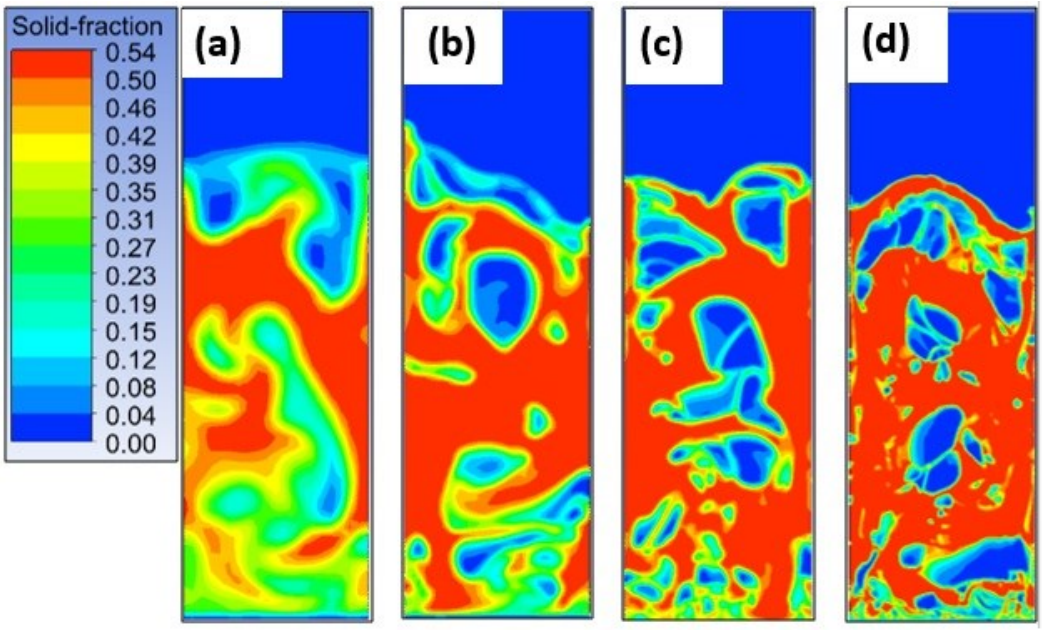

Figure 4.2 - Solid volume fraction contours at time 20 s. for U=0.2 m/s. From left to right 4 decreasing mesh size 7.62 (a), 3.81 (b), 1.905 (c), 0.635 (d) mm

Mesh spacing (mm)	ΔP(KPa)	Time averaged void fraction
Δ= 7.62 (a)	4.144	0.64
Δ= 3.81 (b)	4.119	0.59
Δ= 1.905 (c)	4.026	0.61
Δ= 0.635 (d)	4.045	0.62

Table 4-2 - Mesh sensitivity outputs used to assess the convergence of numerical solution

Δtime 2-40 s	HPC	Number of Cells	Total simulation time (h)
2D – 7.62 mm	16	1333	46
2D – 3.81 mm	16	5333	63
2D – 1.905 mm	16	21333	96
2D – 0.635 mm	32	19200	264
3D – 3.81 mm	48	285000	336

Table 4-3 - Simulations performances: effect of mesh refinement on the total CFD simulation time for the 2D and 3D model. Simulations run on HPC machines (Mammoth Parallel II) at the University of Sherbrooke

Based on these results square meshes of 1.905 mm side, corresponding approximately to 10 times the particles Sauter diameter, were chosen to investigate the 2D model sensitivity.

4.5. RESULTS & DISCUSSION

CFD simulation results were analyzed to test the TFM model sensitivity as well as its accuracy in matching empirical data. The key parameter used to assess the CFD models accuracy was the experimental pressure drop across the bed. Specifically the Power Spectrum Density (PSD) analysis was used, attempting to quantify the effect of bubbles motions and bed mass oscillation on the pressure drop signal. Once the time-dependent pressure drop signal was obtained, two other main mathematical steps were followed to investigate the pressure fluctuation distribution. First, a power spectral density (PSD) of the signal was calculated, showing the frequency distributions of these oscillations. To this purpose a Fast Fourier Transform was applied to the original signal, cutting the first 2 seconds of each simulation in order to exclude the transitory behaviour of the system. Then an integral calculation of this PSD distribution was computed in order to show the cumulate frequency growth. This last step has been put forward just to ease the reading and the interpretation of the PSD distribution itself. Moreover it can be noticed that the final value of the PSD integral also represents the total "energy" reached by the original signal in time. Besides being an useful indicator of the bubbling vigor, this value was also used in certain case to normalize the PSD curves (dividing their cumulative distribution by this value) and make these independent from the time scale of the pressure drop signal (see section 5.1). Accordingly only the shape of the PSD growth could be observed and analyzed. To carry out the model validation, a proper campaign of measurement was carried out covering both the "fixed" and the "bubbling" bed regimes. A dedicated experimental test allowed identifying a minimum time threshold to ensure a representative PSD of the model, which will be explained in the following section.

4.5.1. Experimental tests to evaluate the dependency of PSD distribution on time.

The time-pressure drop signal shows random pressure fluctuations because of the intrinsic stochastic behavior of bubbles. Therefore, the results are always different for a given set of geometries and operating conditions. Because of this variability, an alternative strategy would logically be required to univocally trace the "fingerprint" of bubble formation and motion inside the reactor. To this purpose the signal was processed using *Fast Fourier Transform* (FFT) algorithm to obtain a frequency spectrum distribution and its corresponding integral (over the frequency domain) which, at this point, were no longer specific of the singular experiment. However, in order to gain a good PSD resolution, the time horizon of these experiments had to be considerably wider as compared to the one required by the single bed oscillation. Such an issue could be comparable to the choice of a representative sample size in statistics and therefore three experiments involving different duration (40 s., 5 min., 1 h.) were carried out. The three corresponding normalized cumulative PSD's are plotted in Figure 4.3. The integral of PSD function was preferred to have a better definition of the curves. Normalization is required here to overcome the intrinsic effect of different time duration on the total energy of the original signal (which is intrinsically linked to it by definition).

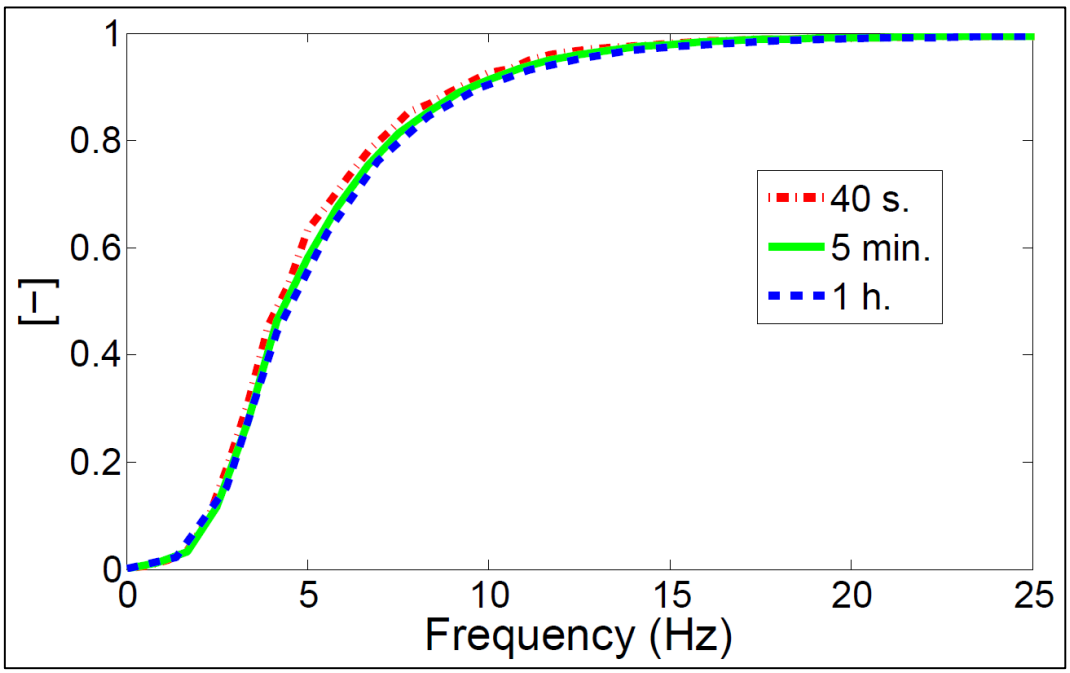

Figure 4.3 - Normalized PSD integral for 3 different empirical tests performed in the bubbling regime (according to operating conditions reported in section 2) : 40 s (red), 5 min (green), 1 h (blue)

All 3 tests show a very similar trend where the curves corresponding to tests 2 and 3 are almost overlapping while test 1 (40 s. test) present minor differences due to some missing peaks in the spectrum, which ultimately results in a less regular growth of the cumulative distribution. Nevertheless, according to these results, it has been concluded that 40 seconds can reasonably be accepted as an end-time reference for CFD simulations. The post-processing data of shorter tests (not reported in this work) revealed a very poor PSD distribution because of a significant lack of frequencies ultimately suggesting not to reduce any further the flow time for CFD simulations. Under the chosen numerical setup, high performance computers (HPC) can solve 40 s of real time in approximately 5 days (for the 2D model) using a 0.075 inches mesh grid. The 0-25Hz range in the frequency spectrum covers almost the entire distribution of pressure fluctuations showing that the specific fingerprints of bubbles is confined in this limited range with a major concentration of peaks in the 3-5 Hz range. The lack of a single, dominant frequency ("natural" frequency of bed mass oscillation) is not surprising and can be explained by the existence of different modes of bed oscillations which alter the natural frequency of gas-solid interactions in the fluidized bed [96]. Bi [93] reported that these different modes are to be taken into account in such a system because of their direct impact on the pressure drop spectrum of the signal. Moreover the major concentration of peaks in the lower part of the frequency spectrum is deemed to be strongly linked to bubbles formation and eruption as also found by Peirano and co-workers [55].

4.5.2 TFM vs Experiments: Model validation methodology

Fixed regime

Despite the main purpose of this work being the investigation of the bubbling regime, it could be as well useful to validate the CFD model in the fixed regime. Details of the mechanical properties of the solid phase and their mathematical formulations, as implemented inside the CFD model, can be found in Table 4.4. The latter is valid for simulations both in the bubbling and fixed regime (with only a different definition of the frictional pressure term for fixed condition). This type of analysis was principally aimed to assess whether or not the value of minimum fluidization velocity (*Umf*) used inside the CFD (as one of two calibration points for our customized drag law) can also be properly predicted

by the CFD model. To this purpose, six superficial velocity values were used for empirical tests and corresponding CFD simulations. As mentioned, the transition from the fixed to the bubbling regime is not abrupt, and consequently it is difficult to identify a precise and representative value of *Umf*. As explained in the last part of section 3 the *Umf* represents, in the CFD model, an important calibration point impacting on the ultimate value of the drag coefficient. Consequently three values of *Umf* (in the range identified for the experiments) were tested by providing them as an input to the CFD model (used within the drag calibration algorithm). Three corresponding sets of simulations were performed based upon these values and the six superficial velocity used for the fixed regime as shown in Figure 4.4. Simulation results showed good agreement with the experimental curve where the average relative error varies around 10% for all three cases. A bigger gap was observed for lower superficial velocities and a smaller error when the bed approaches the transition to a fluidized regime. The end flow-time of these simulations was set to 10 seconds since in the fixed regime, the steady state is reached quickly. The best match with the experiments was found using a value of U_{mf}=0.06 m/s (as drag law calibration point) when the superficial velocity was such as to approach the bubbling condition. Thus using the highest value of superficial velocity tested, U_o=0.0548 m/s, we obtained a relative error between experiments and CFD around 1%. Results also showed that numerical results are closer to empirical values at lower superficial velocity when the smallest U_{mf} (0.055 m/s) is used into the CFD drag law. For intermediate superficial velocities, the simulation performed using U_{mf}=0.058 m/s provided better results. Consequently there is not an unique trend on the best value of U_{mf} to be employed into the CFD drag law and the impact of this parameter on CFD outputs was also tested for the bubbling regime.

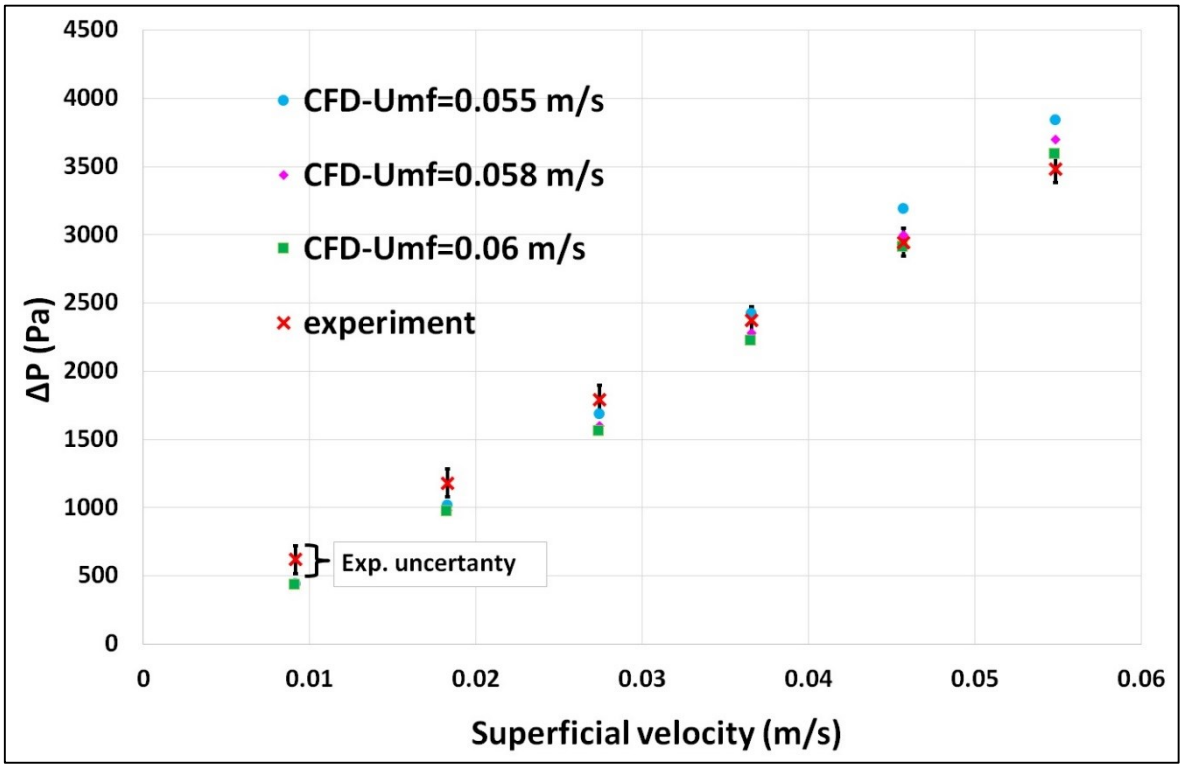

Figure 4.4 - Experimental and CFDs time-averaged pressure drops for different superficial velocity tested in the fixed regime. CFD simulations were performed based on a different Umf (used within the drag calibration algorithm). The graphic also depicts the experimental uncertainty produced by the differential pressure gauge precision

Bubbling regime

Once the air velocity exceeds a critical value (U_{mf}), bubbles are generated above the air distributor and moves upwards tending to grow and coalesce. The pressure fluctuations across the bed are greatly influenced by the gas velocity because of the drag effect brought on the particles that ultimately reflects on the bubbles formation and motion [94].To this purpose a value of U_o = 0.2 m/s (approximately 3.5 times the U_{mf}) was used as boundary condition for the CFD simulations of the bubbling regime. In addition a no slip condition was set both for the primary and the secondary phase at the wall. Given the primary importance of the drag effect in cold fluid dynamic applications and according to preliminary CFD tests and literature review [62], the adjusted Syamlal-O'Brien model has been chosen and used for all CFD simulation in this work. More details about the solid phase properties and mathematical formulation that was set in the CFD model (for the bubbling regime) can be found in Table 4.4.

Phase-Material	Properties	Units	Model
Allumina (granular)	Granular temperature model	-	Phase property
	Particle Diameter	µm	190
	Granular viscosity	kg/m-s	Gidaspow
	Granular bulk viscosity	kg/m-s	Lun-et-al
	Frictional viscosity	kg/m-s	Shaeffer
	Frictional pressure	Pascal	Based KTGF*
	Frictional modulus	Pascal	Derived
	Granular temperature	m2/s2	Algebraic
	Solid pressure	Pascal	Lun-et-al
	Radial distribution	-	Lun-et-al
	Elasticity modulus	Pascal	Derived
			*Johnson-et-al(for Fixed-regime)

Table 4-4 - Mechanical properties of solid phase their mathematical formulation used in the CFD model (Ansys/Fluent) to simulate the gas-solid system.

Example of graphical outputs are shown in Figure 4.5 (comparison between experimental values and CFD simulations). Although there are similarities between the two set of data (Figure 4.5, above), the qualitative comparison of the pressure oscillation in time is not sufficient to assess the accuracy of CFD model in reproducing the experimental data. Figure 4.5 (below) shows a divergence between the PSD of the experimental and simulation signals (especially in the first part of the spectrum 0-2 Hz), which is mainly due to the intrinsic inability for the 2D model to capture and predict the exact "fingerprint" of bubbles. That might be due to the natural three dimensionality of the flow, supporting what found in previous works [55], [61].

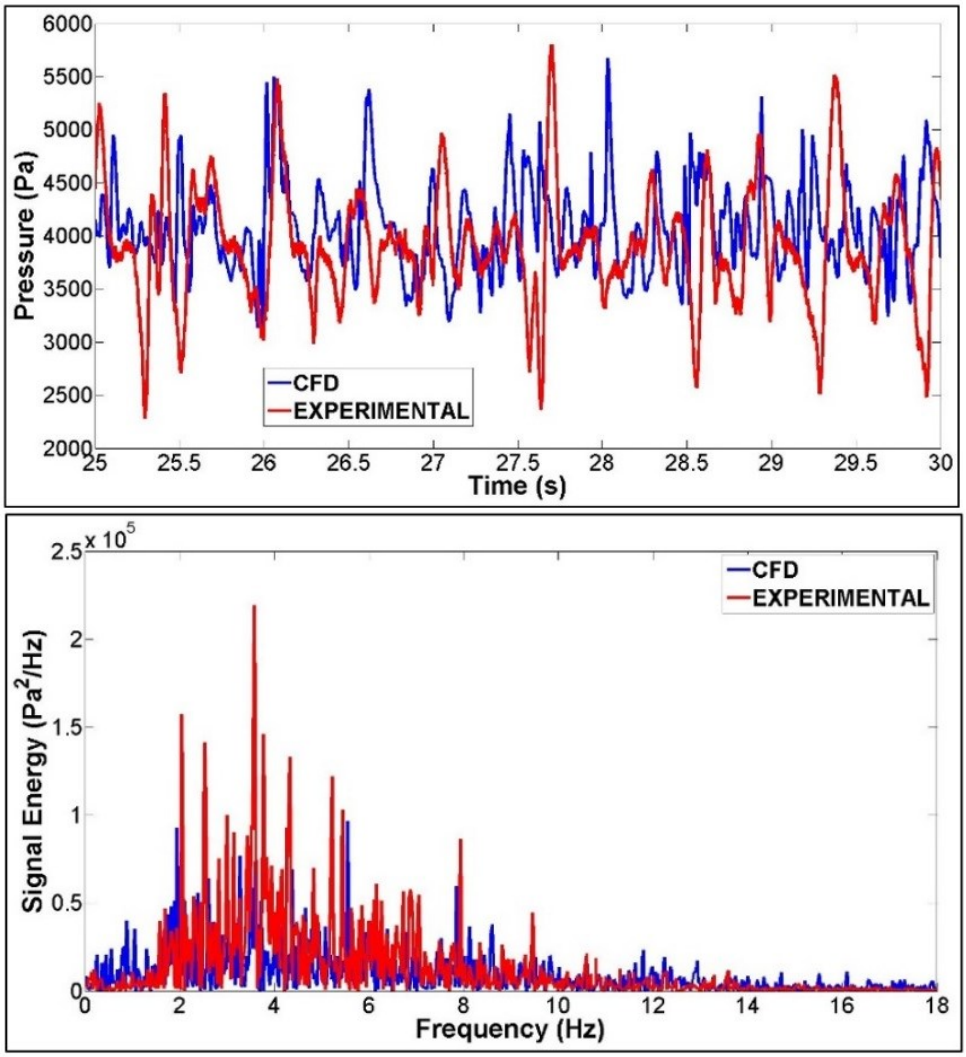

Figure 4.5 - Experimental vs 2D TFM of a bubbling bed using alumina as fluidizing medium: Comparison between the pressure drop signal in time (above) and its corresponding representation in the frequency spectrum (below)

In addition to the pressure drop signal, the distribution of the phase-volume fractions inside the bed is crucial and often used as a key validation point. However, the visual empirical observation of the stochastic evolution of flow patterns (bubble, cluster, channeling phenomenon etc...) is rather challenging. Under the fluidization regime, bubbles move really fast and their presence close to the reactor wall is unpredictable. Their presence can be only observed in the wall proximity (in certain moments) and without any chance to evaluate what occurs deeper inside the system body. In addition the presence of a thin layer of dust between bubbles approaching the reactor wall and the PVC wall itself further complicates the visual analysis.

4.5.3 Model sensitivity

The outputs of the 2D model sensitivity analysis are reported in the following along with the empirical data in order to also assess the accuracy of the numerical results. Together with the principle indicators of time-pressure drop, all the results were compared in terms of PSD cumulative (integral function) that summarizes at best the dynamic behavior of the bubbling system.

Restitution coefficient

As mentioned in section 4.3, this parameter quantifies the loss of energy due to the particles collisions, which impacts the momentum equation for the solid phase in equations (4.7),(4.8),(4.12),(4.14). In this work simulations were repeated using five different values of the restitution coefficient, in the 0.5-1 range and results are compared in Table 4.5 and Figure 4.6.

Δtime 2-40 sec.	Time aver. ΔP(Pa)	Min. (Pa)	Max. (Pa)	Variance ($\boldsymbol{Pa^2}$)	Signal energy ($\boldsymbol{Pa^2}$)* $\mathbf{10^5}$
2D – $\boldsymbol{e_{ss}}$=0.5	4049	2395	6669	178208	1.765
2D – $\boldsymbol{e_{ss}}$=0.7	4052	2738	6163	167538	1.679
2D – $\boldsymbol{e_{ss}}$=0.9	4051	2310	7625	175998	1.762
2D – $\boldsymbol{e_{ss}}$=0.98	4082	2694	5934	176553	1.764
2D – $\boldsymbol{e_{ss}}$=1	4102	2922	6434	150331	1.490
EXP.	3965	1916	6322	204544	2.051

Table 4-5 - Comparison of main statistical indicators (of time-pressure drop) for the Experiment and CFD simulations (varying the restitution coefficient-ess)

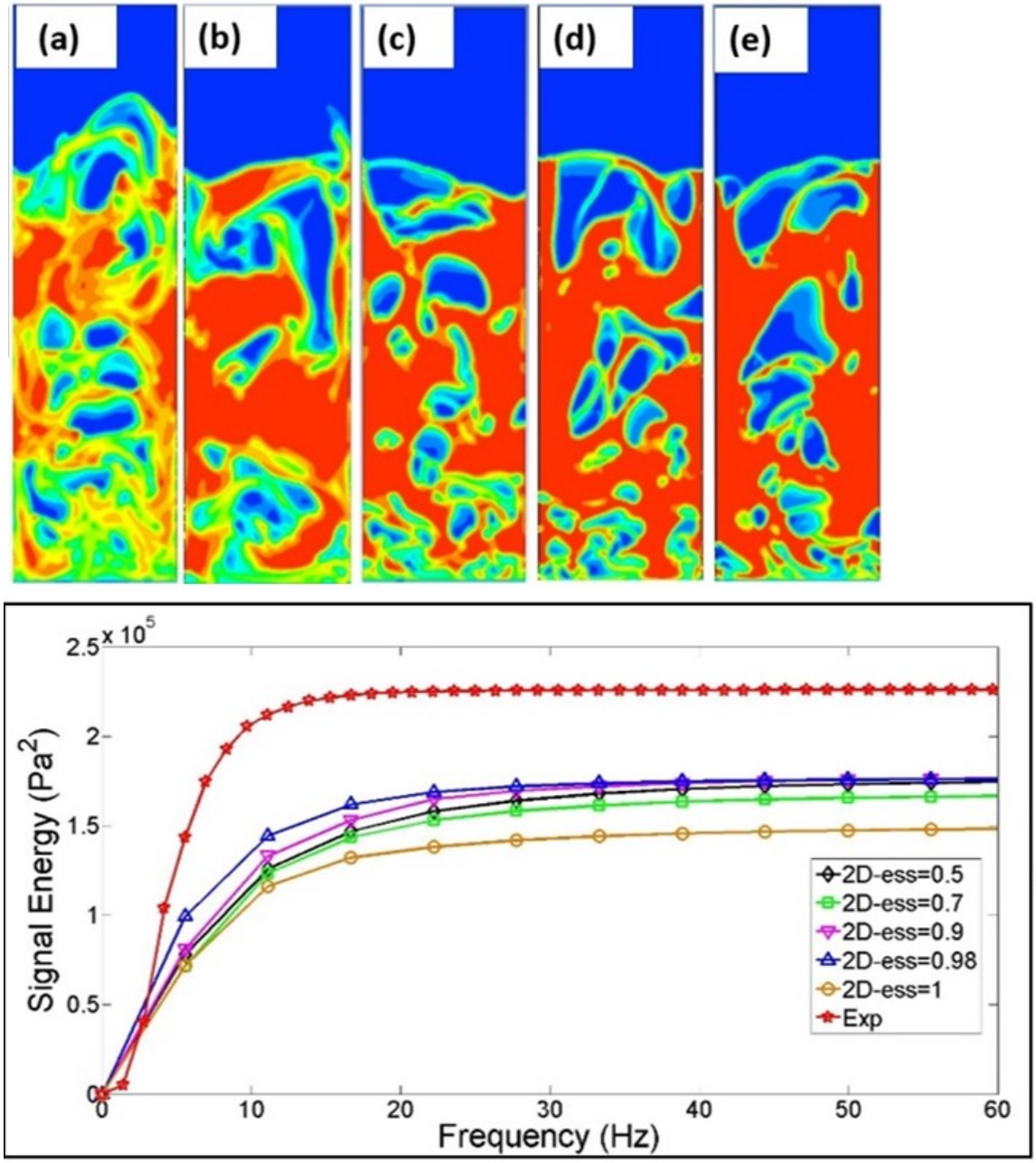

Figure 4.6 - Above: Solid volume distribution (red corresponding to αs=0.54) for ess values of 1(a), 0.98(b), 0.9(c), 0.7(d), 0.5(e). Below: corresponding PSD integral distribution

Results showed that the restitution coefficient does not have a significant impact on the CFD simulations outputs except when ideal collisions are assumed (e_{ss} = 1). This is in agreement with the work of Tagliaferri et al.[65] as well as with what was previously reported in open literature [57], [58].

Esmaili and Mahinpey [62] found comparable results concluding that when collisions becomes less ideal, particles become closely packed in the densest region of the bed resulting in sharper porosity contours and larger bubble. The simulation with e_{ss}=0.7 presented the best match with empirical data in terms of cumulated PSD, showing the lowest concentration of peaks in the first part of the spectrum as compared to the other simulations. In simulation where e_{ss}=1, the absence of sharp and big bubbles leads to a smaller variance of pressure drop and ultimately to a lower final signal energy (see Table 4.5 and Figure 4.6).

Solid Pressure

This parameter plays an important role in the momentum equation (4.2) for the granular phase and, along with shear stress tensor, contains all the parameters describing the intrinsic nature of granular flows.

Open literature shows no clear convergence on the best expression to be used for bubbling fluidized beds [62], [86] and, also for this reason, various formulations of the solid pressure term were investigated. Mathematical expressions for this term can be found in section 3 according to Lun et al.[38], O'Brien [97] and Ma-Ahmadi [98] respectively. This latter, differently from the first two, also embeds the frictional viscosity effects as shown in the equation (4.16).

Δtime 2-40 sec.	Time aver. ΔP(Pa)	Min. (Pa)	Max (Pa)	Variance (Pa^2)	Signal energy (Pa^2)* 10^5
2D - Ps=lun.et al	4051	2310	7625	175988	1.762
2D - Ps=Syamlal O'Brien	4064	2470	6652	205555	1.991
2D - Ps=Ma-Ahmadi	4077	2729	6935	189681	1.899
EXP.	3965	1916	6322	204544	2.051

Table 4-6 - Comparison of main statistical indicators (of time-pressure drop) for the Experiment and CFD simulations (varying the formulations for the solid pressure term - Ps)

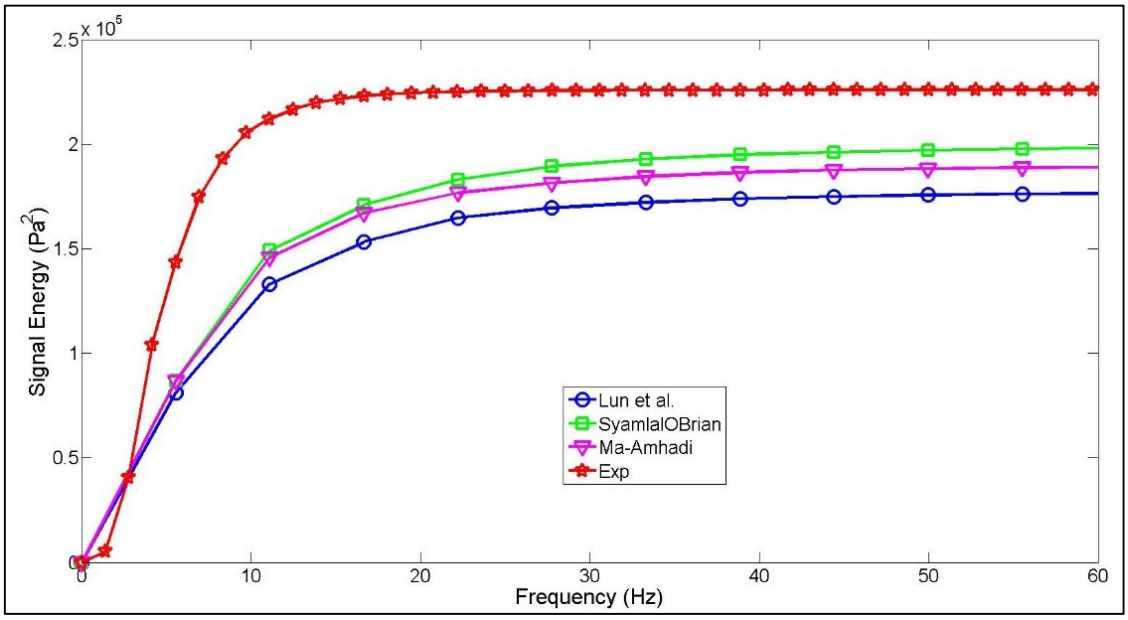

Figure 4.7 - PSD cumulative trend for the experiment (red) and three CFD simulations based upon three different formulations of the solid pressure term

Similarity between the Ma-Ahmadi and Syamlal-O'Brien model are depicted by the overlap within the 0-20 Hz range (Figure 4.7). The Syamlal-O'Brien model provides the best estimation in terms of the final total power achieved (with respect to the empirical data of our experimental bench, see Table 4-6). This model produced a slightly superior signal energy when compared to the Ma-Ahmadi expression. However this little gap is due to the presence of peaks at frequencies higher than 20 Hz, which cannot be observed on the experimental PSD. This result may seem surprising since major contribution to particles momentum exchange arises from collisions in the dilute part of the bed and above all from particles friction, in the denser zones, which is accounted in the Ma-Ahmadi formulation through the frictional viscosity. However, in the TFM approach, the frictional viscosity is derived from the frictional pressure, which is only based on the solid fraction distribution inside the bed, and not on the real properties of solid particles such as their static, dynamic and rotational frictional components (that can be instead defined when using a Discrete Element Method (DEM) for particle-particle interactions). The importance of including a proper closure for particles friction, including also the rotational dynamic and effects (not accounted in this TFM study), has been very thoroughly explained and justified by Yang et al. [99] in their recent TFM work.

Minimum fluidization velocity (drag law)

In this study, focusing on a cold multiphase system, the drag force is the dominant term coupling the two phases. The adjusted Syamlal O'Brien drag law was chosen because of his superior accuracy, also in agreement to what was previously found in literature [62], [63], [86]. As explained in section 4.3, this drag law is particularly sensitive to the empirical value of the void fraction and the minimum fluidization velocity. While the former can be quite univocally computed (knowing the bed weight and the bed volume occupied by the solid phase when the fluidization onset occurs) the latter is often more complex to estimate (as we experienced in this case of study where the progressive transition between the fixed and the bubbling regime can be noticed). Three simulations corresponding to three different values of U_{mf} were carried out without modifying anything else in the operating condition setup or numerical settings.

Δtime 2-40 sec.	Time aver. ΔP(Pa)	Min. (Pa)	Max. (Pa)	Variance (Pa^2)	Signal Energy (Pa^2)* 10^5
2D - Umf=0.06	4051	2393	7637	184297	1.853
2D - Umf=0.058	4053	2762	6774	177677	1.773
2D - Umf=0.055	4082	2557	7146	207083	2.021
EXP.	3965	1916	6322	204544	2.051

Table 4-7 - Comparison of main statistical indicators (of time-pressure drop) for the Experiment and CFD simulations (changing the Umf to be used within the drag calibration algorithm)

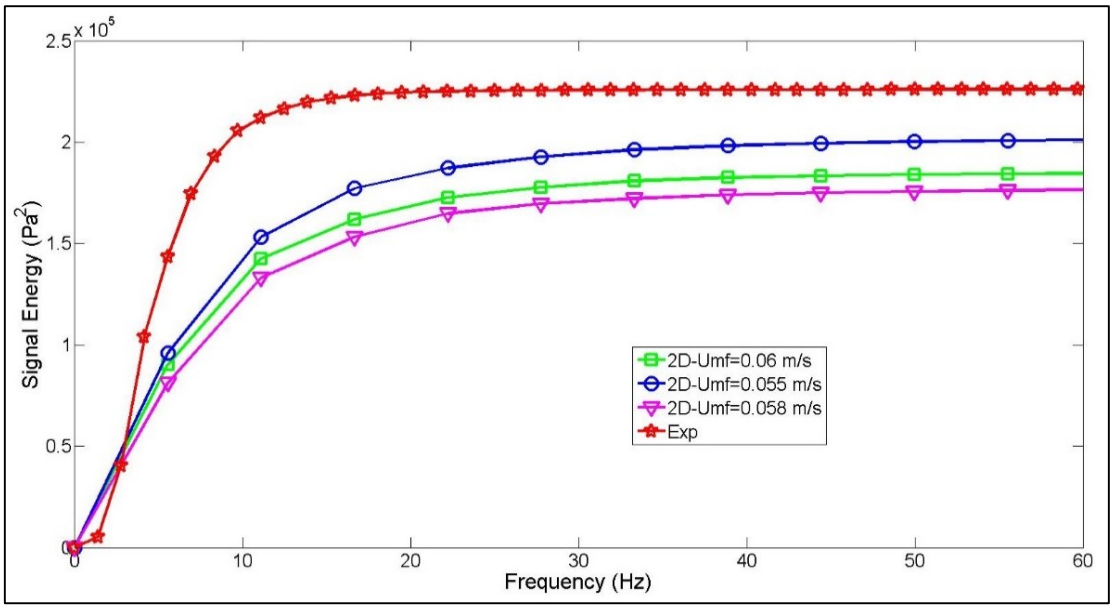

Figure 4.8 - PSD cumulative trend for the experiment (red) and three CFD simulations based upon three different value of minimum fluidization velocity (Umf)

Results shown in Table 4.7 and Figure 4.8 depicts the sensitivity of the model to a U_{mf} variation. The CFD simulation with U_{mf}=0.055 m/s shows the best match with the empirical data in terms of pressure drop variance and final energy despite an over-prediction of 500 Pa both for the maximum and minimum oscillation peaks found in the pressure drop signal. However, as already observed for the solid pressure analysis, the energy gap between the CFD simulation and empirical data has been reduced because of the frequency peaks over the 20 Hz which are absent in the experiments. A better trend was found for the simulation with U_{mf}=0.06 m/s with a minor growth of its PSD integral in the 20-60 Hz range (Figure 4.8). In this case (as also found for the other parameters investigated in this study), all the 2D model simulations showed some deficiency in reproducing the experimental PSD distribution with an unrealistic presence of peaks in the low frequencies zone. The model also depicted a weaker distribution of peaks in the 2-10 Hz range where the experimental PSD already reaches 90 % of its total energy. Nevertheless, the mean pressure drop is correctly predicted in all of three cases, with a relative error found to be between 2% and 3% of the experimental one.

2D vs 3D models - effects induced by numerical geometry

This section focuses on the comparison of CFD results achieved by using 2D models (with two different mesh sizes corresponding to 10 and 20 times the particles diameter) and a 3D set with a relatively coarse grid (hexahedron of 3.81 mm side namely about 20 times the particles diameter) to restrain its computational costs. This particular comparison aimed at showing the potential improvements of 3D simulation while warranting its limitation in matching the total signal energy of the experiment as a result of coarse meshing. All the other numerical settings were the same for these simulations in order to have a fair comparison of the results.

Δtime 2-40 sec.	Time aver. ΔP(Pa)	Min. (Pa)	Max. (Pa)	Variance (Pa^2)	Signal Energy (Pa^2)* 10^5
2D-Δ=0.15in (3.81mm)	4119	2441	7687	182169	1.771
2D-Δ=0.075in (1.91mm)	4051	2393	7637	184297	1.853
3D-Δ =0.15in (3.81mm)	3960	2557	6526	193892	1.9465
EXP.	3965	1916	6322	204544	2.051

Table 4-8 - Comparison of main statistical indicators (of time-pressure drop) for the Experiment and CFD simulations (based upon two mesh grid size in 2D and using a full 3D geometry)

Figure 4.9 (c-d) show how the choice of a coarser mesh (3.81 mm in green vs 1.91 mm in orange) leads to an underestimation of the PSD distribution all over the frequency domain, which is particularly clear after the first 2 Hz. As for the grid sensitivity analysis (see section 4.1), the CFD model ability to capture the real distribution of bubbles as well as their sharp contours gradients is strongly linked to the mesh resolution (thanks to the reduce numerical diffusion). Consequently a finer grid allows for a better accuracy in the prediction of the pressure drop signal and its PSD distribution. Despite the overall general validity of this consideration, it is worth reminding that given the 3D nature of bubbles, the PSD should be used only as a qualitative tool in analyzing results coming from the 2D models. According to the present results for the 2D model (see Table 4.8), a coarser grid leads to an over prediction of the time-averaged pressure drop with a relative error of ~4%, which is almost twice the error of the simulation with the finer grid. The PSD analysis of the 3D simulation (marked in blue in Figure 4.9) shows that the full geometry model does improve the match with the empirical data. This improvement emerges clearly from the observation of the first part of the PSD peaks distribution (0-2 Hz). Here the 3D model and the experiment (marked in red) are in a very good agreement. This relevant improvement is also evident from the analysis of the PSD integral evolution in the 0-4 Hz range (see Figure 4.9-d), where the divergence between 2D (green line) and 3D (blue line) simulations which were run with the same mesh grid, emerges clearly. However, slightly before 2 Hz, the 3D curve starts growing with a weaker intensity (as compared to the experiment) and this is most likely due to the coarse mesh used for this case, which was chosen to limit the duration of the 3D simulation. Further investigation will clarify and quantify the impact of the grid choice on the 3D model as it was done for the 2D case. Besides, the high frequency peaks (> 15 Hz) are still present in the 3D simulation, which means that this error is independent of the 2D/3D approach and it might be an intrinsic limitation of the TFM approach. The presence of low frequency peaks was found to be a limitation of the 2D model, which could not be prevented by any parameters variation in the model sensitivity (performed in this work) and the extension to

a full 3D model brought important improvement confirming what found and recommended by Peirano et al. (2001) and Vega et al. (2011) in their works.

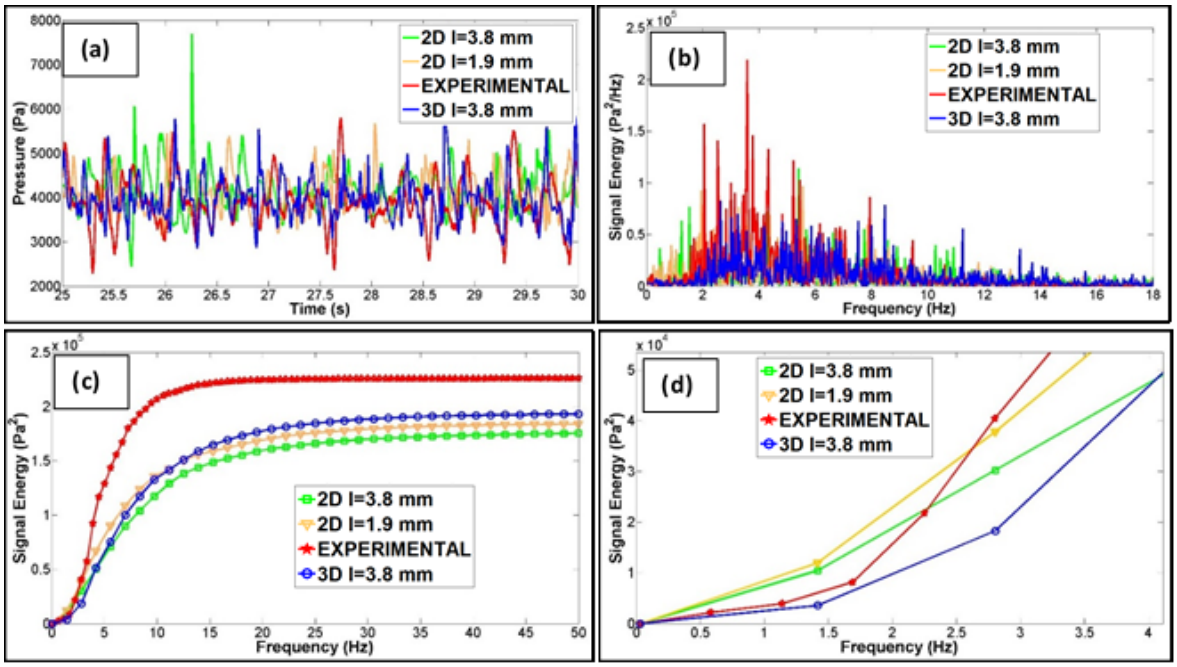

Figure 4.9 - Comparison between the experiment and CFD of fluidized bed reactor: a time-window of the pressure drop signals (a), the corresponding PSD distributions (b), the PSD integral curves in the range 0-50 Hz (c) and its zoom in the range 0-4 Hz

4.5.4 Physical correlation between pressure drop and void fraction (bubbles) distribution.

The physical correlation between pressure drop and void fraction (bubbles) distribution it is quite complex due to the dampened effect of pressure waves propagating through the solid media. Specifically when a bubble reaches the surface the change in the voids distribution over the entire domain comes along with the generation of new pressure waves. However there is always a certain delay in their propagation which result in a time lag of pressure variation. Because of this delay, along with the simultaneous bubbles eruptions and consequent changing of the voids distribution, it is difficult to correlate the pressure oscillations in time and the bubbles displacement. However, as shown by Vega and co-workers [61], it is possible to simplify this analysis by considering the pressure difference between two points in the bed that very close to each other (see Figure 4.10-left hand side). This strategy allows correlating the local pressure drop with a single local bubble, rather than accounting for the global voids distribution in the whole bed. It is possible to locally apply

the *Ergun* Equation, where the pressure drop is strictly linked to the void fraction and the gas velocity. Figure 4.10 shows two extreme cases, first (case-1), a single bubble embeds both check points. In such case the solid fraction drops to a value close to zero because of the dearth of solid obstacles between point A and B. The lack of particles between the 2 points leads to an insignificant pressure drop. Case 2 shows the opposite situation, when both the check points are embedded in the emulsion phase (at high concentration of solid phase), which makes the fluid motion energetically expensive. In both cases the strong link between solid fraction and pressure drop is well depicted in the upper part of Figure 4.10. A third case is also possible, when the solid fraction is close to the maximum packing limit (like in case-2), but a lower value of pressure drop is predicted by the model. Such an occurrence is not surprising, since the gas velocity also plays a role in the gas pressure drop (as shown in the Ergun equation). According to the simulation, the gas velocity at the points A and B is 0.85 m/s for case-2 and 0.6 m/s for case-3, which explains the different simulated pressure drop.

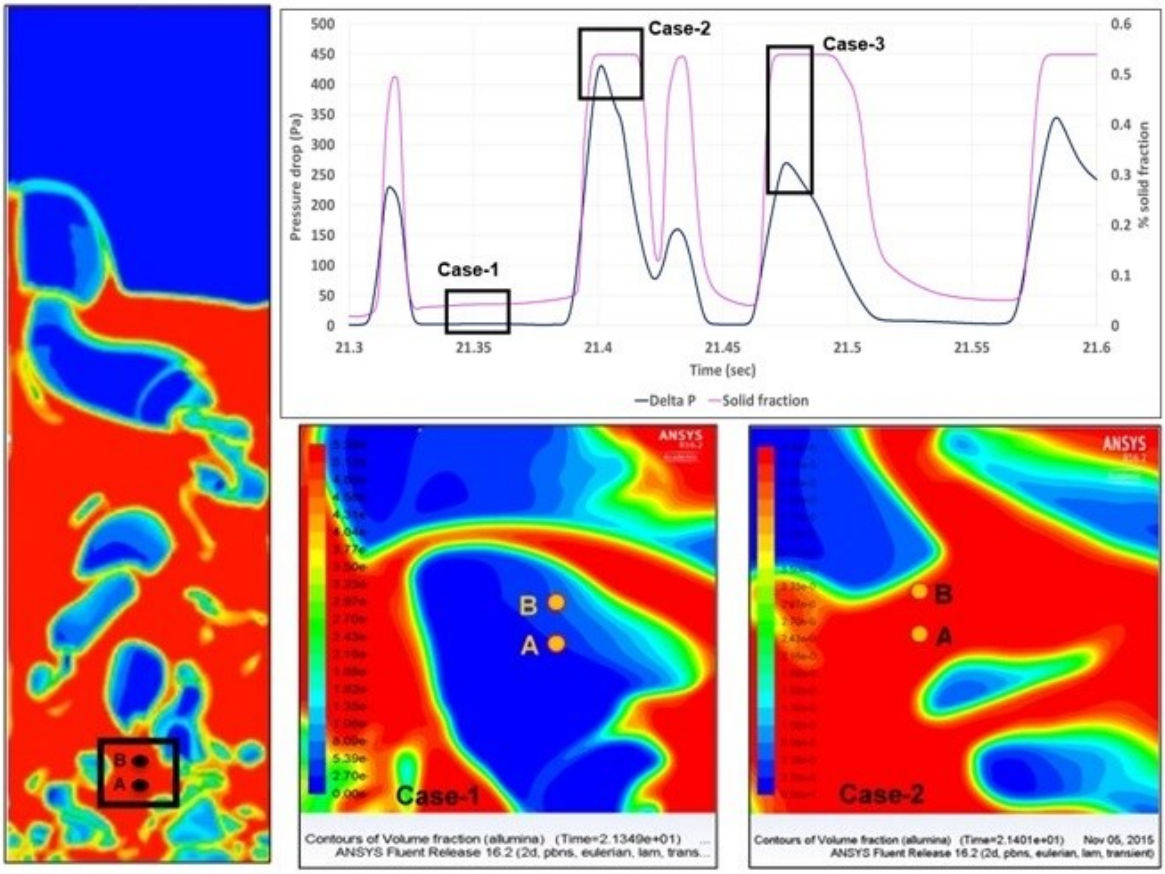

Figure 4.10 - . Correlation between bubbles distribution and pressure drop in bubbling bed reactor: a view of the whole bubble distribution as predicted by CFD-TFM along with the 2 points where pressure is monitored (on the left), the pressure drop trend vs solid fraction for a little time window (top), bubbles distribution in the area of the 2 points for different time (case-1 &case-2, bottom pictures)

4.6 CONCLUSIONS

The results presented in this paper concern the application of a CFD Two Fluid Model (TFM) to a gas-solid fluidized bubbling bed reactor. The power spectral density (PSD) analysis (of pressure drop fluctuations) was used to compare the empirical data with the numerical predictions. The need of containing the computational costs was one of the priority and resulted in finding a flow time threshold for model simulations. Testing the effect of the sampling time on the empirical power spectral density (PSD) of pressure drop fluctuations it was was found that 40 seconds could represent a good compromise to limit the duration of CFD simulations while ensuring the consistency of model validation with empirical data. The mesh size analysis carried out in this study showed that an interval spacing of 10 times the mean particle diameter was able to give acceptable results supporting what found in previous studies. Because of the unclear transition between fixed and bubbling regime, in the present experimental setup, the effect of U_{mf} (used as a parameter in the parametric drag law) on CFD simulations was investigated. The model outputs showed a better agreement with empirical data when the highest U_{mf} value (in the transition zone of the fluidization curve) was used. Beside in the ideal collision case (e_{ss}=1) the effect of the restitution coefficient appeared to be negligible on model predictions as well as the solid pressure term which was tested throughout two different formulations. In general, the 2D model revealed to correctly predict the time-averaged pressure drop and its fluctuations amplitude. Moreover the post processing analysis of 2D simulations revealed a straightforward correlation between the pressure drop and void fraction distribution, confirming the presence of bubbles as the main source of local variation of pressure. A 3D version of the model was also implemented and compared with the 2D model. Despite being based on a “medium” size mesh, the 3D model drastically improved the results over the first part of the spectrum (0-2 Hz), namely where all the previous 2D model simulations failed. The effect of a coarser grid on the numerical PSD was prior assessed allowing to believe how 3D model results may have been closer to the empirical ones also in the remaining part of the spectrum if a finer mesh was exploited. However according to the simulation performances, reported in this work, this would result prohibitive from a computational standpoint especially in the perspective of a model scale up to industrial application. This barrier may possibly be overtaken if: a) coarser particles can be used (which would result in a coarser mesh required to numerical verification); b) a different type of variable analysis is needed possibly

requiring a lower flow time as compared to the one used in this work; c) the study involves macroscopic variables or type of analysis which do not require very fine mesh to be investigated.

Acknowledgement

The authors are grateful to the Industrial Research Chair on Cellulosic Ethanol and Biocommodities of the Université de Sherbrooke and especially its sponsors: The Ministère de l'Énergie et des Ressources Naturelles du Québec (MERNQ), CRB Innovations, Enerkem and Éthanol GreenFIeld Québec Inc. The authors are also grateful to MITACS for Leonardo Tricomi and Dr Tommaso Melchiori's grant and finally Compute Canada for having made possible to perform most of the simulations throughout high performance computing (HPC) machines at the Université de Sherbrooke (Mammoth Parallel 2).

Notation

d_s diameter of particles in the solid phase, m

e_{ss} restitution coefficient between colliding particles of solid phase

$\vec{g}$ vector representation of acceleration due to gravity, 9.81 m/s^2

$g_{o,ss}$ radial distribution function between particles of solid phase

K_{gs} momentum exchange coefficient between gas and solid phase, kg $m^{-3}s^{-1}$

$\dot{m}_{pq}$ mass flow rate from the generic phase p to the generic phase q, kg $m^{-3}s^{-1}$

P pressure, Pa

P_s solid pressure, Pa

P_{frict} frictional component of solid pressure, Pa

t time, s

$\vec{u}_q$ velocity vector of the generic (gas and solid) phase q, m/s

$\vec{u}_g$ velocity vector of gas phase, m/s

$\vec{u}_s$ velocity vector of solid phase, m/s

$\vec{u}_s^{'}$ velocity fluctuation vector of particles, m/s

α_q volume fraction of the generic (gas and solid) phase q

α_g volume fraction of the gas phase

α_s volume fraction of the solid phase

$\alpha_{s,\max}$ maximum packing limit (volume fraction) of the solid phase

Θ_s granular temperature, m^2/s^2

λ_s granular bulk viscosity, Pa*s

μ_g viscosity of gas phase, Pa*s

$\mu_{s,tot}$ total granular viscosity of solid phase, Pa*s

$\mu_{s,col}$ collisional component of total granular viscosity, Pa*s

$\mu_{s,kin}$ kinetic component of total granular viscosity, Pa*s

$\mu_{s,fricl}$ frictional component of total granular viscosity, Pa*s

ρ_q density of the generic (gas and solid) phase q, kg m^{-3}

ρ_g density of the gas phase, kg m^{-3}

ρ_s density of the solid phase, kg m^{-3}

$\bar{\bar{\tau}}_g$ stress-strain tensor for the gas phase, Pa

$\bar{\bar{\tau}}_s$ stress-strain tensor for the solid phase, Pa

5 Numerical investigation of a cold bubbling bed throughout a dense discrete phase model with KTGF collisional closure

Auteurs et affiliation :

- **Leonardo Tricomi :** Département de génie chimique et de génie biotechnologique, Faculté de Génie, Université de Sherbrooke. La Chaire de Recherche Industrielle sur l'Éthanol Cellulosique et les biocommodités (CRIEC-B).
- **Jean-Michel Lavoie :** Département de génie chimique et de génie biotechnologique, Faculté de Génie, Université de Sherbrooke. La Chaire de Recherche Industrielle sur l'Éthanol Cellulosique et les biocommodités (CRIEC-B).
- **Tommaso Melchiori :** Département de génie chimique et de génie biotechnologique, Faculté de Génie, Université de Sherbrooke. La Chaire de Recherche Industrielle sur l'Éthanol Cellulosique et les biocommodités (CRIEC-B).
- **Micael Boulet :** Enerkem Inc., Sherbrooke, Québec, Canada
- **David Chiaramonti :** RE-CORD/Dept.of Industrial Engineering, University of Florence, Florence, Italy

Date de soumission : 8 June 2017

Revue : Biofuels Engineering

Titre en français : "Recherche numérique d'un lit bouillonnant à froid tout au long d'un modèle de phase discrète avec une fermeture collisionnelle KTGF"

Résumé

On a utilisé un modèle hybride de particules denses discrètes d'Euleran-Lagrangian (DDPM) pour simuler numériquement le comportement de bullage d'un réacteur à lit fluidisé. Le modèle exploite le concept des parcelles afin de réduire le nombre de particules qui doivent être simulées, tout en exploitant la théorie cinétique du flux granulaire (KTGF) pour tenir compte de leurs interactions répulsives. Le DDPM-KTGF a été exploré au cours d'une analyse de sensibilité de modèle pour identifier les paramètres les plus influents qui impactent sur la précision et la performance numérique pour évaluer son utilisation potentielle à des fins industrielles. En raison de la simplicité de mesure, ainsi que de sa forte connexion avec la dynamique des fluides du lit, les données de chute de pression ont été utilisées et traitées par l'analyse de distribution de puissance (PSD) pour caractériser empiriquement et numériquement le comportement de ce système sous un régime fluidisé bullant.

Le modèle DDPM-KTGF a été jugé très sensible à la taille du maillage, aux coefficients de restitution et surtout à la loi de traînée. D'un autre côté, une faible sensibilité à la viscosité cinétique, à la pression solide, la répartition radiale ainsi qu'au nombre de colis a été révélée. En plus d'avoir influencé les résultats physiques, le raffinement du maillage était également nécessaire pour numériquement vérifier le modèle et a eu un impact significatif sur la performance de ses simulations. En outre, un obstacle majeur a été trouvé dans l'utilisation de ce modèle pour simuler le régime de lits fixes, montrant la limitation de l'approche KTGF aux régions à forte densité de particules, en raison d'une mauvaise estimation des interactions de force de particules.

Numerical investigation of a cold bubbling bed throughout a dense discrete phase model with KTGF collisional closure

Leonardo Tricomi[a], Tommaso Melchiori[a], David Chiaramonti[b], Micael Boulet[c], Jean Michel Lavoie[a]

[a] Department a of chemical engineering and biotechnology, University of Sherbrooke, Sherbrooke (Québec) CANADA J1K 2R1

[b] RE-CORD/Dept.of Industrial Engineering, Viale Morgagni 40, I-50134, University of Florence, Florence, Italy

[c] Enerkem Inc., 3375 King West St., Sherbrooke, QC J1L 1P8

Abstract

A hybrid Euleran-Lagrangian Dense Discrete Particle Model (DDPM) was used to numerically simulate the bubbling behavior of a fluidized bed reactor. The model exploits the parcels concept in order to reduce the number of particles to simulate while exploiting the Kinetic Theory of Granular Flow (KTGF) to account for their repulsive interactions. The DDPM-KTGF was explored throughout a model sensitivity analysis to identify the most influent parameters impacting on the numerical accuracy and performances to ultimately assess its potential use for industrial purposes. Because of the measurement simplicity as well as its strong connection with the bed fluid-dynamic, pressure-drop data were used and processed by power spectrum distribution (PSD) analysis to empirically and numerically characterize the behavior of this system under a bubbling fluidization regime.

The DDPM-KTGF model was found to be sensitive to mesh size, restitution coefficients and mostly to the drag law. In opposition poor sensitivity to the kinetic viscosity, solid pressure, radial distribution function as well as to the number of parcels was revealed. Besides having an effect on the physical outputs, the mesh refinement was also required to numerically verify the model and significantly impacted on its simulations time-performance. Moreover, a major barrier was found in using this model to simulate the fixed bed regime, showing the

limitation of the KTGF approach to high particle density regions as a result of a poor estimation of particles force interactions.

HIGHLIGHTS

- Experimental analysis of pressure drop fluctuations in a cylindrical bench.
- Implementation, verification and validation of a CFD model of the bench in 2D and 3D geometry.
- CFD sensitivity analysis:
    - Mesh size and parcels number.
    - Kinetic viscosity, Solid pressure, Radial Distribution, Restitution Coefficient, Drag models.

Keywords

Eulerian-Lagrangian Discrete Phase Model (DDPM), KTGF collisional model, Fluidized bed, Pressure drop oscillations, Power Spectral Density

5.1 INTRODUCTION

Fluidized bed reactors are widely employed in the industry, both for chemical and biochemical processes. Among various types of fluidizing systems, bubbling beds offers an optimal heat and mass transfer, promoted by the turbulent bubble motion [20]. Under this regime, bubbles are responsible for the overall mixing among the gas and the solid phases and it is essential to understand their fluid dynamics in order to optimize the whole process. During the last three decades many efforts have been dedicated to characterize the hydrodynamic of gas-fluidized systems throughout numerical simulations in order to efficiently speed up the optimization of their design and ultimately reducing their costs. Currently there are two main (although conceptually different) classes of models that can be employed for the numerical investigation of fluidized beds, namely the Eulerian-Eulerian two fluid model (TFM) and the Eulerian-Lagrangian model with (for this latter) further sub-branches classes based upon the different particles interactions treatment. While in the former both the gas and solid are described as interpenetrating continua, the second one tracks the solid particles in a Lagrangian framework. The DPM approach offers at least two main advantages over his competitor (TFM). First it is more grid-independent because of a limited numerical diffusion and secondly it allows for a more efficient treatment of the particle size distribution, which can bring the description of the solid system closer to reality. However, the pure DPM model does not account for particle-particle interaction and consequently, it is not suitable for dense granular systems where a significant part of the kinetic energy of the system is consumed by collisions and frictional effects. The DDPM

that was used in this work is an extension of the DPM allowing to extend its applicability to dense particle systems. Specifically the DDPM exploits the Kinetic Theory of Granular Flow (KTGF) to describe the evolution of the uncorrelated particles motion and to account for their repulsive collisional forces. These forces are estimated by solving gradients of continuous functions (i.e shear stress tensor and solid pressure term prior calculated on the Eulerian grid) making of the DDPM-KTGF model an hybrid approach to multiphase system. The first version of the KTGF approach has been developed under the hypothesis of frictionless, nearly elastic and non-rotational particles (Gidaspow [49], Jenkins and Savage [37], Lun et al. [81]) and nowadays a few authors are actively working to overtake these unrealistic limitation and include the effect of aforementioned properties [99]. In the present work, simulations were performed using Fluent 16.2, which allowed including both the effect of particle friction in addition to their inelastic nature (by means of restitution coefficients) but without accounting for rotational effect. Cloete et al. [69] made a comparison of TFM and DDPM (both embedding the KTGF approach) to industrial scale application. They proved that DDPM had a better grid independence, ultimately being 20 times faster than its TFM rival model. Furthermore in spite of a small divergence in the axial pressure drop profile between 2D and 3D model (when using the DDPM-KTGF approach) as well as the prediction of bigger bubbles for the 2D model, they did not register any other major divergence in terms of pressure drop nor bed height. In a recent study, Cloete and Amini [68] compared the TFM and the DDPM models under many different operating conditions showing how the DDPM model can achieve the same level of structure resolution than the rival TFM approach using a twofold bigger mesh size with consequent performance speed up. They also highlighted how the DDPM approach gives a more discrete representation of the volume fraction field relative to the smooth bubbles shown by the TFM. The former was also found efficient to capture the channeling behaviour caused by the large stressed induced by particle-particle and particle-wall collision and friction. Finally they highlighted the promising applicability of DDPM for large scale 3D simulations of bubbling fluidized bed reactor.

Given the importance of these findings, in addition to the small literature inherent to the application of this model to bubbling bed (as compared to TFM or DEM approaches), this work was aimed at bringing an insight into the numerical sensitivity of this DDPM-KTGF model as well as to test the performance both of its 2D and 3D versions, in view of a potential

scale-up. Results have been compared in terms of time averaged pressure drop, variance, solid fraction maps (in certain cases) and, above all, by using power frequency spectrum that relates more closely to the bed dynamic. In all cases, the experimental PSD was used as reference to assess the overall accuracy of the model. Simulations performances were also considered to estimate the range of applicability of this model at industrial scale.

5.2 EXPERIMENTAL SET UP

The experimental setup used in this work (shown in Figure 5.1) has been chosen following the assembling method discussed by Conshohocken [75]. The latter comprises of a lab-scale fluidized bed and specific instrumentation measuring and monitoring both the gas flow discharge and the pressure drop along the bed. In the actual work, the reactor body was made of clear PVC, which has been selected to allow a dynamic visual analysis of the process. The body of this system involved a 6" i.d. and 40" height cylinder. The bottom flange allowed stabilisation of the base of the PVC cylinder wall while embedding the porous gas distributor plate. The latter is stainless 316L-made and presents a micro-porosity of 1.3 μm, ensuring an optimal homogenization of the gas prior to the reactor inlet. The choice of such a distributor typology is dual, first contributing to generate small bubbles all over the cross section while ultimately helping avoiding some experimental drawbacks like dead spaces and the back-sitting of solids. Secondly it allows an easier numerical schematization of the inlet boundary condition that can be accounted easily by a 2D geometry, differently from what would be required by other types of air injectors (such as nozzles) where the 3D model would be the only possible choice. This last aspect is crucial to perform CFD simulations with significant time economy in the early stages of model implementation and verification. Moreover the very fine porosity is such to guarantee a local pressure drop (induced by its own intrinsic porosity) comparable to the one along the bed in the fluidization regime. Despite being highly conservative, this precaution is always considered when designing a proper gas distributor in order to avoid potential and possibly persistent gas channeling inside the bed induced by insufficient pressure drop. However, at industrial scale, porous plates are not often employed hence avoiding the risks of clogging, which could be induced

by inert material (that does not fluidize) as well as other compounds that might melt on the distributor surface.

A filter is placed on top of the upper flange to prevent solid particles from being entrained out of the bed during the fluidization regime and, right next to it, a relief valve allowing to avoid any dangerous overpressures. For the tests, the system was operated under ambient conditions and, for validation purposes, the key device was a differential pressure gauge (Kistler 4264A), capable of recording up to 1000 pressure-drop data per second. These latter were then transferred to a Labview acquisition system both to backup data as well as for real time pressure drop monitoring. The pressure drop was measured between two points at the extremities of the cylinder's body. The bottom probe was positioned at 2.5 inches over the porous plate and the upper one was at the proximity of the top flange. Two small meshed screens were put inside the two pipes of the differential pressure gauge to avoid particles entrainment and therefore potential damages to the instrument. An electronic flow meter operating in the range 0-300 SLPM was used to measure the air flow at the inlet. Experiments were performed at 22 °C (room temperature) and 1 atm, conditions that remained constant during the tests. Finally a small light bulb was located in the upper interior section of the reactor flange, lighting up the bed surface hence allowing to take better quality pictures and videos.

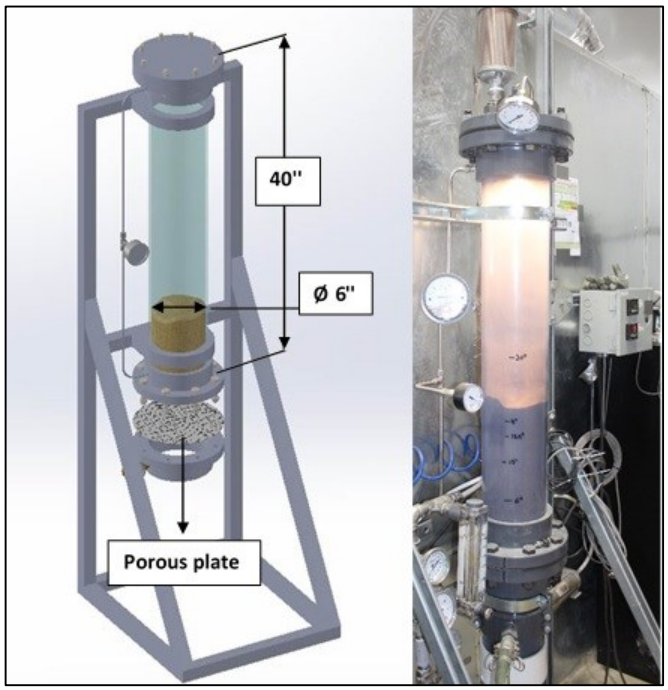

Figure 5.1 - Schematic of test apparatus (left, [75]**) and real lab. scale bench (right) used for this work**

The bed material used for this study is an alumina powder (190 µm Sauter diameter) belonging to the Geldart Group B. Alumina was selected since it is a material often used in industrial-scale gasifiers, where this inert represents by far the major part of the total solid bed mass. Gas and solid properties used both for experiments and corresponding CFD simulations are listed in Table 5.1.

Material	Properties	Units	Value
Allumina	Particle Diameter	µm	190
	Particle density	kg/m^3	3883
	Particle sphericity	-	0.6
	Coefficient of restitution	mm	Varied
	Static bed height	mm	263
	Packing limit	-	0.54
	Friction packing limit	-	0.48
	Initial solid volume fraction	-	0.52
	Angle of internal friction		60°
Air			
	Density	kg/m^3	2.417
	Viscosity	N s/m^2	1.8 X 10^{-5}

Table 5-1 - Materials physical properties for the experimental gas-solid system

The bench was filled with alumina up to a bed height of 263 mm, corresponding to a total mass of approximately 9.5 kg. From the fluidization curve of our experiments (not reported here) a minimum fluidization velocity (U_{mf}) of 0.055 m/s was found. Only one value of superficial velocity corresponding to 3.5 times the U_{mf} was used to simulate the bubbling regime. This value, calculated as a ratio between the flow discharge (measured by the electronic flow meter) and the cross sectional area of the cylinder, was selected in order to ensure a vigorous fluidization regime while avoiding being too close to the upper limit of the electronic unit reading (to avoid potential inaccuracies).

5.3 PHYSICAL MODEL, PARCELS SYSTEM GENERATION AND PRINCIPLE EQUATIONS

Our real system includes gas and solid particles mixed together in an enclosed cylindrical vessel (Figure 5.1). With the air velocity exceeding a critical value (U_{mf}) bubbles generate

at the very bottom and moving upwards tend to grow and coalesce. In this work the CFD model aimed at reproducing the PSD distribution of pressure oscillations induced by bubbles motion inside the bed. The computational costs of describing the singular particle motion (in such a multi-million particle system) would be prohibitive and in order to cope with this technical limitation, some simplification were adopted. Specifically, in order to reduce the total number of equations to be solved inside the numerical system, the "parcels" concept was exploited. A parcel is an artifice allowing regrouping many single particles in one sphere, which is tracked inside the system as if it was a point with a mass equal to the total mass of all the particles contained inside. By doing so the total number of equations to be solved is drastically reduced with great benefit for simulation performances. The number of parcels targeted was controlled by changing their size and consequently, the number of particles per parcel. The ratio between the parcel over the particle diameter is computed and used to ensure the respect of two important aspects. First, it avoids the presence of empty spaces between particles (inside each parcel) which allows to achieve a good match between the simulated and experimental bed height at rest (a certain gap will always be present due to the fact that parcels are considered as perfect spheres while real particles present irregular shapes). Secondly, this coefficient allows a perfect scale up of drag forces and consequently a reliable dynamic behaviour of the parcels system, which in spite of their mass are fluidized as much as single particles. The CFD model used in this work, similarly to TFM approach, also requires extra equations to work as a closure, which can be provided by the constitutive/rheological laws for granular flow. The latter are obtained by applying the kinetic theory of granular flows (KTGF) to account for the particle-particle collision forces. The general form of the equations employed in this DDPM-KTGF model are the following:

Gas phase continuity equation

$$\frac{\partial}{\partial t}\alpha_g \rho_g + \nabla \cdot \alpha_g \rho_g \vec{u}_g = 0 \tag{5.1}$$

Where α_g is the volume fraction of phase g (here gas), ρ_g its density and $\vec{u}_g$ the corresponding velocity vector.

Gas phase momentum equation

$$\frac{\partial}{\partial t}\alpha_g \rho_g \vec{u}_g + \nabla \cdot (\alpha_g \rho_g \vec{u}_g \otimes \vec{u}_g) = -\alpha_g \nabla P + \nabla \cdot \alpha_g \bar{\bar{\tau}}_g + \alpha_g \rho_g g + K_{gs}(\vec{u}_g - \vec{u}_s) \quad (5.2)$$

With P representing the gas-solid shared pressure inside the system, g the gravity and K_{gs} the solid-gas drag factor ($Kg\, m^{-3} s^{-1}$). The gas shear stress tensor is given by:

$$\bar{\bar{\tau}}_g = \mu_g(\nabla \vec{u}_g + (\nabla \vec{u}_g)^T) + (\lambda_g - \frac{2}{3}\mu_g)\nabla \vec{u}_g \cdot I \quad (5.3)$$

Particles motion and collisional model

As mentioned previously, particles are embedded inside parcels and these latter are tracked within the Eulerian frame according to a Lagrangian description of their motion. The driving equation is the second Newton`s law:

$$\frac{d}{dt}\vec{u}_p = K_{gp}(\vec{u}_g - \vec{u}_p) - \frac{g(\rho_p - \rho_g)}{\rho_p} + \frac{\nabla \bar{\bar{\tau}}_s}{\alpha_s \rho_p} - \frac{\nabla P_s}{\alpha_s \rho_p} \quad (5.4)$$

Where α_s is the volume fraction of the solid phase as resulting by an averaging process of the discrete parcels volume within each cell and $\vec{u}_s$ (m/s) is the corresponding average velocity (Figure 5.2).

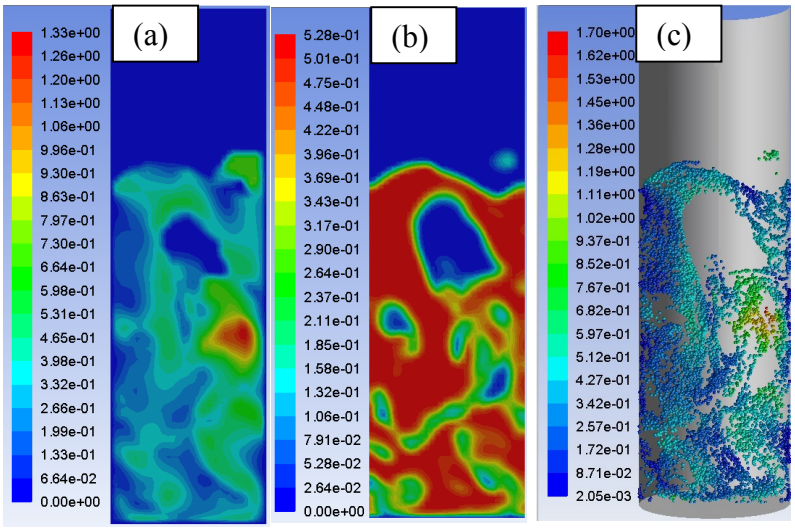

Figure 5.2 – Solid velocity magnitude (a), solid fraction map (b) and parcels tracking map (c) colored by velocity magnitude, where the first two maps (a,b) are obtained as averaging process of parcels volume and their velocity

According to the KTGF approach the particle force interaction is modeled throughout the last two terms of eq. (5.4). These terms are yet accounted for this Lagrangian equation despite having been prior computed in the Eulerian frame (namely cell by cell in the mesh grid chosen to discretize the physical domain). This procedure makes of the DDPM-KTGF a hybrid approach to solid particles modeling. The use of the KTGF theory requires defining a series of properties and closures to characterize the granular flows and ultimately the interaction forces established among particles.

The solid shear stress tensor is defined as:

$$\bar{\bar{\tau}}_s = \mu_{s,tot}(\nabla\vec{u}_s + (\nabla\vec{u}_s)^T) + (\lambda_s - \frac{2}{3}\mu_s)\nabla\vec{u}_s \cdot I \tag{5.5}$$

Where the viscosity coefficients include the combination of different terms:

$$\mu_{s,tot} = \mu_{s,col} + \mu_{s,kin} + \mu_{s,frict} \tag{5.6}$$

$\mu_{s,tot}$ is the total solid shear viscosity resulting from the summation of three different components, which are described below and are correspondingly the collisional [59], kinetic [76] and frictional [77] components of the total sheer stress as derived from the KTGF theory.

$$\mu_{s,col} = \frac{4}{5}\rho_s d_s g_{o,ss}(1+e_{ss})(\frac{\Theta_s}{\pi})^{1/2}\alpha_s{}^2 \tag{5.7}$$

$$\mu_{s,kin} = \frac{10\rho_s d_s\sqrt{\Theta_s\pi}}{96(1+e_{ss})g_{o,ss}}\left[1+\frac{4}{5}g_{o,ss}\alpha_s(1+e_{ss})\right]^2 \tag{5.8}$$

$$\mu_{s,frict} = \frac{P_s \sin\Phi}{2\sqrt{I_{2D}}} \tag{5.9}$$

Where α_s represents the solid-averaged (from parcels position) volume fraction, Θ_s $(m^2 s^{-2})$ the granular temperature, $g_{o,ss}$ the radial distribution [80], $d_s\,(m)$ the solid particle diameter (Sauter), P_s the total solid pressure (below the expression from Lun et al [81]), P_{frict} its frictional component [79], λ_s the solid bulk viscosity [81] accounting for

the resistance of the granular flow to compression and expansion and lastly e_{ss} the restitution coefficient that expresses the ratio between the particle speed after and before collisions. The mathematical description of these variables is given in the following:

$$\Theta_s = \frac{1}{3}\left\langle \vec{u}_s' \cdot \vec{u}_s' \right\rangle \tag{5.10}$$

$$g_{o,ss} = \left[1 - \left(\frac{\alpha_s}{\alpha_{s,\max}}\right)^{1/3}\right]^{-1} + \frac{1}{2}\alpha_s \tag{5.11}$$

$$\lambda_s = \frac{4}{3}\rho_s d_s g_s (1+e_{ss})\left(\frac{\Theta_s}{\pi}\right)^{1/2} \alpha_s{}^2 \tag{5.12}$$

$$P_s = \alpha_s \rho_s \Theta_s + 2\rho_s (1+e_{ss})\alpha_s{}^2 g_{o,ss}\Theta_s + P_{fricts} \tag{5.13}$$

$$P_{fricts} = Fr\frac{(\alpha_s - \alpha_{s,\min})^2}{(\alpha_s - \alpha_{s,\max})^5} \tag{5.14}$$

The Kinetic Theory of Granular Flow [59],[76],[81] links the total kinetic energy of a group of particles randomly moving inside a system to their fluctuating velocity throughout the granular temperature. This variable, representing an unknown of this system, requires an extra conservation equation to be solved. This transport equation derived from kinetic theory takes the form

$$\frac{3}{2}\left[\frac{\partial}{\partial t}(\alpha_s \rho_s \Theta_s) + \nabla\cdot(\alpha_s \rho_s \vec{u}_s \Theta_s)\right] = (-p_s I + \bar{\bar{\tau}}_s) : \nabla \vec{u}_s + \nabla\cdot(k_{\Theta_s}\nabla\Theta_s) - \gamma_{\Theta_s} + \Phi_{gs} \tag{5.15}$$

More details for each term's formulation can be found in [100]. In order to speed up simulations, this last equation was solved in its algebraic form where the contributions of convection and diffusion are neglected. In fact, as also remarked by Cloete and Amini in their work [68], in dense bubbling bed the local generation and dissipation are predominant as compared to convection and diffusion and granular temperature is varying mainly as a result of friction and inelastic collisions. Along with granular temperature, the radial distribution function (eq. 5.11) works as a correction factor to account for the collisional probability between grains when the solid phase becomes dense. There is a significant

difference between the two drag coefficients defined in equations (5.2) and (5.4) (respectively K_{gs} and K_{gp}). While K_{gp} is computed for each parcel and used in their Lagrangian motion equation as part of a forces balance, the former is evaluated in the Eulerian frame, namely per each cell, by summing over the drag forces of each single parcel accounted in each cell. K_{gp} can be described by different mathematical formulations and in this work, a proper user defined function (UDF) was implemented to apply the parametric Syamlal-O'Brien drag law [60] to the DDPM scheme since Fluent 16.2 does not provide this drag law among the default inbuilt formulations when the DDPM scheme is selected. There are several types of drag laws already implemented within the software's environment and some of them are more suited to describe particular systems and conditions (ranging from more diluted to dense beds). In general, the drag law depends on a drag coefficient (*Cd*), which in its turn depends on the local relative velocity between phases and the void fraction. This coefficient depends as well on other factors such as particle size distribution, particle shape, etc. However, it is difficult to characterize the void fraction dependency for any conditions other than for a packed bed or for infinite dilution (single particle model) [86]. In order to bypass this lack of crucial data, some authors attempted to exploit the experimental minimum fluidization velocity of their own system as a calibration point. As an example, *Syamlal and O'Brien* (1987) introduced a method to adjust drag law using the U_{mf} of their system [60]. This approach is based on a special correlation between a single and a multiple-particle systems under settling condition which leads to an accurate estimation of drag coefficient for any volume fraction condition inside the bed. This calibration requires the empirical knowledge of the U_{mf} together the bed`s void fraction at the onset of the fluidization regime. For completeness, our model sensitivity analysis also comprises a drag law comparison, to test the full 3D model accuracy, using the software-inbuilt Gidaspow drag formulation. Besides this numerical test all other simulations have been performed using the UDF customized drag (parametric Syamlal O'Brien), which proved a superior predictability of the bed PSD.

5.4 NUMERICAL SIMULATIONS AND SET UP

The system simulated in this work is a virtual but consistent (in size and boundary conditions) representation of the lab-scale bench shown in Figure 5.1. Most of the simulations were run in a 2D planar geometry which was used to schematize the domain of the real system. However the DDPM-KTGF model allows for fast simulations (as compared to the TFM) under certain limitations, such as low number of parcels and relatively coarse mesh refinement, which translates in the possibility of using also the full 3D geometry. The 3D model was used to analyze mesh sensitivity, number of parcels and drag formulation effects. All the numerical simulations were performed using Ansys-Fluent 16.2 and were run on high performance computing (HPC) machines at the University of Sherbrooke (*Mammoth Parallel 2*).

A phase-coupled Semi Implicit Method for pressure linked equations (PC-SIMPLE) was used, which allowed extending the SIMPLE approach to multiphase cases. According to this method, the pressure values were computed for each time step in the cell centers while the velocities components were calculated at each cell interface. In this staggered scheme, velocities and pressure (for the primary phase) were first calculated, then corrected according to an iterative process in order to respect the continuity constraint. Because of the transient formulation of the problem, a bounded implicit second order scheme was adopted for temporal discretization of time derivate variables. A fixed time step of 10^{-4} sec. was chosen for all the simulations, ensuring a stable convergence. The convergence criteria is based on the residual values of the numerical solutions (for each of the unknown variables) solved inside the Eulerian domain. The tolerances on these residuals were set to the default values of 10^{-3} both for the continuity and velocity components. For spatial discretization, a second order upwind method was chosen in order to minimize the numerical diffusion. With regards to the Lagrangian treatment of particles, a 5-th order Runge and Kutta scheme was chosen to integrate Newton's equations ultimately providing the parcel positions and velocities inside the Eulerian grid. Moreover a smoothing procedure was applied to the current set up in order to avoid the discontinuities given by the discrete nature of DDPM model. Gradients of solid fraction, granular temperature and the velocity itself are used by the KTGF to compute the interactions forces (last two terms of eq. 5.4), which might be significantly

affected by these discontinuities. In order to avoid this circumstance a node-based averaging procedure was exploited as part of the numeric setup offered by the software.

5.5 RESULTS & DISCUSSION

The time-averaged pressure drop as well as the continuous time-pressure signals, cannot fully and univocally characterize the dynamic behaviours of a bubbling multiphase system, since the former is only a physical quantity representative of the bed mass and while the latter an expression of a stochastic event. Kage et al. [90],[91] revealed the presence of three different peaks in the spectrum of pressure oscillation and, above all, he was able to experimentally link them to the bubble generation, eruption and natural oscillation of the fluidizing bed (as a whole). The location of these three principle phenomenon and related peaks (in the frequency domain), along with their intensity, are contributing to the specific growth of the integral PSD function. Given a certain set of operating conditions, the PSD function contains the whole history of pressure fluctuations inside the bed, and consequently represents a key measurement and reference to assess the accuracy of the CFD model and his numerical sensitivity. Consequently, our model sensitivity analysis and validation was based on the spectrum analysis of pressure drop fluctuations which, for a sufficient time scale (as explained in section 5.5.1), provided a scientific characterization of the bed's dynamic. Once the CFD and experimental pressure drop signals were obtained, the power spectral density (PSD) of these signals were calculated to show the frequency distributions of time-pressure drop fluctuations. To this purpose a Fast Fourier Transform (FFT) was applied to the original signal, cutting the first 2 seconds of each simulation in order to exclude the initial transitory behaviour. After this first step, an integral calculation of the PSD distribution was computed, aiming at showing the cumulate frequency growth which was carried out to ease the reading and interpretation of the PSD distribution itself. Moreover, according to the physical meaning of this integral, it was also possible to obtain complementary information about the total "energy" reached by the original signal (in time), which is strictly related to its variance. This value represents an useful indicator of the bubbling vigor since it relates to the peaks in the frequency spectrum which in their turn are affected by the fluctuations amplitude.

Despite the experimental bench having a total height of 40 " (see Figure 5.1) only 20 " were simulated in the CFD model (see Figure 5.4) in order to reduce computational time. This geometrical simplification was adopted in light of some preliminary CFD tests, showing that solid particles (even in presence of major bubbles) were not dragged further than this level.

5.5.1 Experimental tests to evaluate the dependency of PSD distribution on time.

The time-pressure drop signal showed random pressure fluctuations because of the intrinsic stochastic behavior of bubbles. Therefore the results of different tests, repeated under the same operating conditions, were most likely to be different each time. Because of this variability, an alternative strategy is logically to be searched in order to univocally trace the "fingerprint" of bubble formation and motion. To this purpose, the signal was processed using *Fast Fourier Transform* (FFT) algorithm to obtain a frequency spectrum distribution and its corresponding integral (over the frequency domain), which are no longer specific to the singular experiment. However, in order to gain a good PSD resolution, the time scale of these experiments had to be wider as compared to the one required by the single bed oscillation, which is comparable to the choice of a representative sample size in statistics. In this work, experiments with different duration were carried out and results were plotted altogether in order to assess the importance of time scale on the pressure drop statistics and PSD growth. A good agreement was found between a 40 sec. and 5 min. experimental tests (with comparable PSD integral curves, not reported here) suggesting this time scale to be used also as CFD flow time. This way it was possible to ensure an optimal compromise between outputs data reliability (representativeness of bubbling fluctuations) and simulation performances.

5.5.2 Fixed regime

In order to tests the accuracy of this numerical model, over a different range of superficial velocity, the CFD model was run in the fixed regime to assess its numerical ability to reproduce the linear part of the fluidization curve and compared the predicted U_{mf} with empirical one. In fact this type of analysis was principally aimed to assess whether or not

the empirical value of U_{mf} used in the CFD simulations (as one of two calibration points for our customized drag law) could also have been properly predicted by the model. Nevertheless it was found that the model is unable to evaluate any reasonable value of pressure drop in this regime. Specifically and as shown in Figure 5.3, the DDPM-KTGF model predicts a distribution of total pressure (for the primary phase) comparable to the hydrostatic pressure that would be generated under the assumption of the solid phase being a liquid. Moreover it was found that the model is totally insensitive to the air superficial velocity in the 0 to Umf (whose value of 0.055 m/s was recovered from the empirical fluidization curve) range. In addition, an unphysical behavior of the overall system of parcels was also observed. While moving downward to the very bottom of the bench they also overlap to an unreliable extent. Such observation inspired caution in using this model to simulate packed bed, since it may not be suitable to predict the right particle force interactions. Specifically in dense regime, when the bed is well settled, the repulsive contact forces between solid particles depend only on the gradient of solid granular pressure (see eq. 5.4 and 5.13) where the only non-zero term is the frictional component of the solid pressure) being the shear stress tensor gradient equal to zero (because solid velocities are nearly null). In such case the model fails to predict the repulsive forces, whose magnitude should balance gravity, causing the parcels unphysical overlapping. This model limitation was found to be in agreement with Chen and Wang [66] findings, who highlighted how the DDPM-KTGF failed in accounting for the volume exclusion effect, which also resulted in the unphysical parcels overlapping in the dense region of the domain, as a result of an over-simplified treatment of particle-particle interactions. More investigation is required to verify whether it is possible to find a different numerical set up to round this problem, thus avoiding this unphysical circumstance. From this understanding, the KTGF approach is not recommendable to study fixed regime and in general high packed beds where, instead, the DEM approach would be more suitable (as a Lagrangian model of dense particle system).

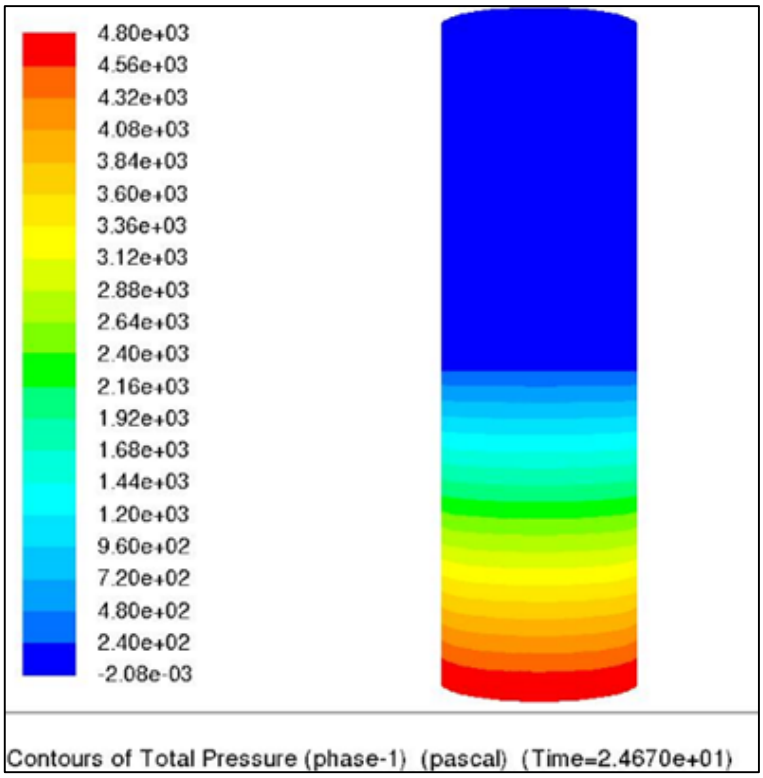

Figure 5.3 – Map distribution for the air (primary phase) total pressure obtained by setting U0=0 m/s: this result highlighted the impossibility of exploiting DDPM-KTGF approach (to fixed regime) as a result of its inaccurate particle-particle interactions evaluation in dense regimes

5.5.3 Bubbling regime

The principle target of this CFD model was to reproduce the PSD distribution of pressure oscillations induced by bubbles motion inside the bed. Numerous studies have investigated the coupling between bubbles dynamics and pressure fluctuations as a convenient way to characterize the transient behavior of a bubbling multiphase system, from the early works published by Davidson and Harrison [29] up to more recent studies [55], [61], [92]. Qingcheng et al. [94] explained the physical origin of pressure fluctuations throughout the observation of a single bubble (produced by pulsed gas method) moving upward in a gas-solid fluidized bed. Pressure fluctuations across the bed are greatly influenced by gas velocity because of the drag effect on particles that ultimately reflects on the formation and motion of bubbles [94].

In this work the parametric Syamlal and O'Brien law was used and this drag formulation was implemented via User Define Function (UDF), compiled and hooked inside the model.

The use of this drag law was supported by preliminary CFD tests, which later became an important part of the model sensitivity, revealing its superior capability, in matching the bed hydrodynamic behavior and pressure drop fluctuations (both recorded in the experiments), as compared to what was predicted by using the Gidaspow (inbuilt) formulation. Moreover this choice was also justified and supported by the hybrid nature of this DDPM numerical approach which, along with the exploitation of the KTGF theory used to account for particle interactions, make the whole model comparable to the TFM approach. Despite a lack of works based on the DDPM-KTGF model and focusing on the effect brought by different drag formulations, literature still presents some valuable information based upon the TFM approach. Different authors [62], [63], using a TFM model, found the parametric Syamlal O'Brien drag formulation to provide more accurate results of pressure drop and bed expansion. A value of U_o = 0.2 m/s, corresponding namely to 3.5 times the minimum fluidization velocity (*Umf*) was used as boundary condition for the CFD simulations of the bubbling regime. A no slip condition was set for the primary phase at the wall while reflect condition was set for particles all over the boundary (walls, inlet and outlet).

More details about the solid phase properties and mathematical formulation as set in the CFD model (for the bubbling regime) can be found in Table 5.2.

Phase-Material	Properties	Units	Model
Allumina (granular)	Granular temperature model	-	Phase property
	Particle Diameter	µm	190
	Granular viscosity	kg/m-s	Gidaspow
	Granular bulk viscosity	kg/m-s	Lun-et-al
	Frictional viscosity	kg/m-s	Shaeffer
	Frictional pressure	Pascal	Based KTGF
	Frictional modulus	Pascal	Derived
	Granular temperature	m^2/s^2	Algebraic
	Solid pressure	Pascal	Lun-et-al
	Radial distribution	-	Lun-et-al
	Elasticity modulus	Pascal	Derived

Table 5-2 - Mechanical properties of solid phase mathematical formulation used in the CFD model (Ansys/Fluent) to simulate the gas-solid system

Besides the characterization of bubbling bed throughout the pressure drop fluctuations, the distribution of the phase volume fractions inside the bed is crucial and often used as a key

validation point [62],[65]. However visual observation of the stochastic evolution of flow patterns (bubble, cluster, channeling phenomenon etc...) inside the experimental bench is rather challenging. This is also limited to wall proximity without any chance to evaluate what occurs deeper inside the system body. Moreover, under fluidization regime, the bubbles move really fast and their presence close to the wall is unpredictable. The presence of a thin layer of dust between bubbles approaching the reactor wall and the PVC wall itself further complicates the visual analysis. Despite these limitations, the use of a commercial video camera revealed to be helpful for a basic and overall assessment of the real system hydrodynamics to be compared to CFD outputs. In order to perform such comparison, 100 frames (pictures) per second were saved during simulations and afterwards put together to form a video whose speed was tuned to perfectly match the flow time simulation with the "real" empirical time.

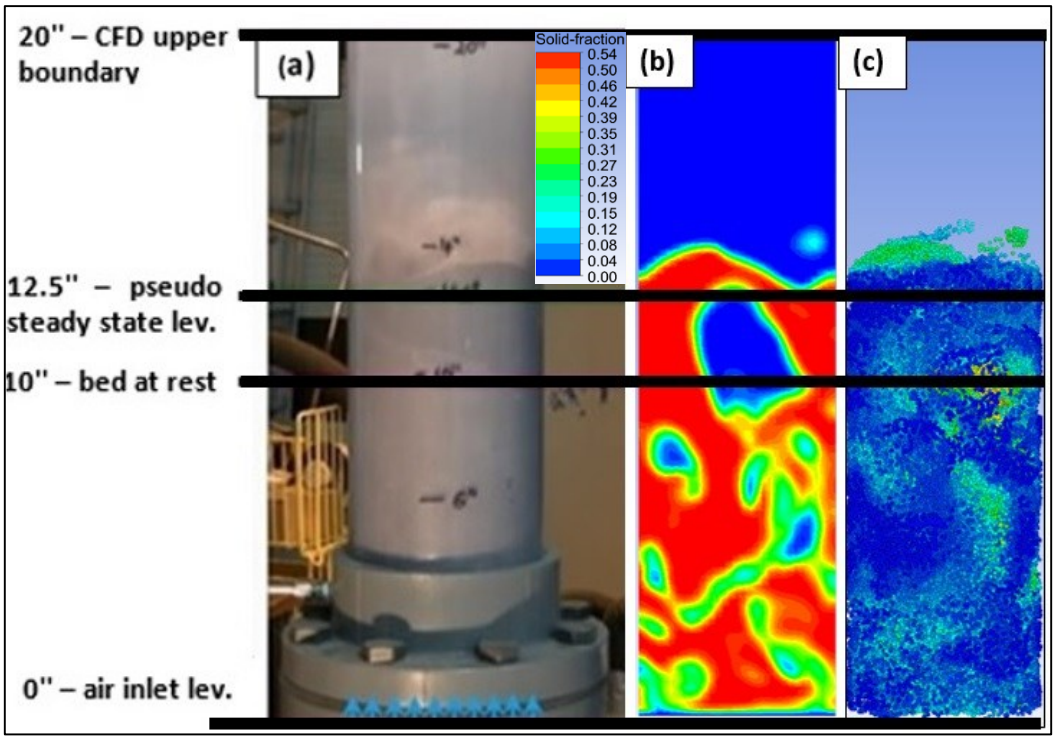

Figure 5.4 - Dynamic visual analysis of the bubbling regime where (a) is the experimental bench reactor, (b) is the 2D cross section of the 3D-DDPM and (c) is the 3D parcels distribution (colored by velocity magnitude, see color-bar in Figure 5.5)

Even though this was only a purely qualitative assessment, the video comparison between CFD and experiments revealed some interesting similarities in the hydrodynamic behavior of bubbles eruptions and mass oscillations. It was also noticed that in all simulations the model was generally predicting a smaller bed expansion in a sense of a lower pseudo state

level of fluctuations as compared to the experiments (Figure 5.4). This may be due to the approximate particle collision forces computed by the model that ultimately results in a too high level of overlapping between parcels (Figure 5.5).

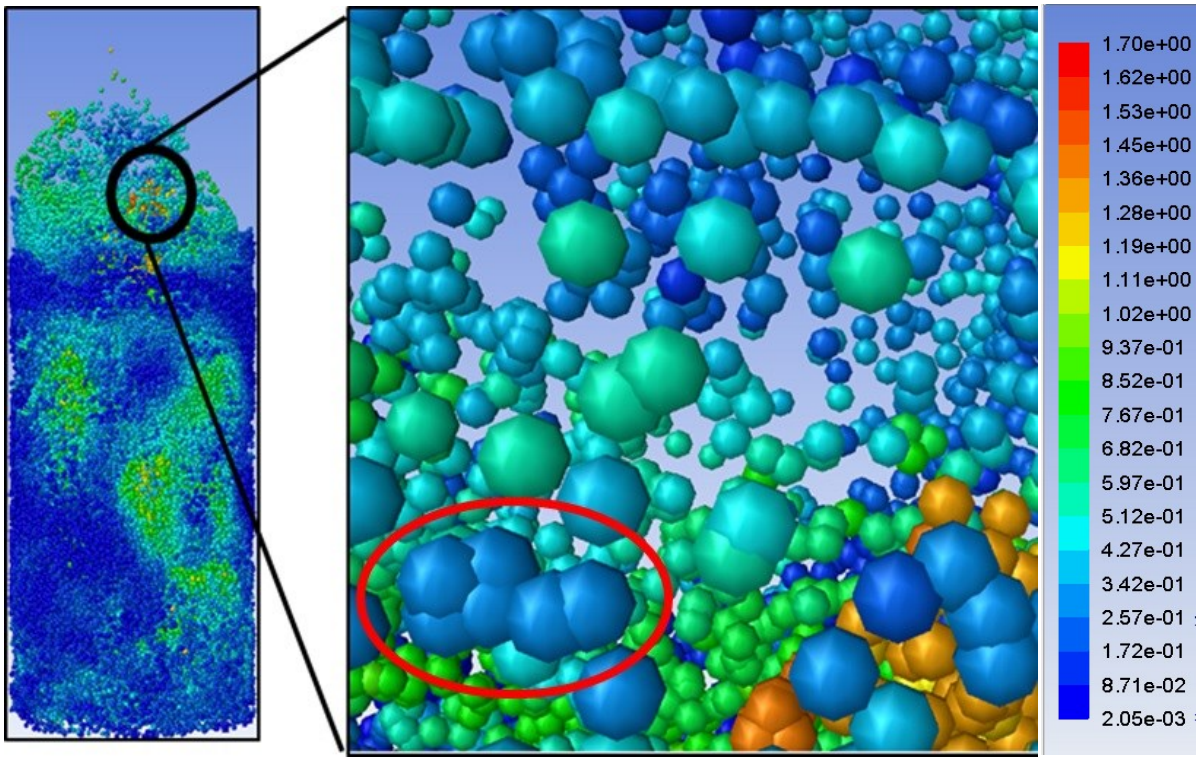

Figure 5.5 – Snap shot of parcels distribution during a simulation in the bubbling regime highlighting the exaggerate overlapping between parcels (colored by their velocity) which resulted in a clustering effect (depicted inside the red circle)

To this regard, a more accurate validation could be obtained following the installation of a proper optical probe system, combined with the utilization of a high performance camera. The latter would allow capturing bubbles details that could be processed downstream throughout an image analysis algorithm to compare the empirical and simulated bed features.

5.5.4 2D and 3D Model sensitivity

Mesh size

Results were here obtained by varying the mesh size of the model, starting from an identical set up based on the mechanical solid properties reported in Table 5.2 and the numeric schemes defined in section 5.4. The number of parcels in the CFD model was fixed to

109.034 units, which was generated with a parcel diameter of 3.5 mm. For the 2D model, the mesh sizes used were 7.62 mm. and 3.81 mm., 1.905 mm., corresponding respectively to 40, 20 and 10 times the particles mean diameter (190 μm) for a total of 1333, 5333 and 21333 square cells. The choice of the exact mesh size was made in order to obtain a precise discretization of the geometry, thus avoiding any cut of cells within the grid while using multiple values of particles size (which is often used as a reference in this gas-solid multiphase system when assessing the mesh grid effect on numerical solutions [58], [56]). For the 3D model, however only two mesh size have been investigated corresponding to 24857 (7.62 mm.) and 81600 cells (5.08 mm.). Table 5.3 and table 5.4 as well as Figure 5.6 and Figure 5.7 show the results obtained for this study.

Δtime 2-40 sec.	Time aver. α_g	Time aver. ΔP(Pa)	Min. (Pa)	Max. (Pa)	Variance $(\boldsymbol{Pa^2})$	Signal energy $(\boldsymbol{Pa^2})* \boldsymbol{10^5}$
2D – 7.62 mm.	0.631	4049	1921	7168	220856	2.1899
2D – 3.81 mm.	0.607	3882	1949	8401	237970	2.3862
2D – 1.905 mm.	0.608	3905	2304	7288	232153	2.3629
3D – 7.62 mm.	0.662	4159	3480	5120	38600	0.38738
3D – 5.08 mm.	0.621	4084	3025	6043	111361	1.0855
EXPERIMENTAL		3965	1916	6322	204544	2.051

Table 5-3 - Comparison between the main statistical indicators (of time-pressure drop signal) for the empirical data as compared to 2D/3D CFD simulations when modifying the mesh size

Δtime 2-40 sec.	HPC	Total simulation time (hours)
2D – 7.62 mm.	3*	15
2D – 3.81 mm.	5*	25
2D – 1.905 mm.	16	180
3D – 7.62 mm.	24	37
3D – 5.08 mm.	32	122

Table 5-4 - Simulations performances: effect of mesh refinement on the total CFD simulation time
*** Simulations run on local workstation Intel® Core™ i7-3960X CPU@3.30GHz, 64 GB (RAM); all other simulations have been performed on HPC machines (Mammoth Paralle II) as explained in section 5.4**

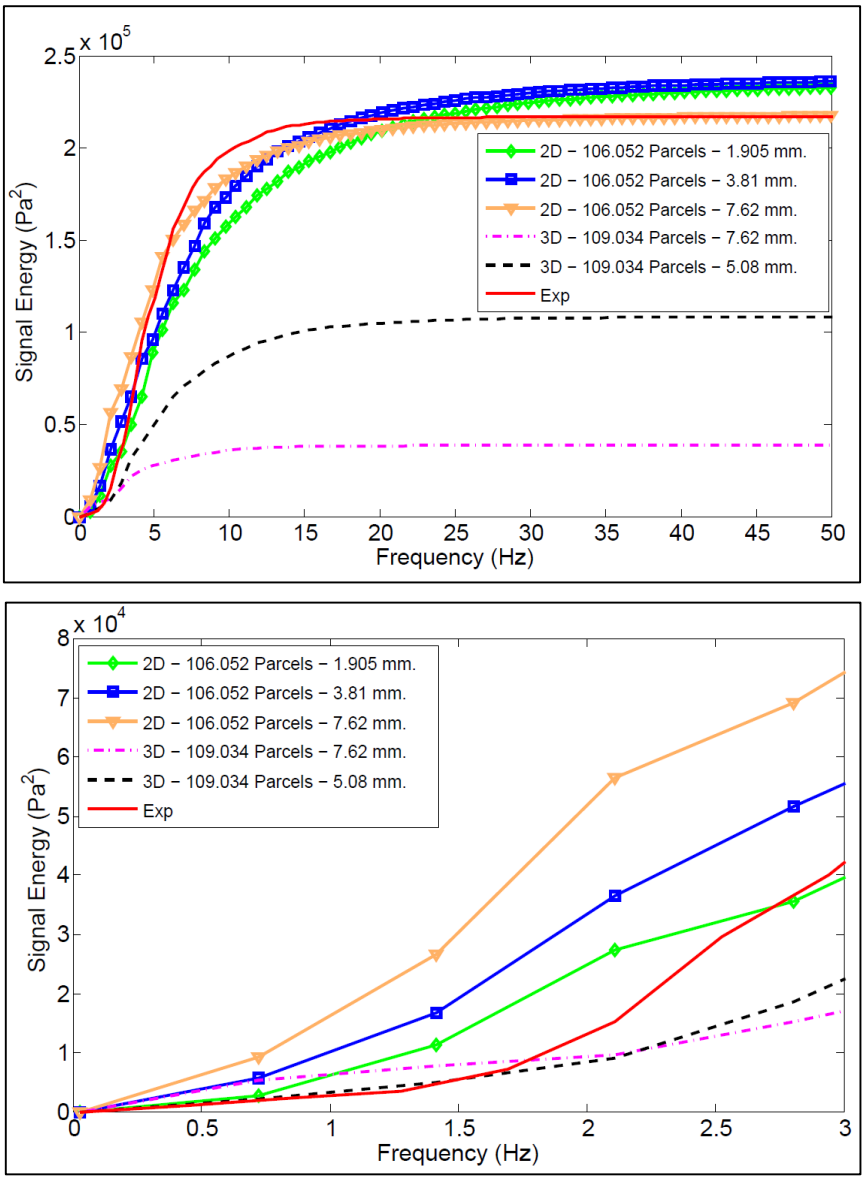

Figure 5.6 – PSD integral curves for 2D and 3D DDPM simulations obtained for different mesh size: above the spectrum in the range 0-50 Hz, below a zoom in highlighting the closer match, in the 0-2Hz range, between the experiments and CFD when the 3D model with finer mesh is used.

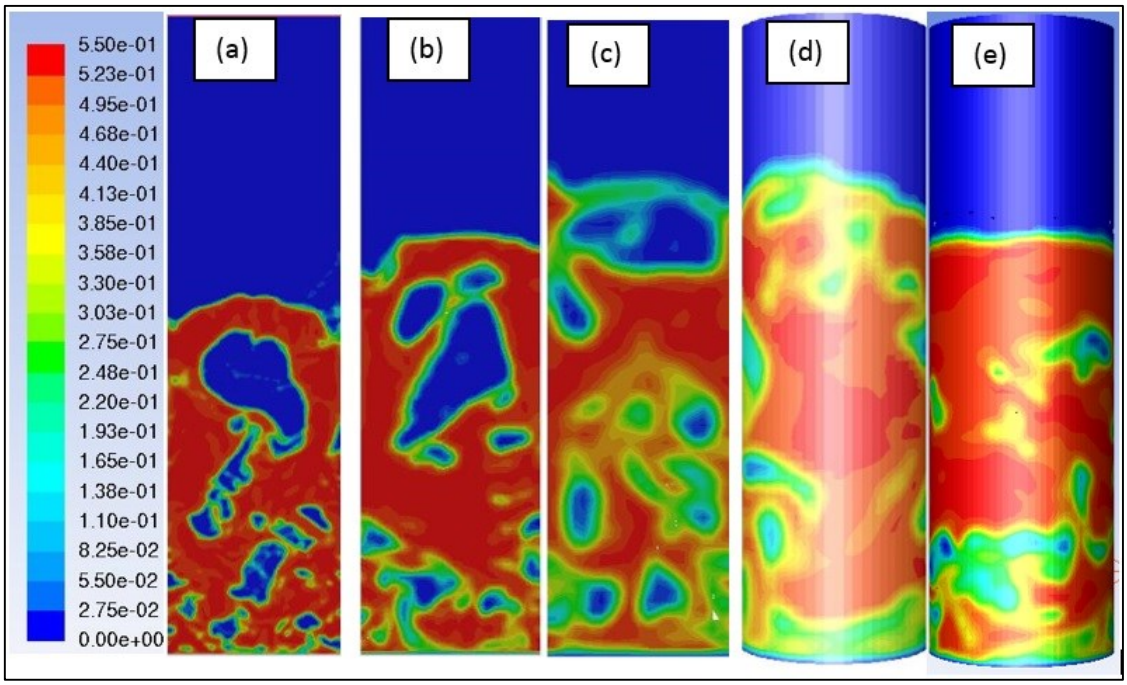

Figure 5.7 – Mesh refinement effect on the predicted CFD solid map distribution of the bubbling bed: from the left to the right the 2D-1.905 mm. (a), 2D-3.81 mm.(b), 2D-7.62 mm.(c), 3D-7.62 mm.(d), 3D-5.08 mm.(e)

These results seem to confirm the significant sensitivity of this DDPM-KTGF model with regard to the mesh size. The Lagrangian approach to particles tracking should not be affected by numerical diffusion errors induced by the Eulerian mesh size since the particles positions are tracked in the Lagrangian frame. However there are still two main reasons why this grid independency is not reached by the DDPM-KTGF model when the mesh size varies. First, since the model is hybrid, the primary phase is still solved over the Eulerian grid. Secondly the KTGF approach used to model the particle particle interactions required an averaging process to transport some of parcels properties to the Eulerian frame and this caused a numerical error linked to the cell size where the parcels are placed. For this reason, given a certain distribution of parcels inside the numerical domain, refining the mesh should help increasing the level of accuracy in estimating the solid phase fraction map within the Eulerian grid. Given a certain mesh size, the solid fraction distribution is computed starting with the volume occupied by all parcels, cell by cell. This value is mapped at the center of the cell then used to compute the gradients required for example inside the shear stress tensor. This process can cause very sharp gradients, which can lead to numerical instabilities. Refining the mesh, as said, may help to round up this problem at costs of significantly longer

simulations. In order to avoid such circumstances a node based averaging process has been used in order to ease the convergence of numerical solution. This numerical strategy allowed smoothing out sharp gradients of solid fractions (as well as other parcels properties such as velocities) by distributing the parcels volume over the neighboring nodes according to their position inside various cells since some of them might be placed inside two or three different cells at the same moment. Even though this numerical "trick" is deemed to help reducing the grid dependency of DDPM simulation, the presented results are still showing a significant mesh impact on the numerical solution. The comparison between the 2D and 3D model for the same coarsest mesh size tested in this study (7.62 mm.) could provides a noteworthy information. In this case, the 3D model proved to be more negatively impacted by numerical diffusion as confirmed both by the weaker PSD growth (Figure 5.6) and the solid map distribution (Figure 5.7) with the contours of bubbles (blue zones) hardly captured. One possible explanation is the different number of parcels per cell unit used in the two different cases. At this regard, to rule out any possible impact of number of parcels per number of cells in 2D and 3D cases, a 3D simulation with 3.500.000 parcels was run in order to conserve the parcels/cell ratio but as reported in the following paragraph (parcels number) no specific improvement was noticed.

By comparing the results shown above and taking into account previous findings reported in literature [28], [56], [58] the 1.905 mm. squared mesh (corresponding approximately to 10 times the Sauter diameter of particles) was selected as the value for ensuring the numerical solution convergence and hence suitable for the model sensitivity analysis. This meshing led to an averaged solid fraction convergence (computed as a surface time-averaged integral for a certain bed height, i.e 8 cm. in this study) as well as to the convergence of the averaged pressure drop.

Further consideration seems to be appropriate when it comes to choose a proper mesh size depending on the type of application and numerical outputs used for validation. Some authors [41] had to select a coarse mesh (in the magnitude of 1000 times their mean particle diameter) in order to exploit the DDPM-KTGF model for industrial boiler application. Cloethe et al. [69] carried out 2D simulation on grids spanning from 4 cm to 16 cm and concluded that their model based on the coarser mesh (corresponding to more than 100 times their particle diameter) could be exploited at industrial scale, providing reliable results when

compared to experimental data and also a convergence into CFD outputs as found when using finer meshes. In their study however the authors used only extrapolated data of averaged pressure drop and did not perform any spectrum analysis of bubbles fluctuations (which are more likely representative of the bed dynamic behavior). By comparing the current DDPM results in terms of bubbles shape resolution (see first two pics of Figure 5.7) and averaged pressure drop data (Table 5.3) it was observed that results achieved on the coarser grid (3.81 mm.) were quite comparable to the ones obtained for the finer one (1.905 mm.). However, the comparison of the related PSD pressure drop fluctuations exhibited some divergences. Table 5.4 shows the increasing computational costs of mesh refinement with important differences between a 3.81 mm. and 1.905 mm. (using 2D model). A similar circumstance was found for the 3D model where, despite an increase of HPC exploited, the simulations run on a 5.08 mm. performed four times slower than ones run on a 7.62 mm. mesh. It is therefore evident that the correct assessment of the mesh size is critical in order to achieve accuracy, while limiting the duration of simulations but remains strictly subjected to the specific type of variable outputs than authors intend to study.

Parcels number

As for the mesh study, both the 2D and 3D geometry were exploited to investigate the impact of parcel numbers on the related PSD distribution, hoping to achieve a better model accuracy as it was increased. The variation of bubble contours and displacement inside the bed were also compared (not reported here since no significant variation was found). For the 2D model, based on a 1.905 mm. square mesh, the parcels injection was generated from inside the software by setting the number of particles per parcels to be used. For the 3D model instead the parcel injection was created based upon the choice of their diameter. In this case the 3D study was performed on the coarser mesh (0.3 in) given the exponential increase of CPU demand with mesh size refinement (see table 5.4). In both cases a vital precaution is to generate parcels whose volume is always smaller than any cells inside the Eulerian mesh to avoid numerical instabilities. Results are reported in Table 5.5.

Δtime 2-40 sec.	Time aver. ΔP(Pa)	Min. (Pa)	Max. (Pa)	Variance (Pa^2)	Signal energy $(Pa^2)* 10^5$
2D – 53.000 Parcels	3901	2183	6460	231000	2.2868
2D – 109.034 Parcels	3905	2304	7288	232153	2.3629
2D – 530.260 Parcels	3885	2082	8049	218888	2.2398
2D –1.060.520 Parcels	3895	1615	8424	245514	2.4550
3D – 109.034 Parcels	4159	3480	5120	38600	0.28869
3D – 530.260 Parcels	4202	3482	5018	30716	0.38738
3D – 3.520.895 Parcels	4202	3260	4907	32678	0.24550
EXPERIMENTAL	3965	1916	6322	204544	2.051

Table 5-5 - Comparison between the main statistical indicators (of time-pressure drop) for the experiment and 2D/3D CFD simulations (varying the number of parcels)

Δtime 2-40 sec.	cores	Total simulation time (hours)
2D – 53.000 Parcels	32	133
2D – 109.034 Parcels	32	146
2D – 530.260 Parcels	32	158
2D –1.060.520 Parcels	32	350
3D – 109.034 Parcels	24	35
3D – 530.260 Parcels	24	41
3D – 3.520.895 Parcels	32	88

Table 5-6 - Effect of parcels number on the total CFD time performance including both 2D and 3D simulations

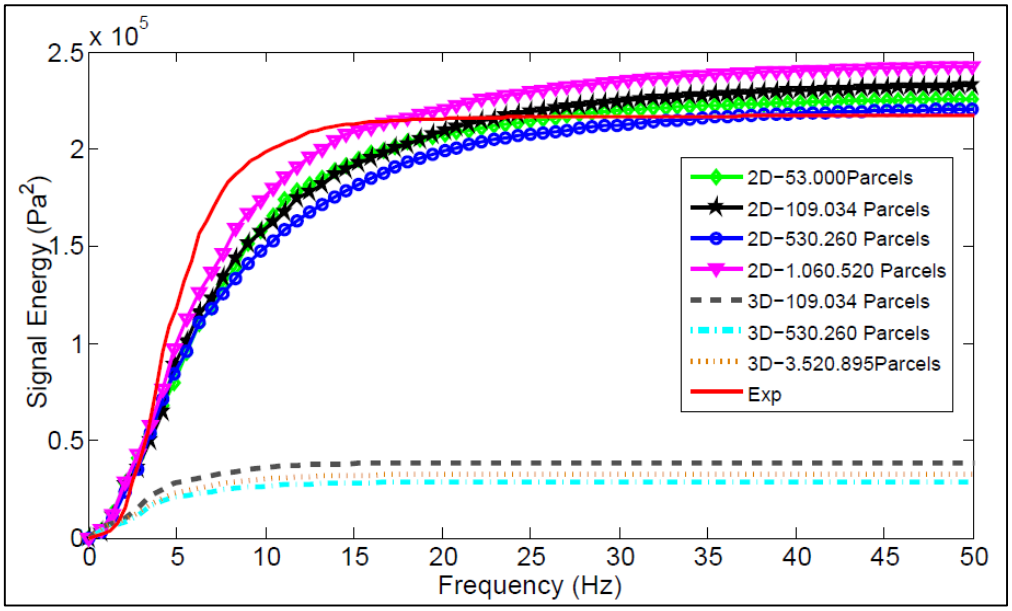

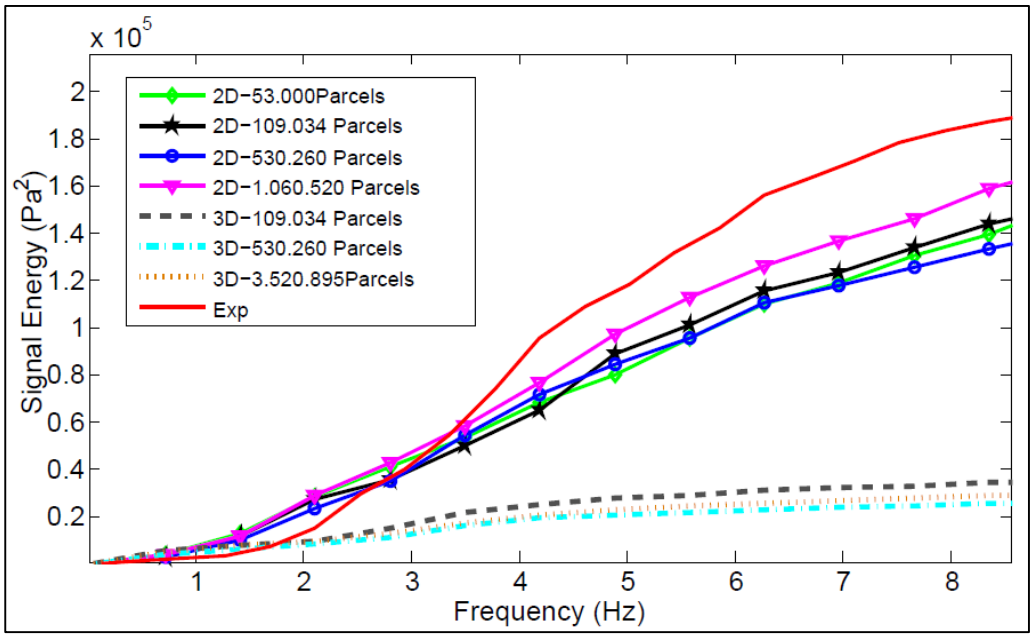

Figure 5.8 – PSD integral curves for 2D and 3D DDPM simulations obtained varying the number of parcels to describe the particles system: above the spectrum the range 0-50 Hz and below a zoom in 0-8 Hz range, where the poor sensitivity of the model to this parameter is observed, in both his 2D and 3D version

Differently from the initial expectations, neither the 2D nor the 3D model (see Figure 5.8), a significant effect of this parameters on the model accuracy was noticed, at least in the range of parcels number here explored. Both classes of simulations (2D and 3D observed separately) presented in fact similar curves all over the spectrum of frequency. So, according to the results presented in this work, this represent a significant finding since it could allow reducing the simulations costs (Table 5.6) while preserving the model results. However, given the importance of mesh refinement on the model accuracy (see previous section), it will be interesting to assess its related impact on model sensitivity as far as the number of parcels is regarded. For this reason the number of parcel effect will be investigated using 3D simulations, on a finer mesh, as part of a future work.

Restitution coefficient

This parameter quantifies the loss of energy due to the particles collisions, which impacts the momentum equation for the solid phase in equations (5.7),(5.8),(5.12),(5.13). In this work, 2D simulations were repeated using five different values of this parameter, in the range 0.5-1. The results are compared in table 5.7 and figure 5.9.

Δtime 2-40 sec.	Time aver. ΔP(Pa)	Min. (Pa)	Max. (Pa)	Variance (Pa^2)	Signal energy (Pa^2)* 10^5
2D – e_{ss}=0.5	2637	554	6404	752577	6.268
2D – e_{ss}=0.75	3878	2276	7781	248703	2.473
2D – e_{ss}=0.9	3901	2183	6460	231000	2.286
2D – e_{ss}=0.98	3885	2210	6384	230767	2.314
2D – e_{ss}=1	3850	1595	7533	373078	3.551
EXPERIMENTAL	3965	1916	6322	204544	2.051

Table 5-7. Comparison of the main statistical indicators (of time-pressure drop) for the Experiment and CFD 2D-simulations (changing the restitution coefficient - e_{ss} values)

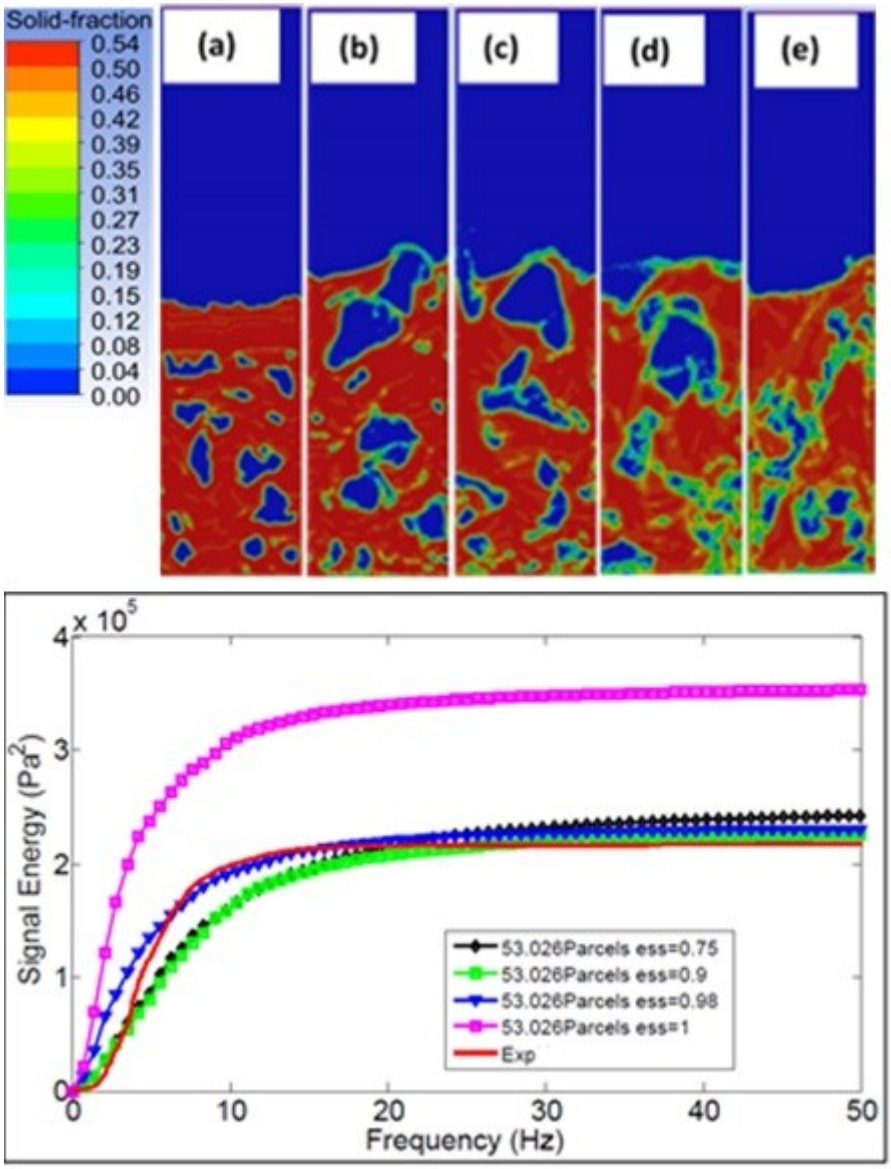

Figure 5.9 – Effect of restitution coefficient on the predicted hydrodynamic: above, solid volume distribution (take at 5 sec. flow time) for different ess values 0.5(a), 0.75(b), 0.9(c), 0.98(d), 1(e); below the PSD integral of CFD simulations and the experiment (continuous red line)

The outputs corresponding to ess = 0.75, 0.9, 0.98 showed a comparable PSD final energy value. However, when set with a value of 0.98, the model gives an important overestimation of the curve growth in the first part of the spectrum (see Figure 5.9). The simulation performed with ess=0.5 showed numerical convergence issues after 10 sec and an unreliable behavior of bubbles who appeared highly fragmented without showing any coalescing behavior (Figure 5.9-a). On the opposite, the simulation performed under the hypothesis of ideal collision (ess=1, Figure 5.9-e) greatly overestimated the experimental PSD curve all over its frequency spectrum. This last simulation also showed the highest variability in term of signal variance and distance between the minimum and maximum values registered (see Table 5.7). Channeling effect (see Figure 5.9-e) and wider bubbles (not displayed in this snap-shot but whose size was very close to reactor diameter which we did not observe in the video of the experiments) were also predicted in this case. From these results was concluded that a representative value of restitution coefficient should be set in the range 0.75-0.9 for this specific type of particles.

Kinetic contribution to total viscosity

The effect of the kinetic contribution to the total viscosity (on the model results) was also investigated using 2D model, varying its related formulation from Gidaspow (default) to Syamlal O'Brien [76] which were both provided as options within the software. This parameter (equation 5.8) influences the total granular viscosity (equation 5.6) and ultimately affects the shear stress tensor magnitude (equation 5.5). The two formulations converge in the high density regime, while showing significant divergences in the dilute one [78]. Given the stochasticity of the bubble behavior it is impossible to pre-emptively assess the evolution of the granular regime inside the bed, and for this reasons both formulations were tested. Principle statistical indicators are reported in Table 5.8.

Δtime 2-40 sec.	Time aver. ΔP(Pa)	Min. (Pa)	Max. (Pa)	Variance (Pa^2)	Signal energy (Pa^2)* 10^5
Gidaspow	3901	2183	6460	231000	2.362
Syamlal O'Brien	3883	2418	6734	244453	2.443
EXPERIMENTAL	3965	1916	6322	204544	2.051

Table 5-8 - Comparison of the main statistical indicators (of time-pressure drop) both for the empirical and CFD 2D-simulations (changing the formulations for kinetic viscosity - $\mu_{s,kin}$)

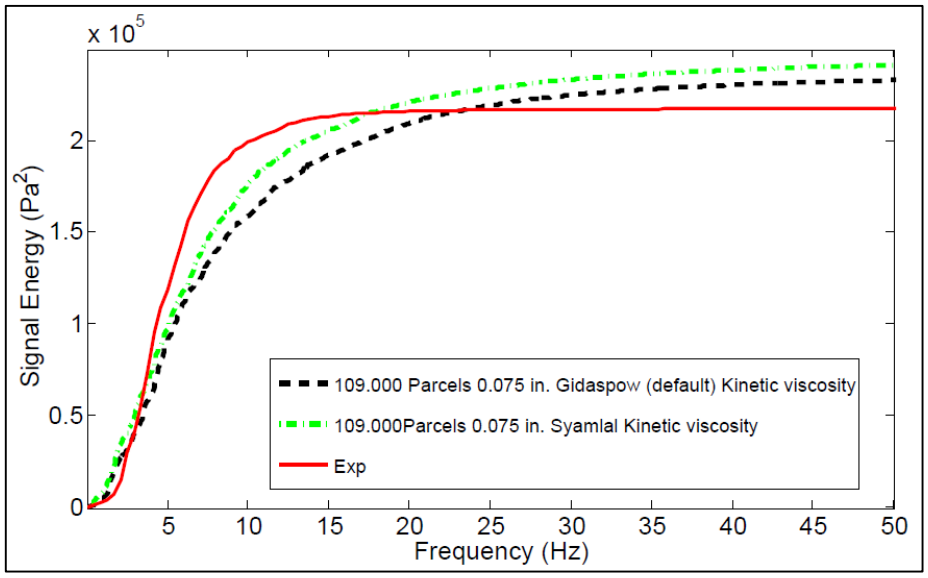

Figure 5.10 - PSD cumulative trend both for the experiment and CFD 2D-simulations results based upon a different kinetic viscosity formulation

The results seem to highlight a small sensitivity of the DDPM model with regards to the kinetic viscosity parameter. From the observation of Figure 5.10 it seems that the only difference is a slight increase (all over the spectrum and more marked after 7.5 Hz) of the signal energy when using the Syamlal kinetic viscosity, which makes the PSD integral of this simulation closer to the experimental one. The validity of these results remained anchored to the use of 2D planar geometry. Future extension of this model may include a similar test, although extended to a full 3D geometry from which a different conclusion might arise.

Radial distribution

The radial distribution function is a parameter used to modify the probability of particle collision depending on their density inside the bed (eq 5.11). This function can vary substantially with the solid fraction [78] impacting on other terms such as solid pressure (eq. 5.13), solid bulk viscosity (eq. 5.12) and kinetic/collisional component of total viscosity (eq. 5.7 and 5.8). There is not an unique formulation for this function in literature and among the various options, the Syamlal O'Brien model [76] was tested which, for high solid

concentration, differs more significantly from the the Lun. et al. expression (provided by default within the software).

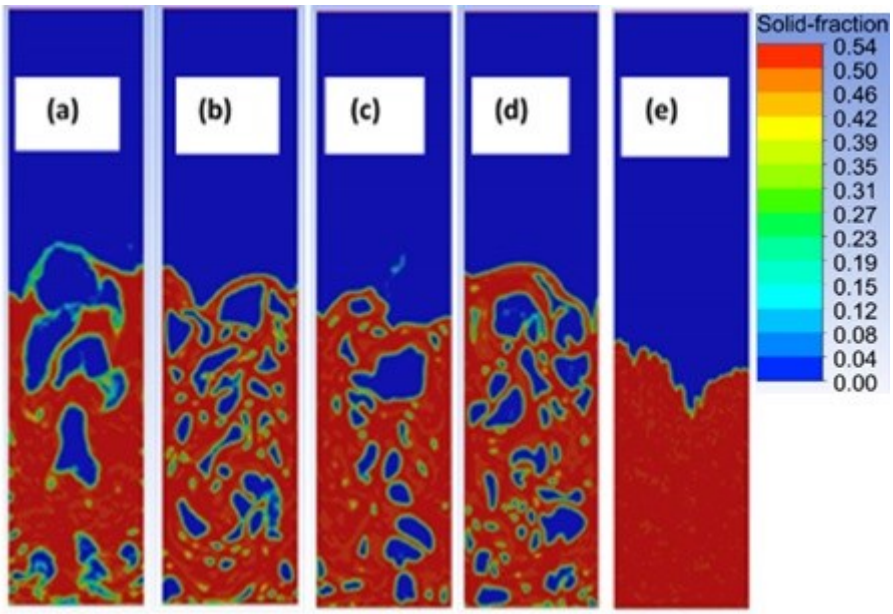

Figure 5.11 – Solid fraction distribution taken during the 2D-simulation performed with Syamlal O`Brien radial distribution at 2 sec. (a), 6 sec. (b), 9 sec. (c), 12 sec. (d), 18 sec. (e)

The Syamlal formulation did not permit achieving a reliable prediction of bubbles distribution (as shown in Figure 5.11). Starting with a pre-existent data file (whose solid map distribution is depicted in Figure 5.11-a) related to a simulation based upon Lun.et al (default option inside the software) radial distribution, the formulation was switched to Syamlal and the simulation continued converging for around 10 seconds (Figure 5.11-(b)-(c)-(d)). After 12 sec the convergence criteria were not met any longer and the whole results went wrong as shown by the unrealistic solid fraction map (Figure 5.11(e)). In the converging period, bubble displacement appeared highly fragmented. Video animation also confirmed the absence of coalescing/breaking process of bubbles, which instead behaved as singular entities hence contradicting the well-acknowledge natural behavior of bubbles inside fluidized beds [28], [55], [56].

Solid Pressure

Various formulations of the solid pressure were also tested using 2D model. The gradient of the solid pressure, along with the shear stress tensor gradient, was ultimately used by the model to compute the particle repulsive forces (eq. 5.4). This variable is a measure of the pressure exerted on the containing wall due to the presence of particles and, along with the shear stress tensor, contains all the parameters describing the intrinsic nature of granular flows. In literature, there is not a clear convergence on the best expression to be used for bubbling fluidized beds [62], [86]. Consequently, the model sensitivity to this granular property was tested using the default Lun. et al. expression [81] that incorporates the kinetic and collisional effect, and Ma-Amhadi expression [98] that also embeds the frictional viscosity effect.

Δtime 2-40 sec.	Time aver. ΔP(Pa)	Min. (Pa)	Max. (Pa)	Variance (Pa^2)	Signal energy (Pa^2)* 10^5
Lun. et al. (default)	3901	2183	6460	231000	2.362
Ma-Amhadi	3907	2275	7142	232116	2.323
EXPERIMENTAL	3965	1916	6322	204544	2.051

Table 5-9 - Comparison of the main statistical indicators (of time-pressure drop) both for the experiment and CFD 2D- simulations (changing the formulations for the solid pressure term – Ps)

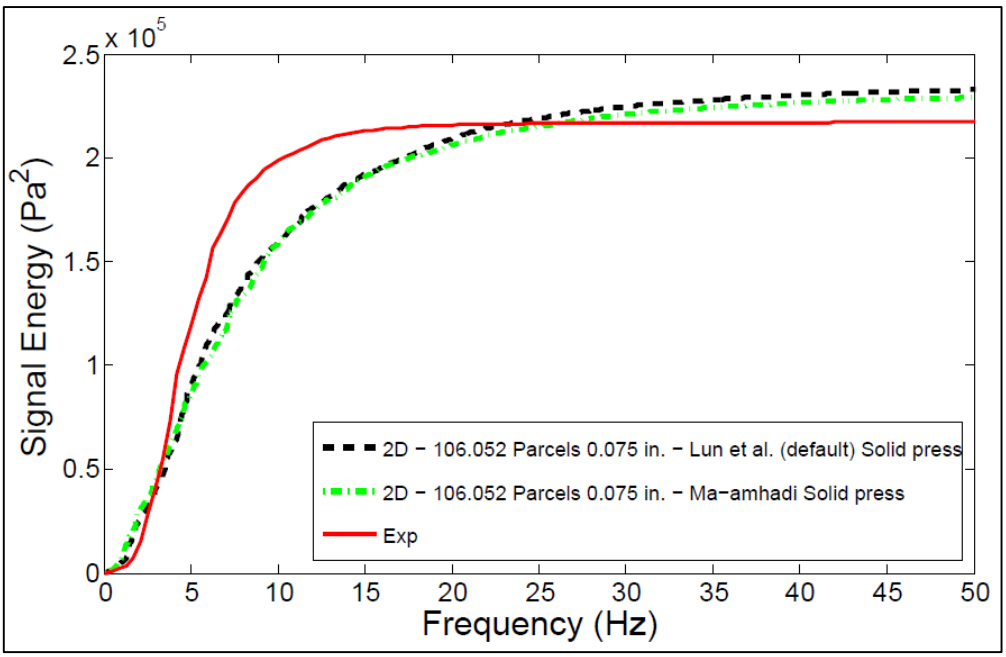

Figure 5.12- PSD cumulative trend both for the experiment and CFD simulations results based upon two different solid pressure expressions

As shown in Figure 5.12, comparable results were obtained for the two CFD simulations with an almost perfect overlapping of the two curves all over the spectrum. Only in a small window between 5 and 10 Hz could some small differences be noticed. This result may seem surprising since major contribution to particles momentum exchange arises from collisions (in the dilute part of the bed) and above all from particles friction in the denser zones (accounted by Ma-Amhadi formulation throughout the frictional viscosity). However in the KTGF model (the same as in the TFM approach) the frictional viscosity is derived from the frictional pressure, which in its turn is only based upon the solid fraction distribution inside the bed, and not on the real properties of solid particles (their static, dynamic and rotational frictional components that can be defined when using a DEM approach). The importance of including a proper closure for particles friction, including also the rotational effects, has been very thoroughly explained and justified by Jang et al. in their recent TFM work [99].

Drag Law

An important results was obtained when using two different formulations to account for the gas drag effect on the particles system. The link between the gas and particles assumes a prime role for the cold bubbling system up to the point of strongly impacting the bed expansion as well as his dynamic behavior (see Esmaili and Mahinpey work [62]). At this purpose we compared the Gidaspow [59] and the parametric Syamlal-O'Brien formulation [60] for which a proper UDF had to be coded and hooked inside the CFD model. In section 5.3 the main features of this parametric drag formulation were discussed and with its superior capability to predict the bed expansion and pressure drop fluctuations can also be found in open literature [62], [63], [86].

Simulations have been performed in a full 3D geometry on a 5.08 mm. hexahedra mesh. Since a weak sensitivity with regards to parcels numbers was found (previously discussed) it was decided to limit this drag test to the minimum number of parcels (relatively speaking to this study, i.e 109.000 units) in order to speed up our simulations. Table 5.10 shows the pressure drop principle indicators obtained with different drag laws while Figure 5.13 and Figure 5.14 depicts the post processing comparison of solid fraction maps (parcels tracking), and the PSD integrals respectively.

Δtime 2-40 sec.	Time aver. ΔP(Pa)	Min. (Pa)	Max. (Pa)	Variance (Pa^2)	Signal energy $(Pa^2)* 10^5$
Syamlal (UDF)	4084	3025	6043	111361	1.085
Gidaspow (Inbuilt)	3946	2712	5402	69434	0.680
EXPERIMENTAL	3965	1916	6322	204544	2.051

Table 5-10 - Comparison of main statistical indicators (of time-pressure drop) for the experiment and CFD simulations (changing the formulations for the drag-law)

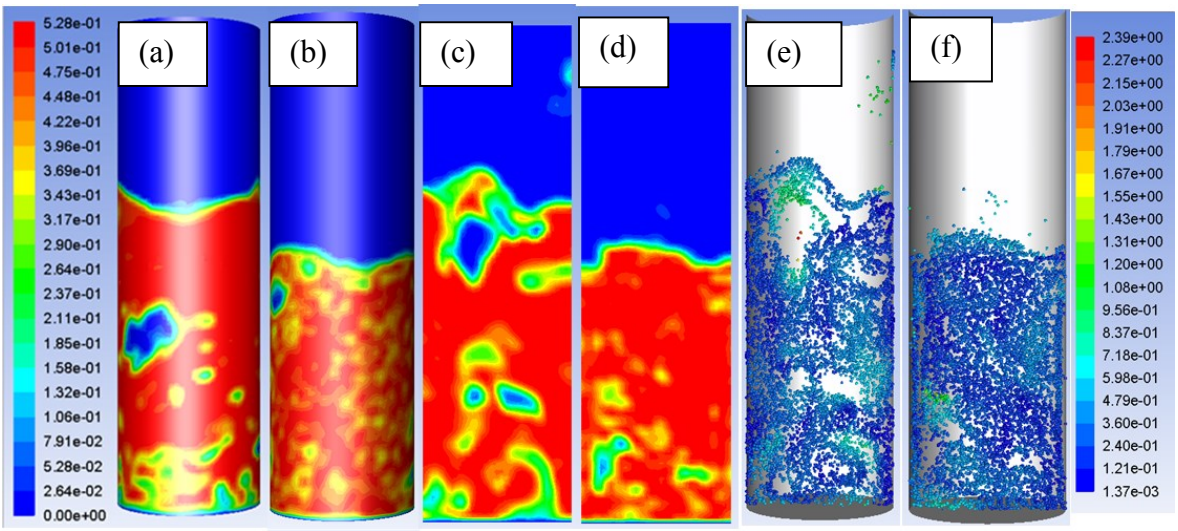

Figure 5.13 – Comparison between the parametric Syamlal O'Brien (UDF) and inbuilt Gidaspow drag laws at 40 sec: From the left to the right, side by side, the solid fraction map in full 3D geometry (a-b), solids fraction map middle cross plane (c-d) and related parcels distribution colored by velocity magnitude (e-f)

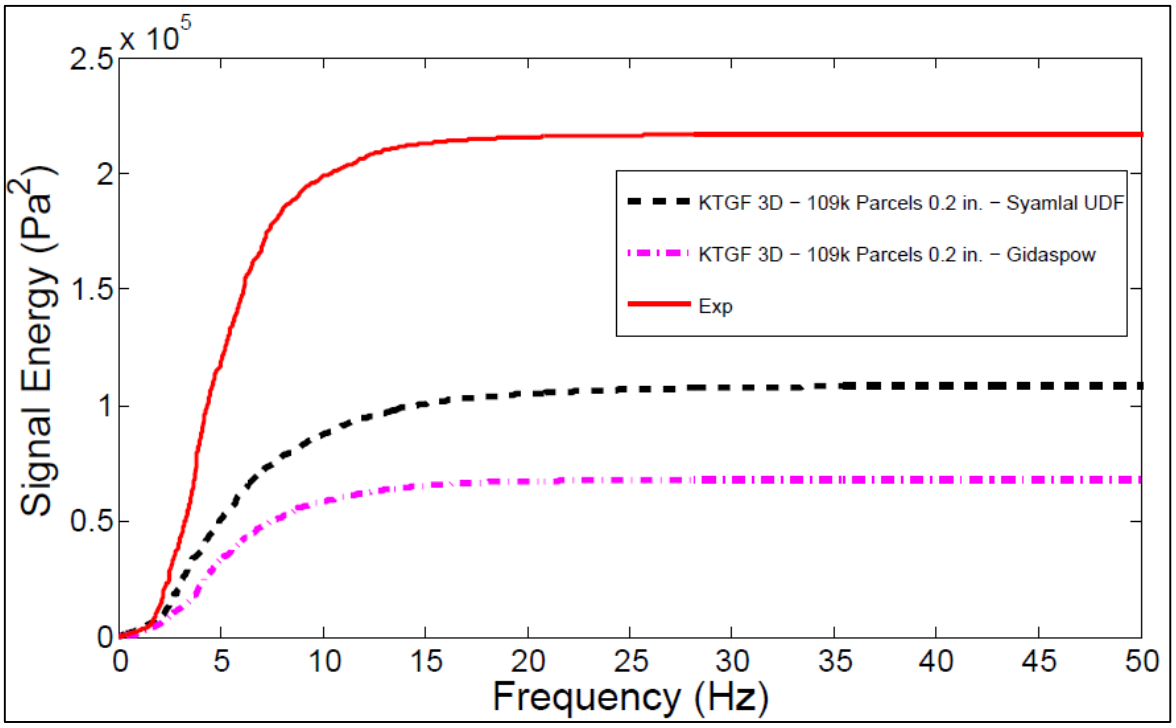

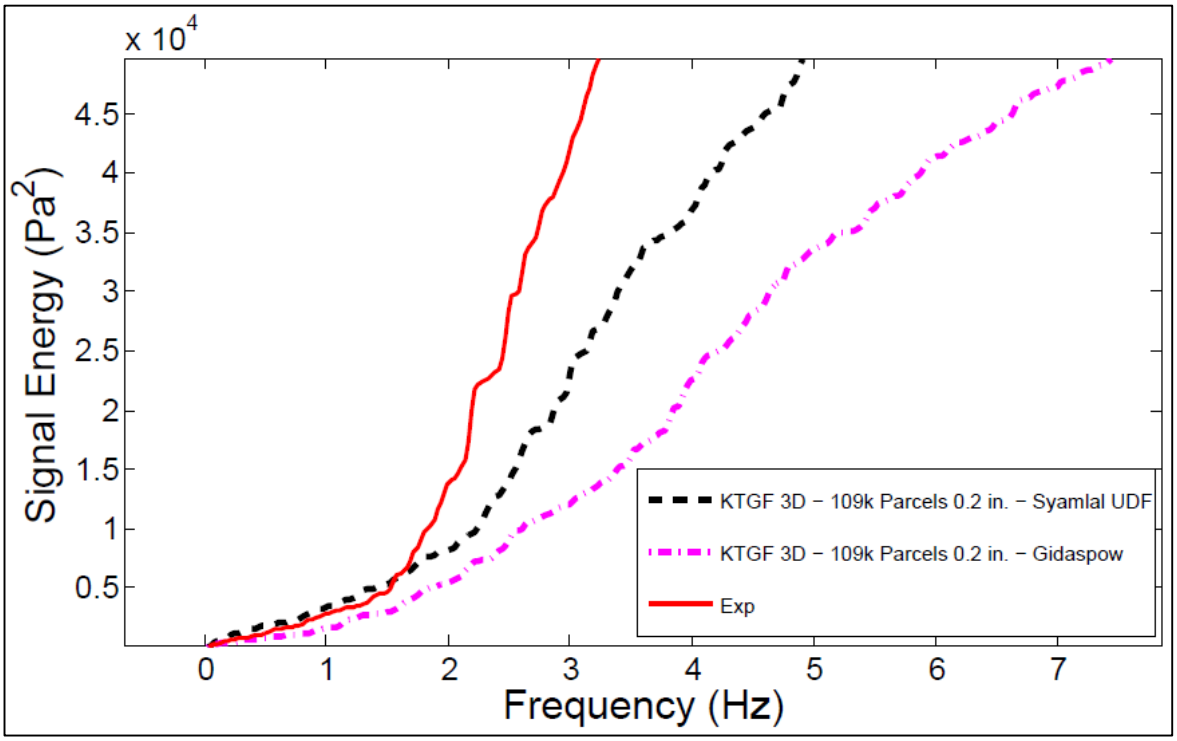

Figure 5.14 - PSD cumulative trend for the experiment and three CFD simulations based upon two different drag-law formulation: Above spectrum in the 0-50Hz, below a zoom in the first part, showing the better accuracy of parametric Syamlal drag.

The analysis of these results supported what previously found by Esmaili and Mahinpey [62] and Vejahati et al. [86] in their TFM works, namely a superior capability of the parametric Syamlal O'Brien drag law in predicting the bed expansion and the PSD integral as result of a more vigorous regime of bubbles inside the bed. This results is significant but not particularly surprising considering that the TFM and the KTGF version of DDPM are very similar in the granular flow property description as well as in the way the repulsive forces (of solid particles) are computed. In both models, there is an identical set of properties and mathematical formulations to be set (within the software) which can be appreciated in Table 5.2. Also the drag formulation is quite identical and the difference between the two model lies in the averaging process for the DDPM scheme. For each time step (during the simulation) the drag force exerted by the fluid on each parcel affects the parcel trajectory and velocity (eq. 5.4). In the following time step, starting with the singular velocity of each parcel, the solver is estimating, cell by cell, an average value as representative of the solid phase velocity (seen as a continuum inside the cell) to be used for the drag term inside the momentum conservation equation for the primary phase (eq. 5.2). The significance of this

result derives instead from another the following considerations: bubbles shape and motion are the macroscopic results of pressure and velocity field of the gas (primary phase) found as a solution of his governing equation. The momentum conservation for the gas is strongly affected by the drag term and so the solution of the equation itself where this term is present (eq. 5.2). Pressure drop fluctuations are directly linked to bubbles displacement as Vega et al. highlighted in their work [61] and thus the PSD analysis of these fluctuation becomes implicitly a way to estimate the accuracy of the solution for the gas phase. The closer match to experimental PSD (Figure 5.14) reached by the Syamlal- UDF drag simulation is evident all over the frequency spectrum, as well as the total signal power (Table 5.10) that was found to have increased as much of 35 % as compared to the simulations run with the Gidaspow drag law. As shown in Figure 5.13, and as could be observed on related video animations (here not shown), when the Gidaspow drag is used, bubbles present a slower and less clear-cut formation, as compared to the other case run with the parametric Syamlal drag. Blue zones corresponding to 100% air fraction are formed at higher level and do not have the time to grow and coalescence, ultimately resulting in a weaker overall fluidization behavior and bed expansion.

5.6 CONCLUSIONS

In the present study, the cold fluid-dynamic of a multiphase bubbling system was investigated using an Eulerian-Lagrangian Dense Discrete Particle Model (DDPM) coupled with the Kinetic Theory of Granular Flow (KTGF). The experimental setup comprises of a transparent PVC cylindrical body filled with inert Geldart group B particles and homogeneously fluidized with a porous plate. The pressure drop fluctuation across the bed was very representative of its bubbling behavior and consequently the (frequency) power spectrum distributions (PSD) analysis was used both to test the CFD model sensitivity as well as to assess his accuracy with regards to the empirical data. The model was found to be mesh dependent because of his hybrid conception and the effect of mesh size was analysed. The DDPM-KTGF model was not found suitable to describe the fixed regime, where the high density of solid phase proved the KTGF theory to be far away from his field of application. In this circumstance the model strongly underestimate the particle repulsive contact forces leading to an unreliable overlapping extent. The number of parcels, in the

range tested in this study, did not affect significantly neither the shape nor the final signal power of PSD curves whilst impacting on the simulation performances. Both the effect of the solid pressure term and kinetic viscosity seemed to be quite irrelevant in 2D simulations. More insight into their effective contribution, along with the number of parcels, is expected by using 3D simulation on a finer mesh. Two different formulations for the radial distribution functions were tested whose results showed the poor suitability of Syamlal O'Brien model in predicting a plausible bubbles behavior. The model showed a quite important sensitivity to the restitution coefficient with bubbling behavior becoming more vigorous with higher values of this parameter. From the observation of present results this parameter should be set in the range 0.75-0.9 for alumina powder. Finally the drag law impact on the model accuracy was investigated comparing two different formulations. The parametric Syamlal O'Brien drag law provided a superior accuracy while the use of the Gidaspow formulation resulted in an underestimation of bubbling vigour as also confirmed by related PSD integral curve. Confirming what found by Peirano et al. in their work [55], the 2D model could be considered as a fair representation of the bed behaviour in terms of expansions, bubble shape and size as well as in predicting the averaged pressure drop across the bed. Divergence with the experiment arose mainly in the first part of the spectrum (in the range 0-3 Hz, independently from the specific formulation used for various parameters) most likely because of the three dimensionality of bubbles. A great improvement was achieved by using a 3D full geometry approach, whose PSD matched very closely the empirical one in the first 2.5 Hz, namely where the 2D model showed major limitations. The DDPM-KTGF CPU-performance was observed to be strongly affected by the chosen mesh size. This aspect seems to limit the possibility to employ this model to industrial scale, at least for this type of analysis (PSD), even though the choice of the mesh size remain anchored to the specific variable analysis or data to be predicted.

Acknowledgement

The authors are grateful to the Industrial Research Chair on Cellulosic Ethanol and Biocommodities of the Université de Sherbrooke and especially its sponsors: The Ministère de l'Énergie et des Ressources Naturelles du Québec (MERNQ), CRB Innovations, Enerkem and Éthanol GreenFIeld Québec Inc. The authors are also grateful to MITACS for Leonardo Tricomi and Dr Tommaso Melchiori's grant and finally Compute Canada for having made

possible to perform most of the simulations throughout high performance computing (HPC) machines at the Université de Sherbrooke (Mammoth Parallel 2).

Notation

d_s diameter of particles in the solid phase, m

e_{ss} restitution coefficient between colliding particles of solid phase

$\vec{g}$ vector representation of acceleration due to gravity, 9.81 m/s^2

$g_{o,ss}$ radial distribution function between particles of solid phase

K_{gs} momentum exchange coef. between gas and continuum solid phase, kg m^{-3}s^{-1}

K_{gp} momentum exchange coefficient between gas and single parcel, kg m^{-3}s^{-1}

$\dot{m}_{pq}$ mass flow rate from the generic phase p to the generic phase q, kg m^{-3}s^{-1}

P_s solid pressure, Pa

P_{frict} frictional component of solid pressure, Pa

$\vec{u}_q$ velocity vector of the generic (gas and solid) phase q, m/s

$\vec{u}_g$ velocity vector of gas phase, m/s

$\vec{u}_s$ velocity vector of solid phase, m/s

$\vec{u}_s^{\,'}$ velocity fluctuation vector of particles, m/s

Greek letters

α_q volume fraction of the generic (gas and solid) phase q

α_g volume fraction of the gas phase

α_s volume fraction of the solid phase

$\alpha_{s,\max}$ maximum packing limit (volume fraction) of the solid phase

Θ_s granular temperature, m^2/s^2

λ_s granular bulk viscosity, Pa*s

μ_g viscosity of gas phase, Pa*s

$\mu_{s,tot}$ total granular viscosity of solid phase, Pa*s

$\mu_{s,col}$ collisional component of total granular viscosity, Pa*s

$\mu_{s,kin}$ kinetic component of total granular viscosity, Pa*s

$\mu_{s,frict}$ frictional component of total granular viscosity, Pa*s

ρ_q density of the generic (gas and solid) phase q, kg m^{-3}

ρ_g density of the gas phase, kg m^{-3}

ρ_s density of the solid phase, kg m^{-3}

$\bar{\bar{\tau}}_g$ stress-strain tensor for the gas phase, Pa

$\bar{\bar{\tau}}_s$ stress-strain tensor for the solid phase, Pa

6 GENERAL CONCLUSIONS

Gasification of biogenic carbon contained in the Refused Derived Fuels (RDF) from Municipal Solid Waste (MWS) is considered as a very promising alternative to incineration and landfilling [9].

Important efforts have been devoted to prove the profitability of MSW gasification on industrial scale, primarily optimizing the fluidized bed configurations [13]. The ability to investigate this complex technology throughout proper numerical platforms can bring a decisive breakthrough in developing a valuable and efficient scaling up to RDF applications [101].

The present study was motivated by the need of investigating the accuracy, sensitivity and performance of different CFD models to investigate a cold lab-scale bubbling fluidized system representative of the real gasifiers unit.

In order to characterize the dynamic behavior of this system, pressure drop data across the bed were first measured and then processed to obtain the corresponding Power Spectral Density (PSD) analysis. The latter was ultimately used to compare the experiments with CFD model predictions.

The first model tested in this work was the TFM because of a broader literature associated to its application to fluidized beds, in addition to its being deemed computationally lighter. The model verification revealed that a fine mesh is required to reach convergence of numerical solutions which ultimately reflected long 2D simulations (in the order of one week) and an even longer time for the full 3D model (approximately two weeks using a super computer). The numerical convergence was found for a mesh size equal to ten times the mean diameter of solid particles, supporting what was already reported in literature [28], [58], [65]. The TFM 2D model achieved a very good agreement with the empirical fluidization curve in the fixed regime while it also matched fairly well the empirical PSD growth and its final integral (indicator of the time-pressure drop fluctuations magnitude and variance). Overall the 2D model was shown to correctly predict the time-averaged pressure drop and its fluctuations amplitude as it emerged from the observation of the statistical indicators. Moreover the post-processing analysis of the 2D simulations revealed a straightforward correlation between the pressure drop and void fraction distribution, confirming the presence of bubbles as the main source of local variation of pressure. A 3D version of the model was also implemented and compared with the 2D model. Despite being based on a “medium” size mesh, the 3D model drastically improved the results over the first part of the spectrum (0-2 Hz), namely where all the previous 2D model simulations failed. The effect of a coarser grid on the numerical PSD was prior assessed allowing to

believe how 3D model results may have been closer to the empirical ones also in the remaining part of the spectrum if a finer mesh was exploited.

Beside the well-developed TFM, a more innovative hence less well-established model approach was used as well in this work. A hybrid Euleran-Lagrangian Dense Discrete Particle Model (DDPM) was implemented to characterize the fluid dynamics of the bubbling bed following the same type of data processing as in the TFM study. When compared to it, the DDPM approach presented important advantages such as the discrete characterization of the solid particle system and also a lower computational requirement. This last aspect is due to the exploitation of parcel concept, which reduces the total number of solid particles to track speeding up the computation of their position and velocities in the Lagrangian frameworks as compared to the analogous computation in the TFM approach. This advantage resulted in the possibility of performing a higher number of 3D simulations to explore more extensively the DDPM-KTGF accuracy and numerical sensitivity. However, similarly to the TFM scheme, this numerical approach was also found to be mesh-dependent and consequently its performance was greatly limited by the respect of a maximum mesh size threshold. This drawback is probably due to the particle collisions which are estimated starting from terms computed on the Eulerian mesh in a similar manner to what accounted by the TFM approach. One major limit was found in applying this model to the study of the fixed regime, where the KTGF theory failed in predicting particle contact forces (and ultimately the volume exclusion effects) which led to an unreliable behavior of the system. A great improvement was achieved using a 3D full geometry approach, whose PSD matched very closely the empirical one in the first 2.5 Hz, namely where the 2D model showed major limitations.

Both models were tested in a similar manner, namely investigating the effect of various parameters/functions formulations (specific of granular flows) as well as inter-phases drag forces on their accuracy, while assessing their performances in view of a potential scale-up. As far as the first class of parameters is regarded, both model showed major sensitivity to a variation of the restitution coefficients even if with some differences. Conversely, while some parameter formulations showed an unsuitable applicability to the model (like for the radial distribution functions investigated with the DDPM-KTGF model), other parameters variation (such as the solid pressure term investigated in both models) did not affect the numerical results significantly, reflecting a relative poor model sensitivity. As a common point, both models were found pretty sensitive to the drag formulation confirming the primary importance of the inter-phase drag momentum exchange in cold gas-solid bubbling systems. Moreover, both the TFM and DDPM-KTGF approach showed that a significant

improvement, in matching the low frequencies part of the experimental PSD (namely in the part of the spectrum that majorly relates to bubbles formation) was possible when a 3D model was used. However in order to run the 3D model, a quite coarse mesh had to be used, which limited the ability for the model to catch up with the empirical PSD growth and its final integral.

Lastly a third numerical model which can more accurately describe the particle collisions (Discrete Element Method, DEM) was implemented and partially investigated at the very end of this PhD work. While some results have been already collected, some other will be needed in order to accurately investigate this Lagrangian model. However the results collected so far seem very promising in the perspective of a potential applicability of this model to industrial applications.

Overall, results obtained from this whole study allowed identifying the predominant barrier in the fine mesh (required for numerical verification and to capture the bubbles contours) which limited the performance of both these two models and ultimately their applicability to industrial scale. For a certain mesh size, a different accuracy between 2D and 3D models was observed when comparing the experiments with simulations based upon the PSD analysis. While from a performance standpoint, only 2D simulations seemed to show the potential applicability to industrial scale, with the possibility of predicting fairly well some important features (the pseudo steady state level of bed fluctuations, bubbles explosion, solid movement), the extent of the related PSD accuracy is questionable. Conversely, 3D models can potentially catch both the tri-dimensional nature of bubbles and their sharp contours (if a fine mesh is used), which is reflected in the closer match between empirical and numerical PSD (clearly evident in the first part of the spectrum), but the expected simulation time for industrial application appears prohibitive. That is why none of these models can provide a straightforward answer to the research question formulated at the end of the introduction especially if the validation analysis relies on PSD analysis. However, these models may still meet the industrial scopes if: a) coarser particles can be used reflecting the possibility to employ a coarser mesh for numerical verification purposes; b) a different type of variable analysis is needed possibly requiring a lower flow time as compared to the one used in this work; c) the study involves macroscopic variables or types of analysis, which do not require very fine mesh to be investigated and correctly predicted.

The focus of this work was put on the investigation of the model accuracy and numerical sensitivity for which only one set of empirical data (corresponding to one set of operating condition) was used as experimental reference. However, a broader spectrum of operating conditions will be necessary in

in order to enforce the validation stage and consequently the robustness of CFD models, which will probably be part of a future investigation.

CONCLUSION

La gazéification des combustibles dérivés refusés (RDF) à partir de déchets solides municipaux (MWS) est considérée comme une alternative très prometteuse à l'incinération et à la mise en décharge [9].

Des efforts importants ont été faits pour prouver la rentabilité de la gazéification MSW à l'échelle industrielle, surtout en optimisant les configurations de lit fluidisé [13]. La capacité d'étudier cette technologie complexe avec des plateformes numériques appropriées pourrait permettre une percée importante dans le développement industriel de la technique pour l'utilisation du RDF [101].

La présente étude a été motivée par la nécessité d'étudier la précision, la sensibilité et la performance de différents modèles CFD pour l'étude d'un lit fluidisé d'échelle laboratoire et non réactif opérant en régime bullant, semblablement aux unités industrielles.

Afin de caractériser le comportement dynamique de ce système, les données de perte de charge sur le lit ont d'abord été mesurées et ensuite traitées pour obtenir l'analyse de densité spectrale de puissance (PSD) correspondante. Ce dernier était finalement utilisé pour comparer les expériences avec les prédictions du modèle CFD.

Le premier modèle testé dans ce travail était le TFM en raison d'une littérature plus importante associée à son application sur des lits fluidisés, en plus d'être considérée comme plus légère. La vérification du modèle a révélé qu'un maillage fin est nécessaire pour atteindre la convergence des solutions numériques qui reflète finalement de longues simulations 2D (dans l'ordre d'une semaine) et un temps encore plus long pour le modèle 3D complet (environ deux semaines à l'aide d'un superordinateur). La convergence numérique a été trouvée pour un maillage égal à dix fois le diamètre moyen des particules solides, en soutenant ce qui a déjà été rapporté dans la littérature [28], [58], [65]. Le modèle TFM 2D a obtenu un très bon accord avec la courbe de fluidisation empirique dans le régime fixe alors qu'il correspondait aussi bien à la croissance empirique du PSD et à son intégrale finale (indicateur de la variation de la variation de la pression du temps et de la variance).

Dans l'ensemble, le modèle 2D a correctement pu prédire la chute de pression calculée dans le temps et son amplitude de fluctuations, à partir de l'observation des indicateurs statistiques. De plus, l'analyse post-traitement des simulations 2D a révélé une corrélation directe entre la baisse de pression et la distribution de la fraction de vide, ce qui confirme la présence de bulles comme principale source de variation de pression locale. Une version 3D du modèle a également été implémentée et comparée

au modèle 2D. En dépit d'être basé sur un maillage de taille "moyenne", le modèle 3D a considérablement amélioré les résultats sur la première partie du spectre (0-2 Hz), à savoir où toutes les précédentes simulations du modèle 2D ont échoué. L'effet d'une grille plus gros sur le PSD numérique a été préalablement évalué, ce qui permet de comprendre comment les résultats du modèle 3D ont pu être plus proches des résultats empiriques, même dans la partie restante du spectre si un maillage plus fin était exploité.

Cette barrière peut être dépassée si: a) des particules plus grosses peuvent être utilisées (ce qui entraînerait un maillage plus grossier requis pour la vérification numérique); b) un type différent d'analyse variable est nécessaire nécessitant éventuellement un temps d'écoulement inférieur par rapport à celui utilisé dans ce travail; c) l'étude implique une variable macroscopique ou un type d'analyse qui ne requiert pas de maillage très fin à étudier.

Outre le TFM bien développé, une approche modèle plus innovante et moins bien établie a également été utilisée dans ce travail. Un modèle hybride Euler-Lagrangian Dense Discrete Particle Model (DDPM) a été implémenté pour caractériser la dynamique des fluides du lit bouillonnant suivant le même type de traitement des données que dans l'étude TFM. Par rapport à cela, l'approche DDPM présentait des avantages importants tels que la caractérisation discrète du système de particules solides et une exigence de calcul plus faible. Ce dernier aspect est dû à l'exploitation du concept de parcelle, qui réduit le nombre total de particules solides pour suivre l'accélération du calcul de leur position et de leurs vitesses dans les cadres lagrangiens, par rapport au calcul analogue de l'approche TFM

Cet avantage a entraîné la possibilité d'effectuer un plus grand nombre de simulations 3D pour explorer plus largement la précision DDPM-KTGF et la sensibilité numérique. Cependant, de manière similaire au système TFM, cette approche numérique a également été jugée dépendante du maillage et, par conséquent, sa performance a été fortement limitée par le respect d'un seuil de taille de maillage maximal. Cet inconvénient est probablement dû aux collisions de particules qui sont estimées à partir de termes calculés sur le maillage eulérien d'une manière similaire à celle prise en compte par l'approche TFM. Une limite majeure a été trouvée dans l'application de ce modèle à l'étude du régime fixe, où la théorie du KTGF a échoué dans la prévision des forces de contact des particules (et finalement des effets d'exclusion de volume) qui ont conduit à un comportement peu fiable du système. Une très bonne amélioration a été obtenue en utilisant une approche 3D géométriquement complète, dont le PSD correspondait très étroitement à l'empirique dans le premier 2,5 Hz, à savoir où le modèle 2D présentait des limitations majeures.

Les deux modèles ont été testés d'une manière similaire, à savoir étudier l'effet de diverses formulations de paramètres / fonctions (spécifiques des flux granulaires) ainsi que des forces de traction inter-phases sur leur précision tout en évaluant leurs performances en fonction d'une augmentation potentielle. En ce qui concerne la première classe de paramètres, les deux modèles ont montré une sensibilité majeure à une variation des coefficients de restitution, même si avec certaines différences. À l'inverse, bien que certaines formulations de paramètres aient montré une applicabilité 160 inadaptée au modèle (comme pour les fonctions de distribution radiale étudiées avec le modèle DDPM-KTGF), d'autres paramètres de variation (comme le terme de pression solide étudié dans les deux modèles) n'ont pas affecté les résultats numériques de manière significative, reflétant une sensibilité relativement faible au modèle. En tant que point commun, les deux modèles ont été jugés très sensibles à la formulation de force d traînée confirmant l'importance primordiale de l'échange de moment de glissement inter-phase dans les systèmes de bouillonnement gaz-solide à froid. En outre, l'approche TFM et DDPM-KTGF a montré qu'une amélioration significative, dans l'adaptation de la partie des fréquences basses du PSD expérimental (notamment dans la partie du spectre qui concerne principalement la formation de bulles) était possible lorsqu'un modèle 3D était utilisé. Cependant, pour exécuter le modèle 3D, il fallait utiliser un maillage assez grossier, ce qui a limité la capacité du modèle à rattraper la croissance empirique du PSD et son intégrale finale.

Enfin, un troisième modèle numérique qui décrit plus précisément les collisions de particules (Méthode d'élément discrète, DEM) a été mis en œuvre et a été partiellement étudié à la fin de ce travail de doctorat. Bien que certains résultats aient déjà été recueillis, d'autres seront nécessaires afin d'enquêter avec précision sur ce modèle de Lagrange et d'évaluer la possibilité de l'utiliser pour des applications industrielles.

Dans l'ensemble, les résultats obtenus à partir de toute cette étude ont permis d'identifier la barrière prédominante dans le maillage fin (nécessaire pour la vérification numérique et la capture des contours des bulles) qui a limité les performances de ces deux modèles et, finalement, leur applicabilité à l'échelle industrielle. Pour une certaine grandeur de maillage, une précision différente entre les modèles 2D et 3D a été observée lors de la comparaison des expériences avec des simulations basées sur l'analyse PSD. Bien que du point de vue de la performance, seules les simulations 2D semblent montrer l'applicabilité potentielle à l'échelle industrielle, avec la possibilité de prédire assez bien certaines caractéristiques importantes (le niveau pseudo-étatique des fluctuations du lit, l'explosion des bulles, le mouvement solide), l'étendue de la précision du PSD connexe est discutable. À l'inverse, les modèles 3D peuvent potentiellement prédire à la fois la nature tridimensionnelle des

bulles et leurs contours profonds (si un maillage fin est utilisé), ce qui se traduit par une correspondance plus étroite entre PSD empirique et numérique (clairement évident dans la première partie du spectre), mais le temps de simulation prévu pour une application industrielle semble prohibitif. C'est pourquoi aucun de ces modèles ne peut fournir une réponse directe à la question de recherche formulée à la fin de l'introduction, surtout si l'analyse de validation repose sur l'analyse PSD. Toutefois, ces modèles peuvent encore atteindre les étendues industrielles si: a) des particules plus grosses peuvent être utilisées, ce qui reflète la possibilité d'utiliser un maillage plus gros à des fins de vérification numérique; b) un type d'analyse variable différent est nécessaire, pouvant requérir un temps d'écoulement inférieur par rapport à celui utilisé dans ce travail; c) l'étude implique des variables macroscopiques ou des types d’analyse, qui ne requièrent pas de maillage très fin pour être étudié et correctement prédit.

L'accent de ce travail a été mis sur l'étude de la précision du modèle et de la sensibilité numérique pour laquelle un seul ensemble de données empiriques (correspondant à un ensemble de conditions de fonctionnement) a été utilisé comme référence expérimentale. Cependant, un plus large éventail de conditions de fonctionnement sera nécessaire pour faire respecter la phase de validation et, par conséquent, la robustesse des modèles CFD, qui feront probablement partie d'une enquête future.

REFERENCES

[1] A. Kumar, D. D. Jones, and M. A. Hanna, "Thermochemical biomass gasification: A review of the current status of the technology," *Energies*, vol. 2, no. 3, pp. 556–581, 2009.

[2] D. O. Hall, F. Rosillo-Calle, J. Woods, and R. H. Williams, *Biomass for energy: Supply prospects. Renewables for fuels and Electricity*. Washington, DC, 1993.

[3] G. Fischer and L. Schrattenholzer, "Global bioenergy potentials through 2050," *Biomass and Bioenergy*, vol. 20, no. 3, pp. 151–159, 2001.

[4] M. Hoogwijk, A. Faaij, R. van den Broek, G. Berndes, D. Gielen, and W. Turkenburg, "Exploration of the ranges of the global potential of biomass for energy," *Biomass and Bioenergy*, vol. 25, no. 2, pp. 119–133, 2003.

[5] R. D. Perlack, L. L. Wright, A. F. Turhollow, and R. L. Graham, "Biomass as feedstock for a bioenergy and bio-products industry: The technical feasibility of billion-ton annual supply," 2005.

[6] B. C. Gates, G. W. Huber, C. L. Marshall, P. N. Ross, J. Siirola, and Y. Wang, "Catalysts for Emerging Energy Applications," *MRS Bulletin*, vol. 33, no. 4, pp. 429–435, 2008.

[7] S. Thorsell, F. M. Epplin, R. L. Huhnke, and C. M. Taliaferro, "Economics of a coordinated biorefinery feedstock harvest system: Lignocellulosic biomass harvest cost," *Biomass and Bioenergy*, vol. 27, no. 4, pp. 327–337, 2004.

[8] P. Basu, "Biomass Gasification, Pyrolysis, and Torrefaction," Second Edi., Elsevier, Ed. 32 Jamestown Road, London NW1 7BY, UK 525, 2013, pp. 253-255–258.

[9] "GSTC (2017).'Waste to Energy Gasification'. Available on :http://www.gasification-syngas.org/applications/waste-to-energy-gasification/ (accessed/cited in May 2017)." .

[10] "Jim Yong Kim, (2012). What a Waste: A Global Review of Solid Waste Management. Available from: https://www.worldbank.org/en/about (accessed/cited in May 2017)." .

[11] "Alex Ramon., (2006). Negative impacts of incineration-based waste-to-energy technology Available from: http://www.alternative-energy-news.info/negative-impacts-waste-to-energy/ (accessed/cited in May 2017)." .

[12] “climatetechwiki (2012).‘Gasification of Municipal Solid Waste for Large-Scale Electricity/Heat’. Available on :http://www.climatetechwiki.org/technology/msw (accessed/cited in May 2017).”

[13] U. Arena, “Process and technological aspects of municipal solid waste gasification. A review,” *Waste Management*, vol. 32, no. 4, pp. 625–639, 2012.

[14] K. Sipilä, “New power production technologies: various options for biomass and cogeneration.,” *Bioresour. Technol.*, vol. 46, pp. 5–12, 1993.

[15] K. J. Whitty, H. R. Zhang, and E. G. Eddings, “Emissions from Syngas Combustion,” *Combustion Science and Technology*, vol. 180, no. 6, pp. 1117–1136, 2008.

[16] M. L. Boroson, J. B. Howard, J. P. Longwell, and W. a. Peters, “Product yields and kinetics from the vapor phase cracking of wood pyrolysis tars,” *AIChE Journal*, vol. 35, no. 1, pp. 120–128, 1989.

[17] R. Rauch, J. Hrbek, and H. Hofbauer, “Biomass gasification for synthesis gas production and applications of the syngas,” *Wiley Interdisciplinary Reviews: Energy and Environment*, vol. 3, no. 4, pp. 343–362, 2014.

[18] “Enerkem., (2017). ‘Multifeedstock / multiproduct’ is what differentiates Enerkem’s technology platform: http://enerkem.com/about-us/technology/ (accessed/cited in May 2017).” .

[19] P. Pepiot, C. Dibble, and T. Foust, *Computational fluid dynamics modeling of biomass gasification and pyrolysis. Computational modeling in lignocellulosic biofuel production*, vol. 1052, no. ACS Symposium Series. 2010.

[20] R. I. Singh, A. Brink, and M. Hupa, “CFD modeling to study fluidized bed combustion and gasification,” *Applied Thermal Engineering*, vol. 52, no. 2, pp. 585–614, 2013.

[21] R. W. Breault, “Gasification processes old and new: A basic review of the major technologies,” *Energies*, vol. 3, no. 2, pp. 216–240, 2010.

[22] A. Molino, S. Chianese, and D. Musmarra, “Biomass gasification technology: The state of the art overview,” *Journal of Energy Chemistry*, vol. 25, no. 1, pp. 10–25, 2016.

[23] S. T. Mac an Bhaird, P. Hemmingway, E. Walsh, A. L. Maglinao, S. C. Capareda, and K. P.

McDonnell, “Bubbling fluidised bed gasification of wheat straw-gasifier performance using mullite as bed material,” *Chemical Engineering Research and Design*, vol. 97, pp. 36–44, 2015.

[24] D. Kunii and O. Levenspiel, *Fluidization Engineering*. 2013.

[25] C. G. Philippsen, A. C. F. Vilela, and L. D. Zen, “Fluidized bed modeling applied to the analysis of processes: Review and state of the art,” *Journal of Materials Research and Technology*, vol. 4, no. 2, pp. 208–216, 2015.

[26] D. Geldart, “Types of Gas Fluidization,” *Powder Technology*, vol. v 7, n 5, p. p 285-92, 1973.

[27] “G.Rovero(2012).Optimization of Spouted Bed Scale-Up by Square-Based Multiple Unit Design. http://www.intechopen.com/books/advances-in-chemicalengineering/optimization-of-spouted-bed-scale-up-by-square-based-multiple-unit-design (cited on May 2017).” .

[28] M. A. van der Hoef, M. Ye, M. van Sint Annaland, A. T. Andrews, S. Sundaresan, and J. A. M. Kuipers, “Multiscale Modeling of Gas-Fluidized Beds,” *Advances in Chemical Engineering*, vol. 31, pp. 65–149, 2006.

[29] J. F. Davidson and D. Harrison, *Fluidised particles*. New York: Cambridge University Press, 1963.

[30] S. Elgobashi, “Particle-laden turbulent flows: Direct simulation and closure models,” *Appl.Sci.Res*, vol. 48, pp. 301–304, 1991.

[31] J. A. M. Kuipers and W. P. M. van Swaaij, “Computational Fluid Dynamics Applied To Chemical Reaction Engineering,” *Advances in Chemical Engineering*, vol. 24, pp. 227–328, 1998.

[32] Y. Bao and J. Meskas, “Lattice Boltzmann Method for Fluid Simulations - Report-2011-pp.1-16.”

[33] “Heat and Mass Transfer Technological Center (CTTC)-Universitat Politècnica de Catalunya BARCELONA TECH (UPC), (2017). Multi-phase modelling. Available from: http://www.cttc.upc.edu (accessed/cited in May 2017).” .

[34] A. Balcázar, N., Castro, J., Rigola, J., Oliva, “DNS of the wall effect on the motion of bubble swarms DNS of the wall effect on the motion of bubble swarms DNS of the wall effect on the

motion of bubble swarms," *Procedia Computer Science*, vol. 108, pp. 2008–2017, 2017.

[35] N. Balcázar, O. Lehmkuhl, J. Rigola, and A. Oliva, "A multiple marker level-set method for simulation of deformable fluid particles," *International Journal of Multiphase Flow*, vol. 74, pp. 125–142, 2015.

[36] Y. Tang, Y. M. Lau, N. G. Deen, E. A. J. F. Peters, and J. A. M. Kuipers, "Direct numerical simulations and experiments of a pseudo-2D gas-fluidized bed," *Chemical Engineering Science*, vol. 143, pp. 166–180, 2016.

[37] J. T. Jenkins and S. B. Savage, "A theory for the rapid flow of identical , smooth , nearly elastic, spherical particles," *J. Fluid Mech.*, vol. 30, no. 1983, pp. 187–202, 1983.

[38] C. K. K. Lun, S. B. Savage, D. J. Jeffrey, and N. Chepurniy, "Kinetic theories for granular flow: inelastic particles in Couette flow and slightly inelastic particles in a general flowfield," *Journal of Fluid Mechanics*, vol. 140, no. 1, p. 223, 1984.

[39] H. P. Zhu, Z. Y. Zhou, R. Y. Yang, and A. B. Yu, "Discrete particle simulation of particulate systems: A review of major applications and findings," *Chemical Engineering Science*, vol. 63, no. 23, pp. 5728–5770, 2008.

[40] Ansys, "ANSYS FLUENT Theory Guide," vol. 15317, no. October, Canonsburg, PA: Ansys,Inc, 2012, pp. 511–545.

[41] W. P. Adamczyk, W. Gabriel, M. Klajny, P. Kozołub, A. Klimanek, and R. A. Białecki, "Modeling of particle transport and combustion phenomena in a large-scale circulating fluidized bed boiler using a hybrid Euler – Lagrange approach," *Particuology*, vol. 16, pp. 29–40, 2014.

[42] T. B. Anderson and R. Jackson, "Fluid mechanical description of fluidized beds: Equations of motion," *Ind. Eng. Chem. Fund.*, vol. 8, p. 137, 1969.

[43] S. Sundaresan, K. Anderson, and R. Jackson, "Instabilities and the formation of bubbles in fluidized beds," *J. Fluid Mech.1*, vol. 303, p. 327, 1995.

[44] J. A. M. Kuipers, K. J. van Duin, F. H. P. van Beckum, and W. P. M. van Swaaij, "A numerical model of gas-fluidized beds," *Chemical Engineering Science*, vol. 47, 1992.

[45] Y. P. Tsuo and D. Gidaspow, "Computations of flow patterns in circulating fluidized beds,"

AIChE Journal, vol. 36, p. 885, 1990.

[46] S. Elgobashi and T. W. Abou-Arab, "A two-equation turbulence model for two-phase flows," *phys. Fluids*, vol. 26, p. 931, 1983.

[47] C. P. Chen, "Studies in two-phase turbulence closure modeling," *Thesis/Dissertation*, 1985.

[48] L. X. Zhou and X. Q. Huang, "Prediction of confined turbulent gas-particle jet by an energy equation model of particle turbulence," *Science in China*, vol. 33, p. 428, 1990.

[49] D. Gidaspow, "Multiphase flow and fluidization: Continuum and kinetic theory descriptions," New York: Academic press, 1994, p. 467.

[50] Ding J. and D. Gidaspow, "A bubbling fluidization model using kinetic theory of granular flow," *AIChE Journal*, vol. 36, p. 523, 1990.

[51] J. L. Sinclair and R. Jackson, "Gas-particle flow in a vertical pipe with particle-particle interactions," *AIChE Journal*, vol. 35, no. 1473, 1989.

[52] A. Samuelsberg and B. H. Hjertager, "Computational modeling of gas/particle flow in a riser," *AIChE Journal*, vol. 42, p. 1536, 1996.

[53] J. J. Nieuwland, M. van Sint Annaland, J. A. M. Kuipers, and W. P. M. van Swaaij, "Hydrodynamic modeling of gas/particle flows in riser reactors," *AIChE Journal*, vol. 42, p. 1569, 1996.

[54] M. S. Detamore, M. A. Swanson, K. R. Frender, and C. M. Hrenya, "A kinetic-theory analysis of the scale-up of circulating fluidized beds," *Powder Technology*, vol. 116, p. 190, 2001.

[55] E. Peirano, V. Delloume, and B. Leckner, "Two- or three-dimensional simulations of turbulent gas-solid flows applied to fluidization," *Chemical Engineering Science*, vol. 56, no. 16, pp. 4787–4799, 2001.

[56] M. Syamlal and T. J. O'Brien, "Fluid dynamic simulation of O-3 decomposition in a bubbling fluidized bed," *Aiche Journal*, vol. 49, no. 11, pp. 2793–2801, 2003.

[57] T. McKeen and T. Pugsley, "Simulation and experimental validation of a freely bubbling bed of FCC catalyst," *Powder Technology*, vol. 129, no. 1–3, pp. 139–152, 2003.

[58] S. Zimmermann and F. Taghipour, "CFD modeling of the hydrodynamics and reaction kinetics

of FCC fluidized-bed reactors," *Industrial and Engineering Chemistry Research*, vol. 44, no. 26, pp. 9818–9827, 2005.

[59] D. Gidaspow, R. Bezburuah, and J. Ding, "Hydrodynamics of Circulating Fluidized Beds, Kinetic Theory Approach. In: Potter, O.E. and Nicklin, D.J., Eds., Fluidization VII, Proceedings of the 7th Engineering Foundation Conference on Fluidization, Engineering Foundation, New York, 75-82.," 1992.

[60] M. Syamlal and T. J. O'Brien, "The Derivation of a Drag Coefficient Formula from Velocity-Voidage Correlations.," *Unpublished*, no. JANUARY 1994, pp. 1–20, 1987.

[61] M. De Vega, A. Acosta-iborra, C. Sobrino, and F. Herna, "Experimental and computational study on the bubble behavior in a 3-D fluidized bed," *Chemical Engineering Science*, vol. 66, pp. 3499–3512, 2011.

[62] E. Esmaili and N. Mahinpey, "Advances in Engineering Software Adjustment of drag coefficient correlations in three dimensional CFD simulation of gas – solid bubbling fluidized bed," *Advances in Engineering Software*, vol. 42, no. 6, pp. 375–386, 2011.

[63] J. Min, J. B.Drake, T. J.Heindel, and R. O.Fox, "Experimental Validation of CFD Simulations of a Lab-Scale FLuidized-Bed reactor with and without side-gas injection," *AIChE Journal*, vol. 56, pp. 1434–1446, 2010.

[64] J. Jang and H. Arastoopour, "CFD Simulation of Different-Scaled Bubbling Fluidized Beds. Engineering Conferences International-The 14th International Conference on Fluidization – From Fundamentals to Products," 2013.

[65] C. Tagliaferri, L. Mazzei, P. Lettieri, A. Marzocchella, G. Olivieri, and P. Salatino, "CFD simulation of bubbling fluidized bidisperse mixtures: Effect of integration methods and restitution coefficient," *Chemical Engineering Science*, vol. 102, pp. 324–334, 2013.

[66] X. Chen and J. Wang, "A comparison of two-fluid model, dense discrete particle model and CFD-DEM method for modeling impinging gas-solid flows," *Powder Technology*, vol. 254, pp. 94–102, 2014.

[67] S. Cloete, "Evaluation of a Lagrangian Discrete Phase Modeling Approach for Resolving Cluster Formatin in CFB Risers," in *International Conference on Mutliphase Flow*, 2010.

[68] S. Cloete and S. Amini, "The dense discrete phase model for simulation of bubbling fluidized

beds: Validation and verification. ICMF-2016 – 9th International Conference on Multiphase Flow," 2016.

[69] S. Cloete, S. T. Johansen, M. Braun, B. Popoff, and S. Amini, "Evaluation of a Lagrangian Discrete Phase Modeling Approach for Application To Industrial Scale Bubbling Fluidized Beds," *Proceedings of the 10th International Conference on Circulating Fluidized Beds and Fluidization Technology - CFB-10*, vol. 7, no. 2013, pp. 1–8, 2011.

[70] S. Cloete, S. T. Johansen, and S. Amini, "Performance evaluation of a complete Lagrangian KTGF approach for dilute granular flow modelling," *Powder Technology*, vol. 226, pp. 43–52, 2012.

[71] J. R. Grace and F. Taghipour, "Verification and validation of CFD models and dynamic similarity for fluidized beds," *Powder Technology*, vol. 139, no. 2, pp. 99–110, 2004.

[72] AIAA, "Guide for the Verification and Validation of Computational Fluid Dynamics Simulations." AIAA-G-077-1998, Am.Inst.Aeronaut.Astronaut., 1998.

[73] VGB technical commitee, "Gas Distributor Plates in Fluidized Bed Systems." VGB TECHNISCHE VEREINIGUNG DER GROSSKRAFTWRKSBETREIBER E.V, 1994.

[74] "Steven Hugill (4th September 2013).'Where there's muck there's gas . . .', available on: http://www.thenorthernecho.co.uk/business/spotlighton/10653594.Where there is muck there is gas/ (accessed/cited in May 2017)."

[75] "ASTM D7743-12 Standard Test Method for Measuring the Minimum Fluidization Velocities of Free Flowing Powders, ASTM International, West Conshohocken, PA, 2012, https://doi.org/10.1520/D7743-12." Conshohocken, West, pp. 1–8, 2013.

[76] M. Syamlal, W. Rogers, and O'Brien T.J., "MFIX Documentation: Volume 1 Theory Guide, National Technical Information Service, Springfield, VA, 1993 (DOE/METC 9411004, NTIS/DE9400087)." .

[77] D. G. Schaeffer, "Instability in the evolution equations describing incompressible granular flow," *Journal of Differential Equations*, vol. 66, no. 1, pp. 19–50, 1987.

[78] Ansys, "Lecture 5: Particulate Flows. Advanced Multiphase Course," Canonsburg, PA: Ansys,Inc, 2014.

[79] P. C. Johnson and R. Jackson, “Frictional–collisional constitutive relations for granular materials, with application to plane shearing,” *Journal of Fluid Mechanics*, vol. 176, no. 1, p. 67, Mar. 1987.

[80] S. Ogawa, A. Umemura, and N. Oshima, “On the equations of fully fluidized granular materials,” *Appl. Math*, vol. Phys.. 31, p. 483, 1980.

[81] C. K. K. Lun, S. B. Savage, D. J. Jeffrey, and N. Chepurniy, “Kinetic theories for granular flow: inelastic particles in Couette flow and slightly inelastic particles in a general flowfield,” *Journal of Fluid Mechanics*, vol. 140, no. 1, p. 223, 1984.

[82] S. Ergun, “Fluid Flow Through Packed Columns,” *Chem. Eng. Prog.*, vol. 48, pp. 89–94, 1952.

[83] D. Gidaspow, “Hydrodynamics of Fluidization and Heat Transfer: Supercomputer Modeling,” *Appl.Mech.Rev.*, vol. 39, pp. 1–23, 1986.

[84] J. F. Richardson and W. N. Zaki, “Sedimentation and Fluidization: Part I,” *Trans.Inst.Chem.Eng*, vol. 32, pp. 35–53, 1954.

[85] C. . Wen and Y. H. Yu, “Mechanics of Fluidization,” *Chem. Eng. Prog. Symp. Series*, vol. 62, pp. 100–111, 1966.

[86] F. Vejahati, N. Mahinpey, N. Ellis, and M. B. Nikoo, “CFD simulation of gas-solid bubbling fluidized bed: A new method for adjusting drag law,” *Canadian Journal of Chemical Engineering*, vol. 87, no. 1, pp. 19–30, 2009.

[87] J. Garside and M. R. Al-Dibouni, “Velocity-Voidage Relationships for Fluidization and Sedimentation in Solid-Liquid Systems,” *Industrial & Engineering Chemistry Process Design and Development*, vol. 16, no. 2, pp. 206–214, 1977.

[88] P. A. Cundall and O. D. L. Strack, “A discrete numerical model for granular assemblies,” *Géotechnique*, vol. 29, no. 1. pp. 47–65, 1979.

[89] S. Matsumoto and M. Suzuki, “Statistical analysis of fluctuations of froth pressure on perforated plates without downcomers,” *International Journal of Multiphase Flow*, vol. 10, pp. 217–228, 1984.

[90] H. Kage, N. Iwasaki, Y. Matsuno, and Y. Matsuno, “Frequency analysis of pressure fluctuation in fluidized bed plenum,” *Journal of Chemical Engineering of Japan*, vol. 24, no. 1, pp. 76–

81, 1991.

[91] H. Kage, M. Agari, H. Ogura, and Y. Matsuno, “Frequency analysis of pressure fluctuation in fluidized bed plenum and its confidence limit for detection of various modes of fluidization,” *Advanced Powder Technology*, vol. 11, no. 4, pp. 459–475, 2000.

[92] H. Johnsson and F. Johnsson, “Measurements of local solids volume-fraction in fluidized bed boilers,” *Powder Technology*, vol. 115, no. 1, pp. 13–26, 2001.

[93] H. T. Bi, “A critical review of the complex pressure fluctuation phenomenon in gas-solids fluidized beds,” *Chemical Engineering Science*, vol. 62, no. 13, pp. 3473–3493, 2007.

[94] W. Qingcheng, Z. Kai, and G. Hongyan, “CFD simulation of pressure fluctuation characteristics in the gas-solid fluidized bed: Comparisons with experiments,” pp. 211–218, 2011.

[95] M. Syamlal and T. J. O’Brien, “Simulation of granular layer inversion in liquid fluidized beds,” *International Journal of Multiphase Flow*, vol. 14, no. 4, pp. 473–481, 1988.

[96] J. R. Van Ommen, S. Sasic, J. Van Der Schaaf, S. Gheorghiu, F. Johnsson, and M. Coppens, “Time-series analysis of pressure fluctuations in gas – solid fluidized beds – A review,” *International Journal of Multiphase Flow*, vol. 37, no. 5, pp. 403–428, 2011.

[97] M. Syamlal and T. J. O’Brien, “Computer Simulation of Bubbles in a Fluidized Bed,” *AIChE Symp. Series 85*, pp. 22–31, 1989.

[98] G. Ahmadi and D. Ma, “A Thermodynamical Formulation for Dispersed Multiphase Turbulent Flows,” *Int.J.Multiphase Flow. 16*, pp. 323–351, 1990.

[99] L. L. Yang, J. T. J. Padding, and J. A. M. H. Kuipers, “Modification of kinetic theory of granular flow for frictional spheres, Part I: Two-fluid model derivation and numerical implementation,” *Chemical Engineering Science*, vol. 152, pp. 767–782, 2016.

[100] Ding Jianmin and D. Gidaspow, “A Bubbling Fluidization Model Using Kinetic Theory of Granular Flow,” *AIChE Journal*, vol. 36, no. 4, pp. 523–538, 1990.

[101] N. Couto, V. Silva, E. Monteiro, S. Teixeira, P. S. D. Brito, and A. Rouboa, “Numerical and experimental analysis of municipal solid wastes gasification process,” *Applied Thermal Engineering*, vol. 78, pp. 185–195, 2015.

[102] “Gu Dazhao, Katie Warrick., (2015). Today’s Gasification Market Available from: http://cornerstonemag.net/tag/reducing-emissions-in-china/ (accessed/cited in May 2017).” .

[103] G. A. Bokkers, “Multi-level modelling of the hydrodynamics in gas phase polymerisation reactors,” *Thesis/Dissertation*, 2005.

[104] B. Practice, M. Lambert, M. Braun, D. Dimitrova, J. Schuetze, and D. Stenger, “CFD-DEM, Theory, Numerics, Best Practice,” pp. 1–64, 2017.